

The Effect of Noncondensable Gas on Steam Bubble Collapse Induced Water Hammer

by

Bruce H. Easom

Submitted to the Department of Mechanical Engineering
in partial fulfillment of the requirements for the degree of

Doctor of Science in Mechanical Engineering

at the

MASSACHUSETTS INSTITUTE OF TECHNOLOGY

June 1992

© Massachusetts Institute of Technology 1992. All rights reserved.

Signature Redacted


Author

Department of Mechanical Engineering

May 1, 1992

Signature Redacted

Certified by

 Peter Griffith
Professor of Mechanical Engineering
Thesis Supervisor

Signature Redacted

Accepted by

Ain A. Sonin
Chairman, Departmental Committee on Graduate Students

ARCHIVES
MASSACHUSETTS INSTITUTE
OF TECHNOLOGY

JUN 17 1992

LIBRARIES

The Effect of Noncondensable Gas on Steam Bubble Collapse Induced Water Hammer

by

Bruce H. Easom

Submitted to the Department of Mechanical Engineering
on May 1, 1992, in partial fulfillment of the
requirements for the degree of
Doctor of Science in Mechanical Engineering

Abstract

A series of experiments have shown that adding noncondensable gas to steam can reduce the amplitude of steam bubble collapse induced water hammers by two orders of magnitude. A simple analytical model has been developed to predict the mass of gas required to produce the desired amplitude reduction.

An experimental apparatus was constructed to produce steam bubble collapse induced water hammers with an air/steam mixture variable from 100 percent steam to 100 percent air. The results show that the compressibility of the gas is primarily responsible for the amplitude reduction.

Procedures for using the results to predict water hammer amplitude reduction in other systems are presented.

Thesis Supervisor: Peter Griffith

Title: Professor of Mechanical Engineering

Dedication

To my father

Bruce Eason

Acknowledgments

I wish to express my thanks to Professor Peter Griffith for his guidance and patience in seeing me through this work. I was always amazed at his insight and perception into my problems and in engineering problems in general. Indeed, most engineering problems are caused by “crud, leaks and noise”. I wish to thank the United States Department of Energy for their support of my work which was conducted under their nuclear energy program.

I also wish to thank the two other members of my Doctoral Committee, Professor Ain Sonin and Dean Frank Perkins. I appreciate their time in helping me understand my experimental data.

Mr. Joseph Callegero did all the welding on the experimental apparatus and procured the necessary materials for its construction. I appreciated his advice and expertise. He was an excellent advocate in dealing with suppliers.

I thank my office mates, Keith Crowe, Mark Fenton, Kou-Shing Liang and Andrew Neumann for their companionship and for letting me bounce ideas off them. Explaining my problems to them helped me better understand the problems myself.

Finally I wish to thank my mother for so patiently seeing me through school. She took me by the hand to kindergarten some thirty years ago and she will see me graduate in June.

Contents

1	Introduction	18
1.1	Background	20
1.2	One-dimensional Water Hammer Model	21
1.3	Bubble Collapse Model	22
2	Experimental Apparatus	26
2.0.1	General Arrangement	26
2.0.2	Boiler	28
2.0.3	Superheater Tank	28
2.0.4	Hammer Column	33
2.0.5	Instrumentation	35
3	Noncondensable Gas Tests	39
3.1	Experimental Results	39
3.1.1	Water Hammer Peak Pressure	39
3.1.2	Water Hammer Momentum	40
3.2	Discussion	46
4	Analytical Model	48
4.0.1	Boundary Conditions	50
4.0.2	Nondimensionalization	51
4.0.3	Implementation	52
4.1	Experimental Versus Analytical Results	52
4.1.1	Gamma Sensitivity	55

4.1.2	Pressure-Time Traces	55
4.1.3	Momentum Estimates	60
5	Conclusion	67
A	Experimental Procedures	71
A.1	Noncondensable Gas Tests	71
A.1.1	System Startup	71
A.1.2	Heating Up	72
A.1.3	Making the Mixture	72
A.1.4	Hammer Column Preparation	73
A.1.5	Water Hammer Initiation	74
A.1.6	Post Run Procedures	74
A.2	Pipe Wall Temperature Sensitivity Tests	75
A.2.1	Hammer Column Preparation	75
A.2.2	Water Hammer Initiation	75
A.2.3	Post Run Procedures	76
A.3	Ambient Pressure Sensitivity Tests	76
A.3.1	Hammer Chamber Preparation	76
A.3.2	Water Hammer Initiation	77
A.3.3	Post Run Procedures	77
B	Data Reduction	78
B.1	Noncondensable Gas Tests	78
B.1.1	Gas Fraction Calculations	78
B.2	Hammer Chamber Pressure Calculations	80
B.2.1	Offset Corrections	80
B.2.2	Thermal Effect Corrections	81
B.3	Pipe Wall Temperature Sensitivity Tests	85
B.4	Ambient Pressure Sensitivity Tests	85
C	Time Traces of Selected Data	86

C.0.1	Water Hammer High Pressure Data	86
C.0.2	Water Hammer Low Pressure Data	90
C.0.3	Dump Valve Differential Pressure	90
C.0.4	Dump Valve Position Data	90
D	Ambient Pressure Sensitivity Tests	95
D.1	Apparatus Modifications	95
D.2	Experimental Results	96
D.3	Discussion	96
E	Pipe Wall Temperature Sensitivity Tests	102
E.1	Experimental Results	102
E.2	Discussion	104
F	Application to Other Systems	107
F.0.1	Determine Maximum Pressure (Step 1)	108
F.0.2	Calculate Maximum P^* (Step 2)	108
F.0.3	Calculate B (Step 3)	108
F.0.4	Determine A (Step 4)	109
F.0.5	Calculate M_g (Step 5)	109
F.0.6	Run Simulation of <i>BOING</i> (Step 6)	109
F.0.7	Evaluate Effect on Other Components (Step 7)	110
F.0.8	Determine Location of Gas Injection (Step 8)	110
F.1	Final Comments	110
G	Finite Difference Water Hammer Model	111
H	Pressure Transducer System Step Response	113
H.1	Piezoelectric Transducer	114
H.2	Charge Amplifier	114
H.3	Charge Amplifier Low Pass Filter	114
H.4	FM Tape Recorder and Structural Dynamics Analyzer	115

I	Instrumentation	119
I.1	Hammer Chamber Pressure	119
I.2	Dump Valve Differential Pressure	120
I.3	Boiler Pressure	120
I.4	Superheater Tank Pressure	120
I.5	Gas Bottle Pressure	123
I.6	Operating Temperatures	125
I.7	Dump Valve Position Indicator	125
I.8	Tape Recorder	126
I.9	Structural Dynamics Analyzer	127

List of Figures

1-1	Water Hammer Events in U.S. Nuclear Power Industry[9]	19
1-2	Water Hammer Model	21
1-3	Water Hammer Pressure at Bottom of Liquid	23
1-4	Dimensionless Bubble Radius Versus Dimensionless Time For a Pentane Bubble Condensing in Subcooled Pentane[6]	24
2-1	Experimental Apparatus General Arrangement	27
2-2	Boiler	29
2-3	Superheater Tank	30
2-4	Circulation Fan Distribution Schematic	32
2-5	Hammer Column	34
2-6	Instrumentation	36
3-1	Water Hammer Peak Pressure Versus Gas Fraction	41
3-2	Water Hammer Peak Pressure Versus Gas Fraction (Expanded)	42
3-3	Liquid Slug Momentum Versus Gas Fraction	44
3-4	Liquid Slug Momentum Versus Gas Fraction (Expanded)	45
4-1	Analytical Model Schematic	49
4-2	Noncondensable Gas Tests - Experimental Versus Analytical Results	53
4-3	Experimental Versus Analytical Results - Expanded	54
4-4	Gamma Sensitivity	56
4-5	Analytical and Experimental Data for Point "a" in Figure 4-3	57
4-6	Analytical and Experimental Data for Point "b" in Figure 4-3	58

4-7	Analytical and Experimental Data for Point "c" in Figure 4-3	59
4-8	Freefall Model	61
4-9	Freefall Momentum	62
4-10	"A" Estimated From Freefall	63
4-11	"A" Estimated From Freefall (Expanded)	64
4-12	Maximum Water Hammer Pressure From Analytical Model	66
B-1	Instruments Used for Gas Fraction Measurements	79
B-2	Hammer Chamber Pressure Transducer Thermal Effect	83
B-3	Thermal Effect Correction Versus Gas Fraction	84
C-1	High Pressure Data for Points in Figure 3-1	87
C-2	High Pressure Data for Points in Figure 3-1 (Expanded)	88
C-3	Hammer Chamber Low Pressure Data for Points in Figure 3-1	91
C-4	Dump Valve Differential Pressure Data for Points in Figure 3-1	92
C-5	Dump Valve Position Data for Points in Figure 3-1	93
D-1	Apparatus Modified for Ambient Pressure Sensitivity Tests	97
D-2	Water Hammer Peak Pressure Versus Ambient Pressure	98
D-3	Pressure Versus Time Data for Points "a" and "b" in Figure D-2	99
D-4	Liquid Slug Momentum Versus Ambient Pressure	100
E-1	Water Hammer Peak Pressure Versus Liquid/Wall Temperature Dif- ference	103
E-2	Liquid Slug Momentum Versus Liquid/Wall Temperature Difference	105
E-3	Pressure Versus Time Data for Points "a", "b" and "c" of Figure E-1	106
H-1	Piezoelectric Pressure Transducer System Schematic	113
H-2	Step Response of FM Tape Recorder and Structural Dynamics Analyzer	115
H-3	Transducer System Step Response	118
I-1	Superheater Tank Pressure Gauge and Diaphragm Arrangement	123

List of Tables

I.1	Hammer Chamber Pressure Instrumentation Specifications	121
I.2	Dump Valve Differential Pressure Instrumentation Specifications . . .	122
I.3	Boiler Pressure Gauge Specifications	122
I.4	Superheater Tank Pressure Gauge and Diaphragm Specifications . . .	124
I.5	Gas Bottle Pressure Gauge Specifications	124
I.6	Thermocouple Reader Specifications	125
I.7	Dump Valve Position Indicator Specifications	126
I.8	FM Tape Recorder Specifications	127
I.9	Structrual Dynamics Analyzer Specifications	127

Nomenclature

A	analytical model dimensionless parameter	[<i>nondimensional</i>]
B	analytical model dimensionless parameter	[<i>nondimensional</i>]
c	speed of sound in liquid	[<i>ft/s</i>]
C_a	capacitance of charge amplifier	[<i>farads</i>]
f	transducer thermal effect scaling factor	[<i>nondimensional</i>]
g	gravitational acceleration	[<i>ft/s²</i>]
g_o	gravitational constant	[<i>lb_m - ft/lb_f - s²</i>]
$G(s)$	pressure transducer system transfer function	[<i>nondimensional</i>]
$G_c(s)$	charge amplifier transfer function	[<i>1/farad</i>]
$G_s(s)$	FM tape recorder/structural dynamics analyzer transfer function	[<i>psi/volt</i>]
$G_t(s)$	piezoelectric pressure transducer transfer function	[<i>psi/Cb</i>]
J_a	Jacob number	[<i>nondimensional</i>]
k_{steel}	thermal conductivity of steel	[<i>btu/hr - ft - F</i>]
k_{water}	thermal conductivity of water	[<i>btu/hr - ft - F</i>]
K	constant of polytropic process $PV^\gamma = K$	[<i>lb_f - ft^{3γ}/ft²</i>]
K_s	FM tape recorder/structural dynamics analyzer calibration constant	[<i>psi/volt</i>]
K_t	piezoelectric pressure transducer calibration constant	[<i>Cb/psi</i>]
l_{hc}	length of hammer chamber	[<i>ft</i>]
L	liquid column length	[<i>ft</i>]
M_{air}	mass of air in superheater tank	[<i>lb_m</i>]
$M_{air\,charge1}$	mass of the first charge of air	[<i>lb_m</i>]
$M_{air\,tank1}$	mass of air in superheater tank after addition of first charge of air	[<i>lb_m</i>]
M_g	mass of noncondensable gas	[<i>lb_m</i>]
M_l	mass of liquid	[<i>lb_m</i>]

M_{steam}	mass of steam in superheater tank	[lb_m]
M_{steam_o}	initial mass of steam in superheater tank	[lb_m]
P	pressure	[lb_f/ft^2]
P^*	nondimensional pressure	[<i>nondimensional</i>]
P_a	ambient pressure	[lb_f/ft^2]
P_{atm}	atmospheric pressure (absolute)	[lb_f/ft^2]
P_d	pressure downstream of liquid slug	[<i>psi</i>]
P_e	Péclet number	[<i>nondimensional</i>]
P_h	water hammer pressure as measured by the high pressure transducer	[lb_f/ft^2]
$P_{h_{correction}}$	offset correction constant for high pressure transducer	[lb_f/ft^2]
P_{in}	piezoelectric pressure transducer input pressure	[<i>psi</i>]
P_j	water hammer pressure from Joukowski limit	[lb_f/ft^2]
P_l	water hammer pressure as measured by the low pressure transducer	[lb_f/ft^2]
$P_{l_{correction}}$	offset correction constant for low pressure transducer	[lb_f/ft^2]
P_{out}	structural dynamics analyzer output pressure	[<i>psi</i>]
P_{te}	high pressure transducer thermal effect	[<i>psi</i>]
P_u	pressure upstream of liquid slug	[<i>psi</i>]
P_1	boiler pressure	[<i>psig</i>]
P_2	superheater tank pressure	[<i>psig</i>]
P_3	gas bottle pressure	[<i>psig</i>]
P_4	dump valve differential pressure	[<i>psig</i>]
P_5	ambient pressure	[<i>psig</i>]
P_6	steam jacket pressure	[<i>psig</i>]
Q	noncondensable gas fraction	[<i>nondimensional</i>]
Q_t	piezoelectric pressure transducer output charge and charge amplifier input charge	[<i>coulomb</i>]

r	bubble radius	[ft]
r_o	initial bubble radius	[ft]
R_{air}	ideal gas constant for air	[lb _f - ft/lb _m - R]
s	Laplace transform variable	[1/s]
t	time	[s]
t^*	nondimensional time	[nondimensional]
\hat{t}	nondimensional time (Figure 1-4 only)	[nondimensional]
t_0	beginning time of first pressure spike	[s]
t_1	ending time of first pressure spike	[s]
T_f	low pass filter time constant	[s]
T_{liquid}	temperature of subcooled liquid slug	[F]
T_{steel_o}	initial temperature of steel	[F]
T_{wall}	pipe wall inside temperature	[Rankine]
T_{water}	water temperature	[F]
T_{water_o}	initial temperature of water	[F]
T_1	boiler steam temperature	[F]
T_2	boiler water temperature	[F]
T_3	superheater tank gas temperature (top)	[F]
T_4	superheater tank gas temperature (bottom)	[F]
T_5	gas bottle wall temperature	[F]
T_6	superheater tank bottom drain temperature	[F]
T_7	steam/gas outlet line temperature	[F]
T_8	subcooled water tank temperature	[F]
v	velocity	[ft/s]
v_i	initial velocity of water slug	[ft/s]
v_{steam}	specific volume of steam	[ft ³ /lb _m]
V	volume	[ft ³]
V_B	volume of gas bottle	[ft ³]
V_{o_g}	initial volume of gas	[ft ³]
V_{o_l}	initial volume of liquid	[ft ³]

V_T	volume of superheater tank	[ft^3]
V_1	charge amplifier output voltage and low-pass filter input voltage	[$volts$]
V_2	low-pass filter output voltage and FM tape recorder input voltage	[$volts$]
V_3	FM tape recorder output voltage and structural dynamics analyzer input voltage	[$volts$]
x	distance from hammer chamber bottom to liquid/gas interface	[ft]

Script

A	pipe cross-sectional area	[ft^2]
M	momentum of water slug	[$lb_m - ft/s$]

Greek

β	bulk modulus	[psi]
β	nondimensional bubble radius $\frac{r}{r_0}$ (Figure 1-4 only)	[<i>nondimensional</i>]
β_f^H	final nondimensional bubble radius for a homogenous distribution of noncondensable gas	[<i>nondimensional</i>]
β_f^P	final nondimensional bubble radius for a parabolic distribution of noncondensable gas	[<i>nondimensional</i>]
β_g	bulk modulus of gas	[psi]
β_l	bulk modulus of liquid	[psi]
γ	polytropic exponent	[<i>nondimensional</i>]
ω_{nt}	piezoelectric transducer natural frequency	[rad/s]

ω_{n_s}	natural frequency of FM tape recorder/structural dynamics analyzer	[rad/s]
ρ	mass density	[lb_m/ft^3]
τ	time for hydraulic shock wave to travel length of of water column and back	[s]
τ_{te}	time offset for thermal effect correction	[s]
ζ_t	peizoelectric transducer damping ratio	[nondimensional]
ζ_s	damping ratio of FM tape recorder/structural dynamics analyzer	[nondimensional]

Bars

$\overline{P_{chamber_o}}$	average pressure in hammer chamber during one half second interval before valve opening	[psi]
$\overline{P_h}$	average reading of high pressure transducer during one half second interval before valve opening	[psi]
$\overline{P_l}$	average reading of low pressure transducer during one half second interval before valve opening	[psi]
$\overline{\beta}$	bulk modulus of liquid/gas mixture	[psi]
$\overline{\Delta P}$	average pressure differential across dump valve during one half second interval before valve opening	[psi]

Primes

P'_h	high pressure transducer reading corrected for offset but not thermal effect	[psig]
--------	--	--------

P'_l	low pressure transducer reading corrected for offset but not thermal effect	[<i>psig</i>]
P''_h	high pressure transducer reading corrected for neither offset nor thermal effect	[<i>psig</i>]
P''_l	low pressure transducer reading corrected for neither offset nor thermal effect	[<i>psig</i>]

Chapter 1

Introduction

Water hammers are hydraulic shock waves that travel through piping systems. They are typically of short duration but are capable of generating destructive forces on pipes and supports. Water hammers can occur in steam heating systems, fossil fuel power plants and nuclear power plants. According to Van Duyne and Yow[9], water hammers are one of the main causes of equipment damage in nuclear power plants. This work describes how adding a small amount of noncondensable gas to steam can reduce steam bubble collapse induced water hammer amplitudes and thus reduce damage to piping systems.

There are several mechanisms that cause water hammers in steam or feed water systems. These include:

1. Rapid valve actuation
2. Trapped slug-flow bubble collapse
3. Trapped steam bubble collapse in a closed end pipe.

Figure 1-1 on page 19 shows the number of reported water hammer events in the U.S. nuclear power industry between 1969 and 1987 as reported by Van Duyne and Yow[9]. Of the 120 reported events over half were related to steam bubble collapse. In order to reduce equipment damage, methods are needed to eliminate or mitigate the effects of these water hammers. Bjorge[1] in 1982 determined the conditions

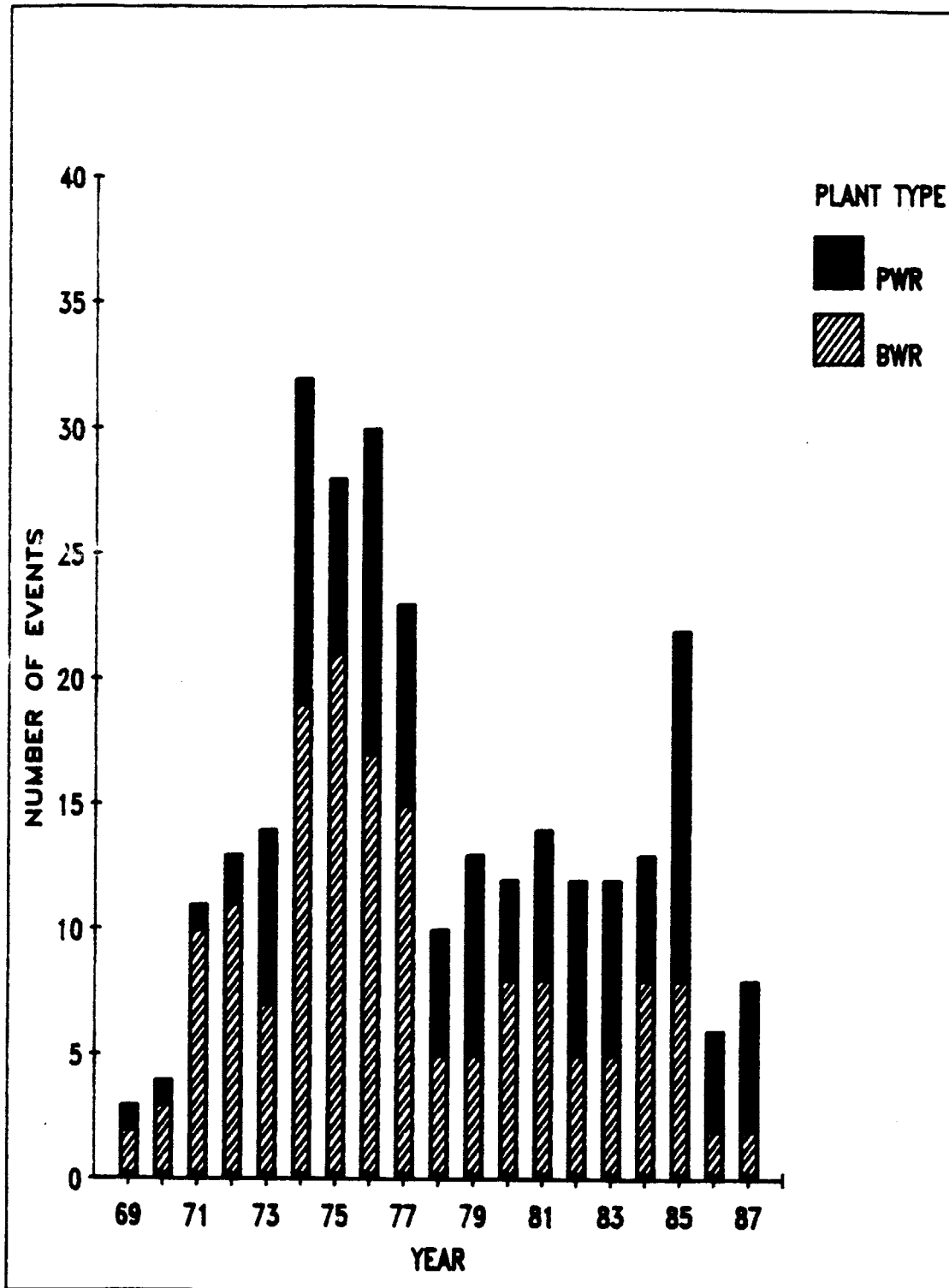


Figure 1-1: Water Hammer Events in U.S. Nuclear Power Industry[9]

that initiate water hammers in steam/water counterflow in horizontal pipes. In 1988 Lobo[5] produced guidelines for piping designers to avoid piping configurations that are prone to water hammers.

For existing plants with water hammer problems there are three categories of corrective action that can be taken. They are given below, generally in order of increasing cost. One can:

1. Change plant operating procedures
2. Perform preventive maintenance on pipes and valves
3. Modify piping configurations

While the first alternative need not be expensive, the other two can be. The work presented here was motivated by the wish to increase the list of options that plant operators have available to eliminate or mitigate problems associated with steam bubble collapse induced water hammers.

1.1 Background

During his work on water hammer inception in horizontal pipes Bjorge noted that trace amounts of noncondensable gas could significantly alter the onset of steam/water counterflow water hammers[1]. The strong effect of small amounts of noncondensable gas in impeding condensation events has also be observed. It seemed reasonable then to expect that adding small amounts of noncondensable gas to steam systems might reduce the intensity of steam bubble collapse induced water hammers. The intent of this work was to verify that noncondensable gas could reduce water hammers and to determine how much gas would be required to attain any desired reduction.

In order to understand how noncondensable gas might be able to affect water hammers, a simple water hammer model will be presented in the next section and then a model of bubble collapse will be discussed in Section 1.3.

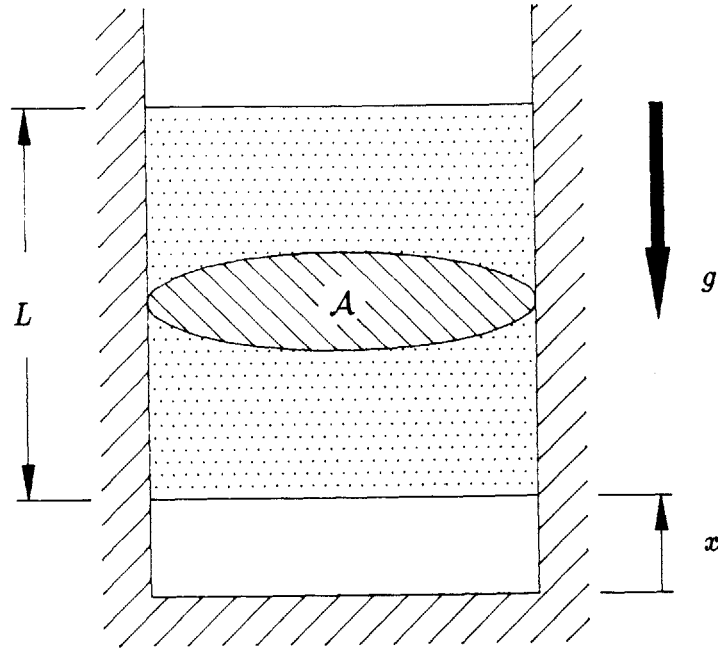


Figure 1-2: Water Hammer Model

1.2 One-dimensional Water Hammer Model

Suppose a bubble of pure steam condenses under a slug of water in a gravity field as shown in Figure 1-2. The velocity of the water slug at the time the steam bubble disappears is given by

$$v_i = -\frac{1}{A} \frac{dV}{dt} \Big|_{v=0} \quad (1.1)$$

If one neglects pipe friction, assumes the shock wave behaves adiabatically and that gravity effects are small, then the water hammer that occurs in the water slug can be modeled by the wave equation

$$\frac{\partial^2 P}{\partial t^2} - c^2 \frac{\partial^2 P}{\partial x^2} = 0 \quad (1.2)$$

where

$$c = \sqrt{\frac{\beta g_o}{\rho}} \quad (1.3)$$

With the following initial conditions

$$v(x, t = 0) = -v_i \quad (1.4)$$

and

$$P(x, t = 0) = 0 \quad (1.5)$$

and the following boundary conditions

$$v(x = 0, t) = 0 \quad (1.6)$$

and

$$P(x = L, t) = 0 \quad (1.7)$$

the solution to Equation 1.2 for the point at $x = 0$ is shown in Figure 1-3 on page 23.

Figure 1-3 shows the pressure oscillates between a pressure of $+P_j$ and $-P_j$ with a period of $\frac{4L}{c}$. P_j is the pressure determined from the Joukowski equation

$$P_j = \frac{\rho v_i \sqrt{\frac{\beta g_o}{\rho}}}{g_o} \quad (1.8)$$

1.3 Bubble Collapse Model

In 1971 Moalem and Sideman[6] solved the problem of a condensing vapor bubble containing noncondensable gas rising through a subcooled, unbounded liquid. The model included heat transfer at the liquid vapor interface and nonhomogeneous concentrations of noncondensable gas within the bubble. The time history of the bubble radius is shown in Figure 1-4[6] on page 24. The bubble radius has been nondimensionalized by dividing by the initial radius and time is nondimensionalized by multiplying by $JaPe^{\frac{1}{2}}$. The results shown are for a pentane bubble condensing in subcooled pentane.

The results show two important points

1. The bubble collapses more slowly when noncondensable gas is present. If the

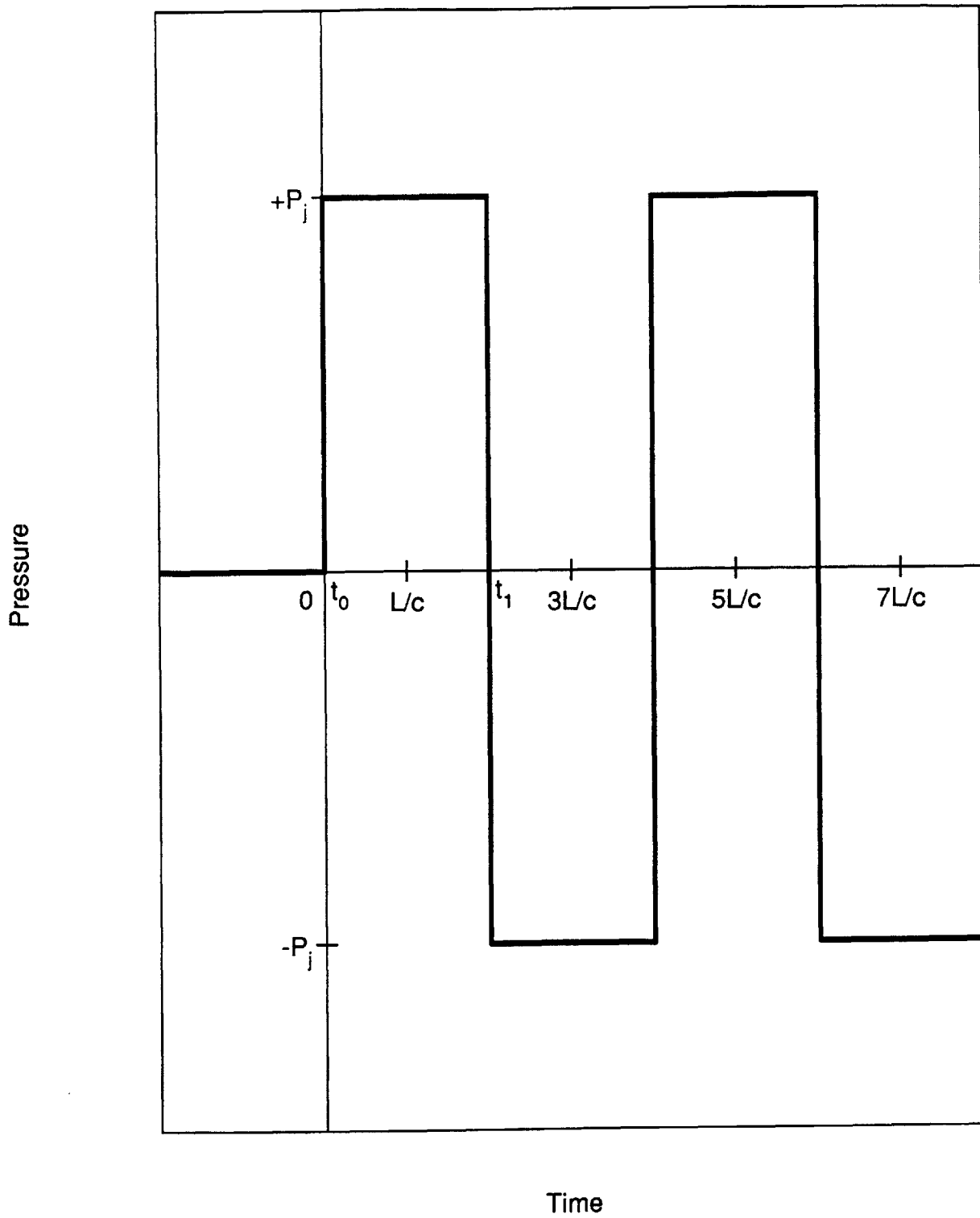


Figure 1-3: Water Hammer Pressure at Bottom of Liquid

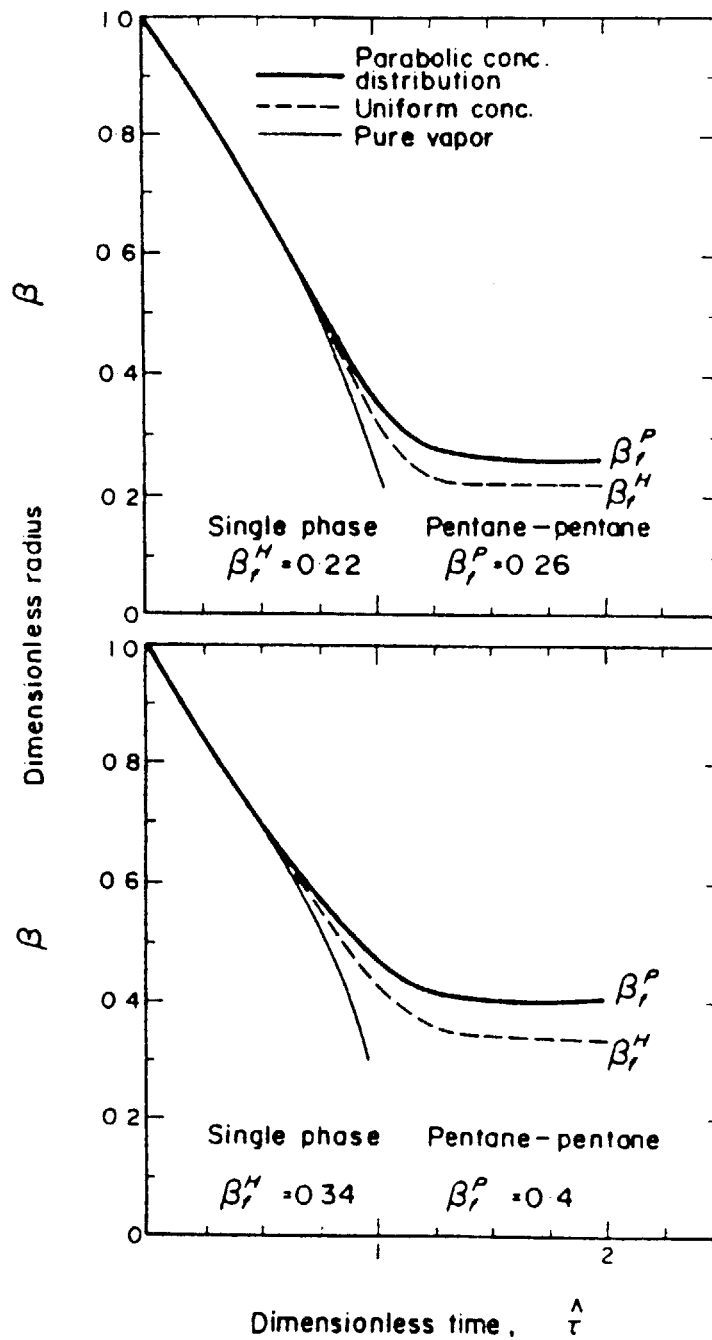


Figure 1-4: Dimensionless Bubble Radius Versus Dimensionless Time For a Pentane Bubble Condensing in Subcooled Pentane[6]

bubble collapses slower, then the velocity of the liquid surrounding the bubble will be lower. Lower liquid velocities mean proportionally lower water hammer amplitudes as shown by Equation 1.8 on page 22. The slower bubble collapse is due to the diffusion resistance provided by the noncondensable gas. The noncondensable gas slows the condensation process by impeding the flow of steam vapor toward the subcooled liquid at the bubble wall. The reduction in bubble collapse rate will be termed the diffusion effect.

2. The bubble radius approaches a steady state non-zero asymptotic radius. Since the bubble does not disappear, the subcooled liquid will have bubbles of noncondensable gas remaining in it. The average bulk modulus of a mixture of liquid and gas is given below.

$$\bar{\beta} = \frac{V_{o_g} + V_{o_l}}{V_{o_g} \frac{\beta_l}{\beta_g}} \beta_l \quad (1.9)$$

Since β_l is about 300,000 psi for water and β_g is about 20 psi for air at atmospheric pressure one can see how a small volume air can significantly decrease $\bar{\beta}$. In fact a liquid to gas volume ratio of approximately 5,000 to 1 reduces β by a factor of 4 and from Equation 1.8, reduces the water hammer amplitude by a factor of two. The effect of adding noncondensable gas is to decrease the bulk modulus and increase the compressibility. This effect will be called the fluid compressibility effect.

By looking back at Equation 1.8 on page 22 one can see how the two effects affect the water hammer amplitude. The diffusion effect reduces v_i which reduces the water hammer amplitude proportionally. The compressibility effect reduces β by dispersing compressible bubbles of gas in the liquid. The two effects are expected to be additive.

The experimental part of this work has been done to determine the magnitude of both the diffusion effect and the fluid compressibility effect. The experimental work is presented in Chapter 3.

Chapter 2

Experimental Apparatus

2.0.1 General Arrangement

The experimental apparatus was built to produce steam bubble collapse induced water hammers with air/steam mixtures of varying composition. The apparatus is shown in Figure 2-1 on page 27. The apparatus consisted of three parts; the boiler, the superheater tank and the hammer column.

The boiler contained an internal heating coil so M.I.T. physical plant steam could be used to generate steam in the boiler. The steam generated in the boiler was passed to the superheater tank through the crossover pipe. Once in the superheater tank, the inlet and outlet valves were shut. A fin type heating coil in the superheater tank allowed the steam to be superheated and a centrifugal fan within the tank force circulated the steam to insure a uniform steam temperature. The small gas bottle to the left of the superheater tank was connected to the tank through two isolation valves. Charges of noncondensable gas were measured in the gas bottle and introduced to the superheater tank through the isolation valves.

The superheated mixture of steam and noncondensable gas was passed to the hammer column through the steam/gas line. It entered the hammer chamber below the closed dump valve. Subcooled water was placed in the pipe above the valve. When the dump valve was opened the subcooled liquid poured into the steam/gas mixture and a steam bubble collapse induced water hammer ensued. Two piezoelectric pres-

SCALE

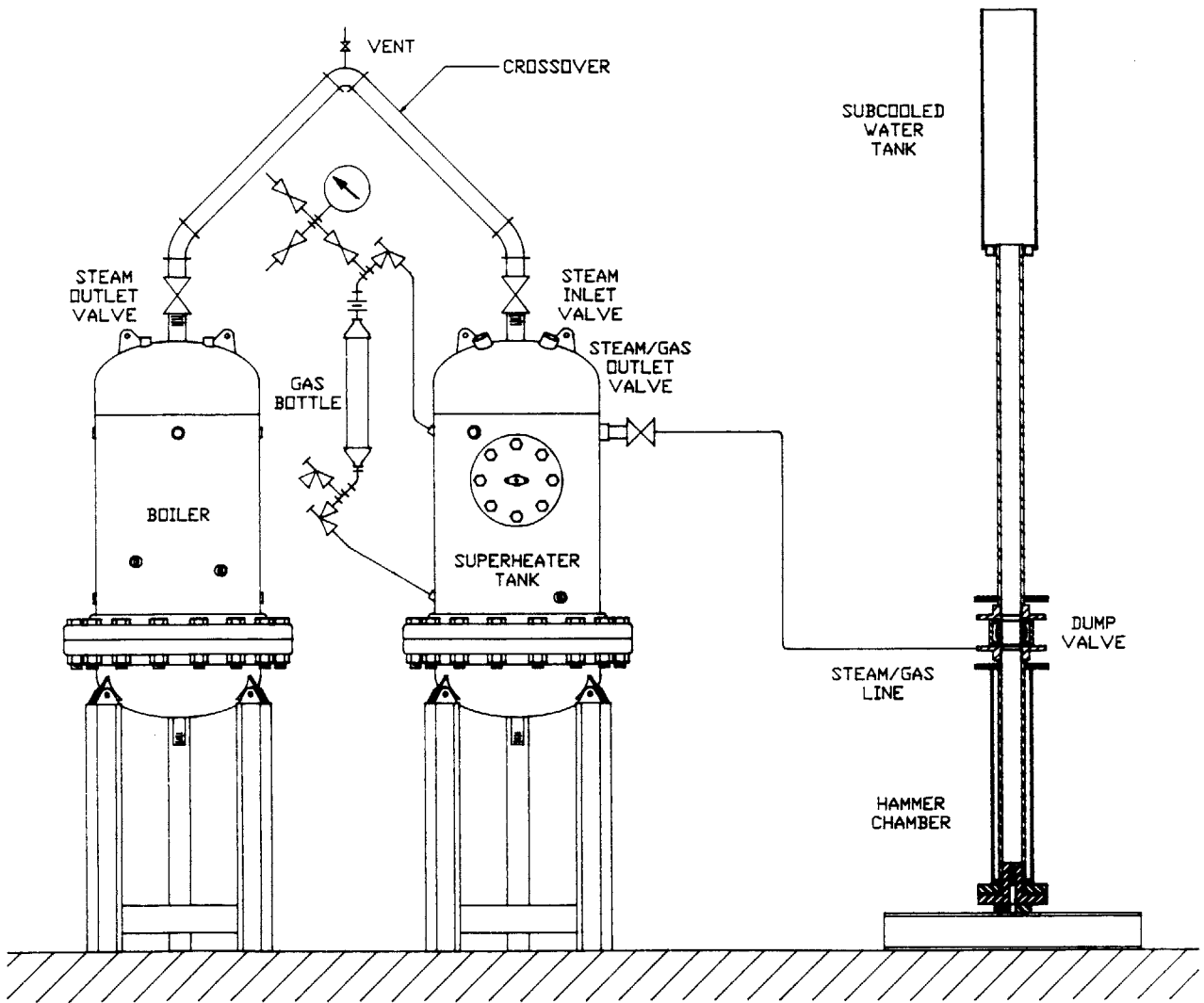
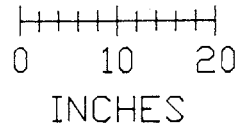


Figure 2-1: Experimental Apparatus General Arrangement

sure transducers in the bottom of the hammer chamber measured the water hammer pressure.

2.0.2 Boiler

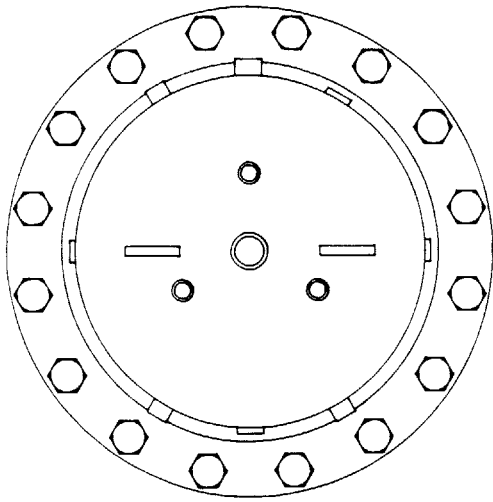
The boiler was built to generate steam having very low concentrations of noncondensable gas. The boiler water was heated using physical plant steam in an internal heating coil. Physical plant steam was not used directly in the steam/gas mixture because it had varying amounts of noncondensable gas in it.

The boiler was designed to allow complete removal of air by filling it with water. The top of the tank was machined to eliminate unnecessary vapor traps and those that remained were fitted with a means to bleed off the trapped air. The boiler is shown in Figure 2-2 on page 29. The boiler was constructed of 18 inch schedule 40 welded steel pipe, two 18 inch elliptical heads and two 150-Pound 18 inch diameter slip on flanges. The boiler had an internal volume of approximately 5 cubic feet. The pressure gauges were fitted with capillary bleeds to remove all air trapped in the gauge sensing lines and in the gauge Bourdon tube itself. The pressure gauge specifications are given in Appendix I.3 on page 120. The pressure relief valves were fitted with manual lifting devices to allow purging of air trapped under the relief valve.

The internal heating coil was made of $15\frac{1}{2}$ feet of $\frac{1}{2}$ inch pipe. 60 psi physical plant steam was supplied through a steam pressure regulator to the heating coil allowing "firing" rates of zero to 180 pounds of steam per hour at 15 psi. The boiler was covered with a one inch thick layer of thermal insulation having a insulation value of $0.07 \frac{btu}{hr-ft-F}$.

2.0.3 Superheater Tank

The superheater tank is shown in Figure 2-3 on page 30. The superheater tank construction was similar to the construction of the boiler. It too had been designed to eliminate vapor traps when filled with water and had been provided a means to bleed off any trapped air. However, it had three features that made it different. First,



SCALE

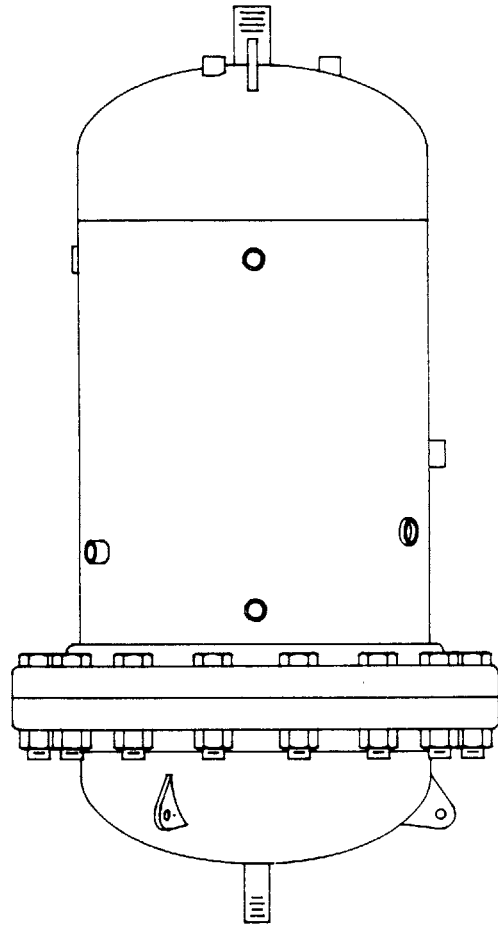
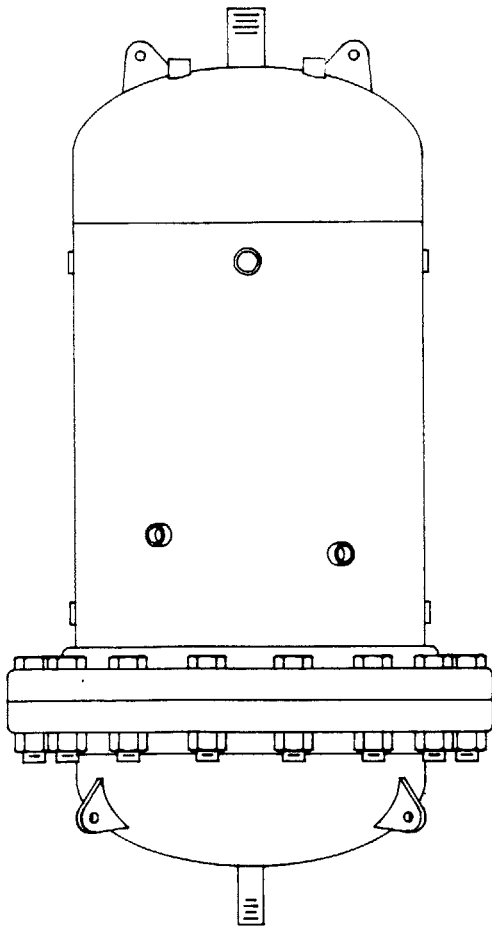
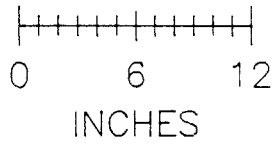
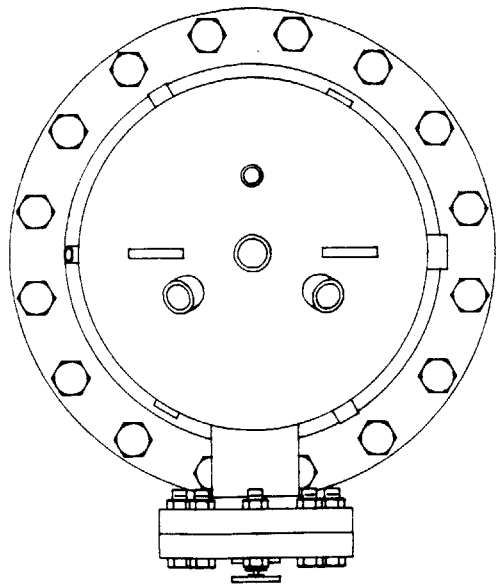


Figure 2-2: Boiler



SCALE

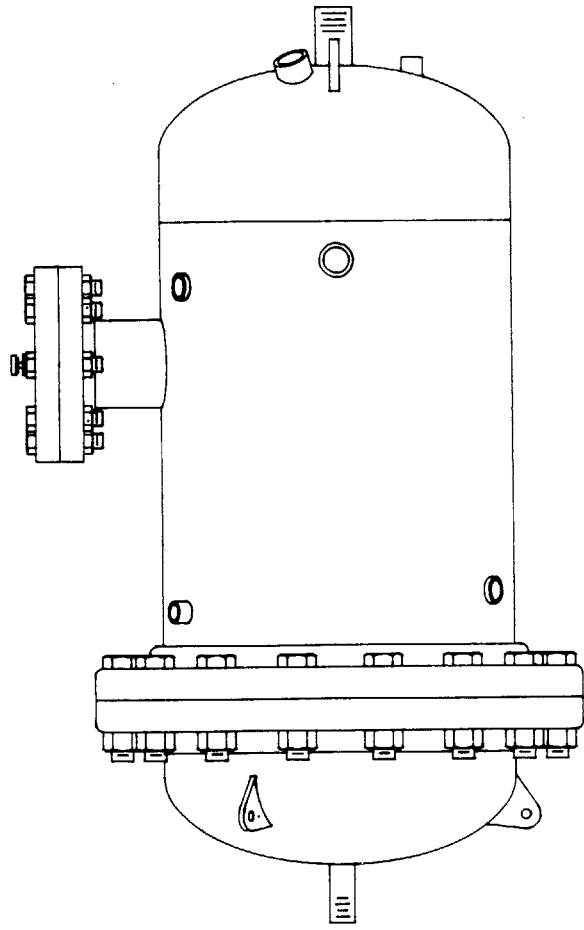
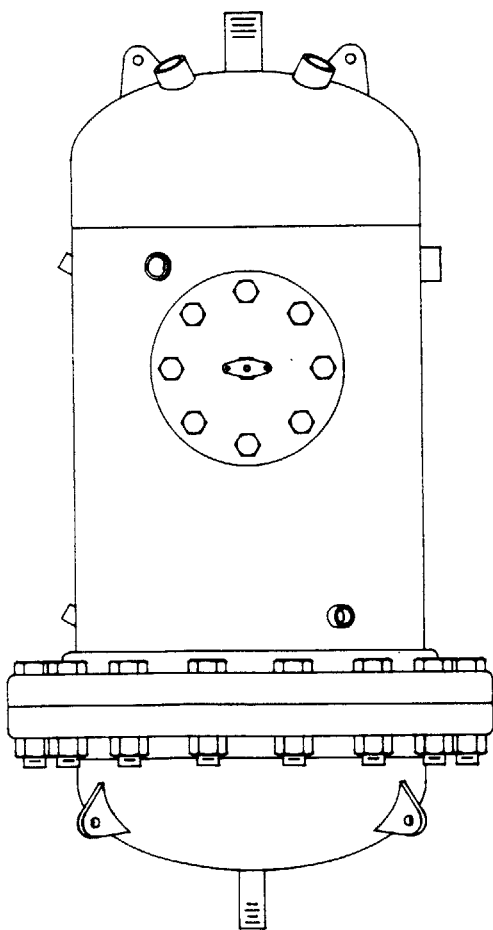
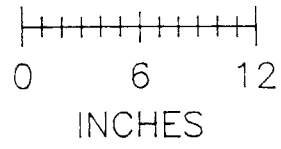


Figure 2-3: Superheater Tank

its internal heat exchanger was a finned tube type. A finned tube heat exchanger was used to enhance heat transfer to the steam/gas mixture. Second, the pressure gauges were fitted with seal diaphragms to prevent steam from entering the pressure gauge Bourdon tubes and condensing, thereby altering the air/steam ratio of the mixture in the superheater tank. The pressure gauge and diaphragm specifications are given in Appendix I.4 on page 120. Third, it had an internal centrifugal forced circulation fan. The fan was driven by an external ac motor through a magnetic coupling. The magnetic coupling eliminated the need for a packing gland and the problems associated with its leakage. The fan was sized to recirculate one tank volume approximately every 8 seconds.

The circulation fan was fitted with an inlet pipe that ran to the bottom of the tank and a manifold that discharged the flow to the top of the tank to provide forced circulation. Connections off the discharge manifold went to the pressure gauge seal diaphragms, underside of the relief valve, to the steam/gas outlet valve and to the upper gas bottle isolation valve. This arrangement is shown schematically in Figure 2-4 on page 32. The discharge piping arrangement insured forced circulation through the gas bottle and through the "dead spaces" at the top of the tank.

The superheater tank had a volume of 5.0027 cubic feet including the volume of the connecting piping between the superheater tank and gas bottle isolation valves. The superheater tank was covered with a one inch thick layer of fiberglass insulation over a one inch thick layer of clay type insulation. The bottom drain was fitted with a type K thermocouple and wrapped with a 400 watt electrical rope heater. The rope heater kept the drain temperature at least 30 degrees above the saturation temperature to insure that no condensate would collect at the bottom of the tank. Electrical rope heaters also wrapped the gas bottle, isolation valves and connecting piping.

The gas bottle had a volume of 0.0169 cubic feet including the piping between the isolation valves and the block valve. The bottle was fitted with a type K thermocouple to measure the outside wall temperature. The bottle and all piping and valves between the superheater tank and block valve were wrapped with an electric rope heater to

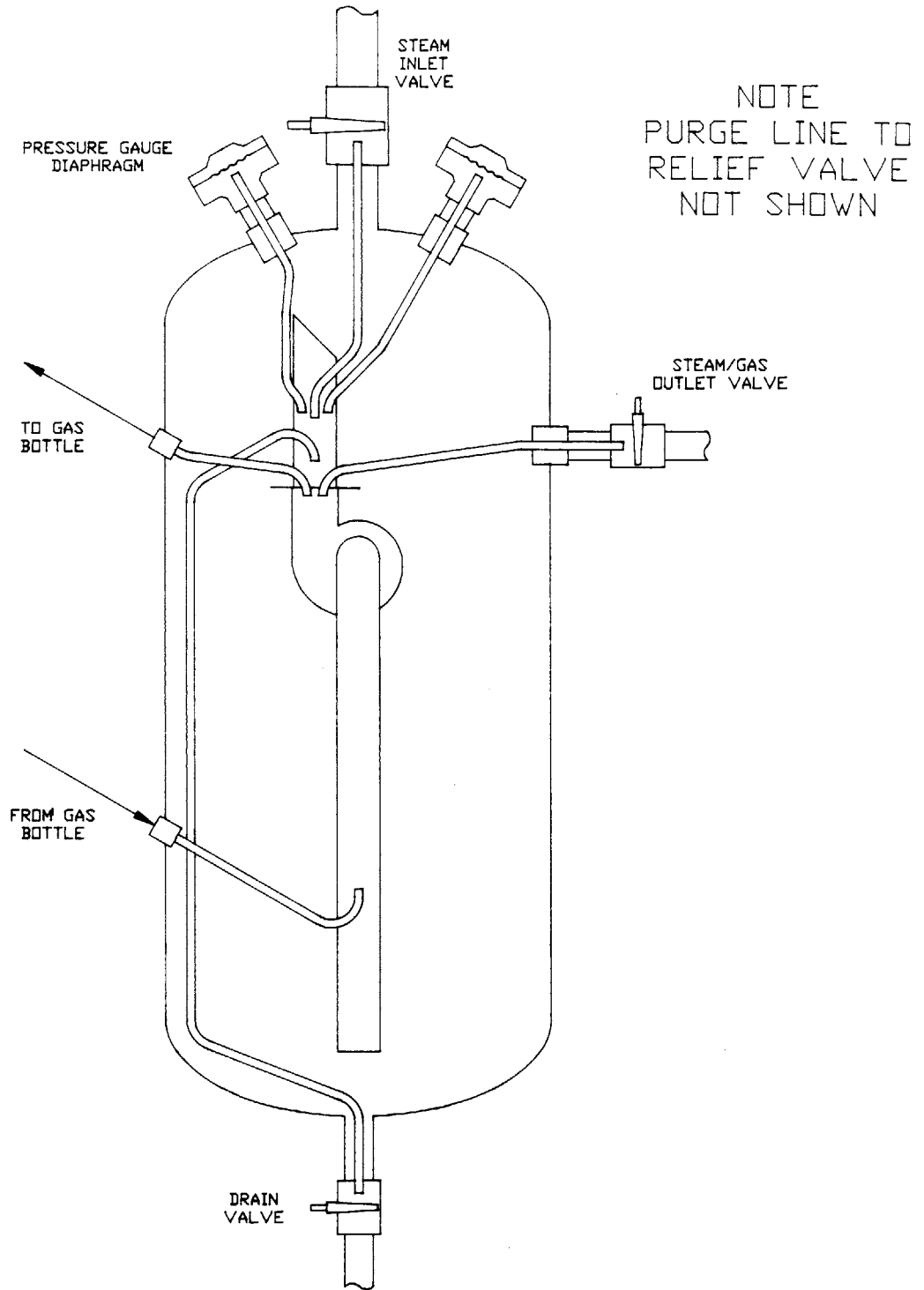


Figure 2-4: Circulation Fan Distribution Schematic

prevent condensation.

2.0.4 Hammer Column

The hammer column is shown in Figure 2-5 on page 34. The dump valve was a two-inch ball valve with a stainless steel ball and teflon seats. Below the dump valve was the hammer chamber which was made of $2\frac{1}{2}$ inch double extra heavy pipe. Surrounding the $2\frac{1}{2}$ inch pipe was a piece of 4 inch standard pipe. The space between them was used as a steam jacket to control the wall temperature of the hammer chamber. The jacket space was supplied with physical plant steam and controlled with a steam pressure regulator and a steam trap. Four drain valves $\frac{1}{8}$ inch in diameter were located in the walls at the bottom of the chamber for draining water and purging the chamber of air.

Two piezoelectric pressure transducers were flush mounted in the bottom of the hammer chamber to measure the water hammer pressure. The transducer specifications are given in Appendix I.1 on page 119. The transducers were nominally identical. Each was connected to a different charge amplifier. One charge amplifier had a very high gain so that the pressure in the chamber prior to the water hammer could be studied and the other had a low gain so that the amplitude of the water hammer could be measured without saturating the charge amplifier.

Above the dump valve was the subcooled water tank. The tank held the subcooled water used to generate the water hammer. The top of the tank was open to the atmosphere and the bottom of the tank was fitted with a drain. When the drain was opened the subcooled water would drain out until a column of $43\frac{5}{8}$ inches remained above the dump valve. The drain allowed repeatable control of the liquid column height. When drained to the $43\frac{5}{8}$ inch height, the liquid column was completely within the $2\frac{1}{2}$ inch double extra heavy pipe between the subcooled water tank and the ball valve. Therefore, when the water hammer was initiated by opening the ball valve, the liquid fell in a column of constant cross-section into the hammer chamber. The tank was fitted with a type K thermocouple to measure the water temperature. A circulating pump recirculated the water from the dump valve back to the tank to

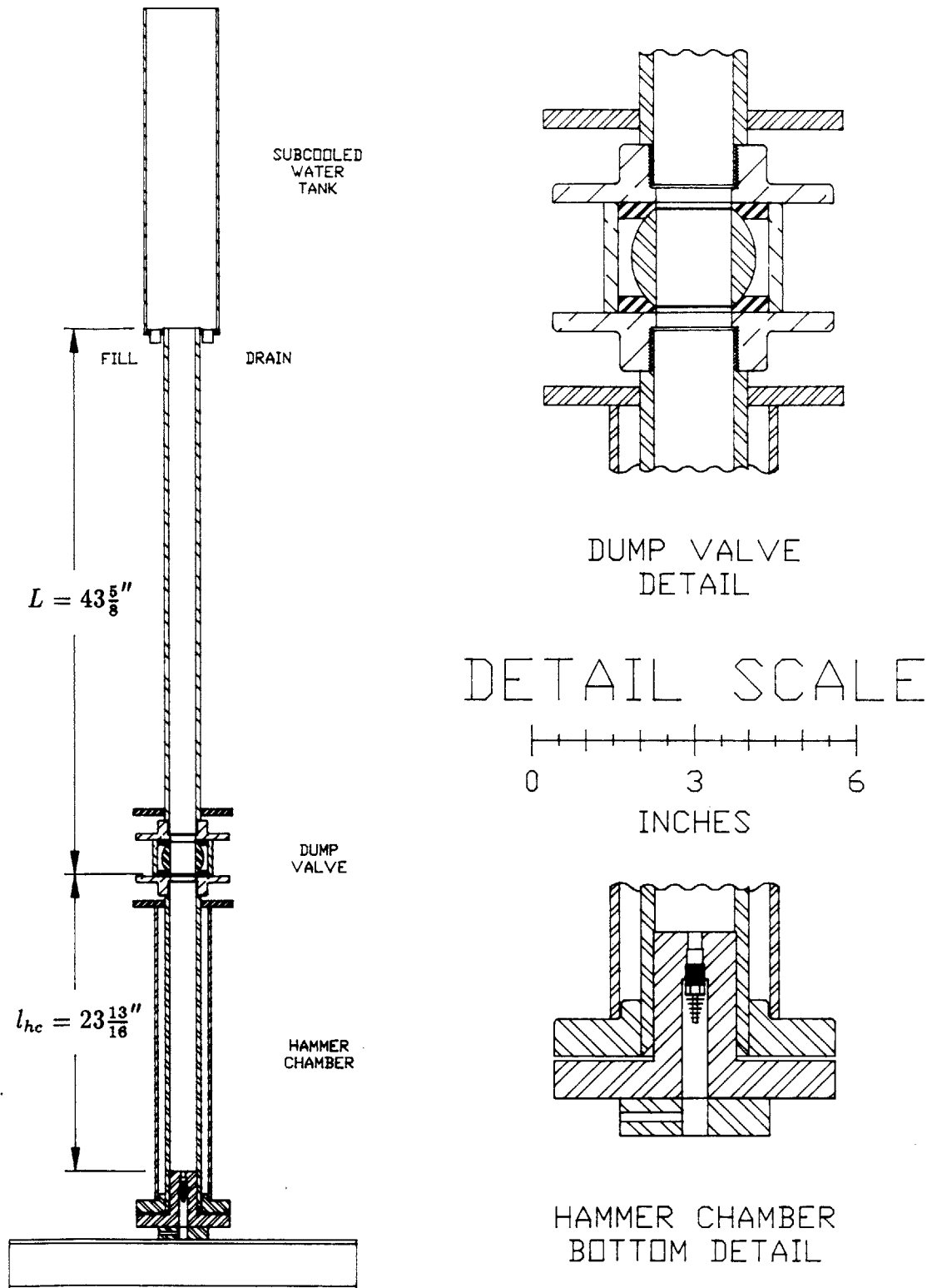


Figure 2-5: Hammer Column

keep the subcooled water in the tank and column at a uniform temperature.

The ball valve had been modified to allow the recirculation of the water trapped in the ball of the closed valve. Also, four steam/gas inlet ports were machined in the valve body beneath the ball to admit the steam/gas mixture to the hammer chamber. The steam/gas inlet line from the superheater tank was wrapped with an electrical rope heater and a type K thermocouple was used to measure the outside wall temperature to insure condensation of the steam/gas mixture did not occur in the steam/gas line.

2.0.5 Instrumentation

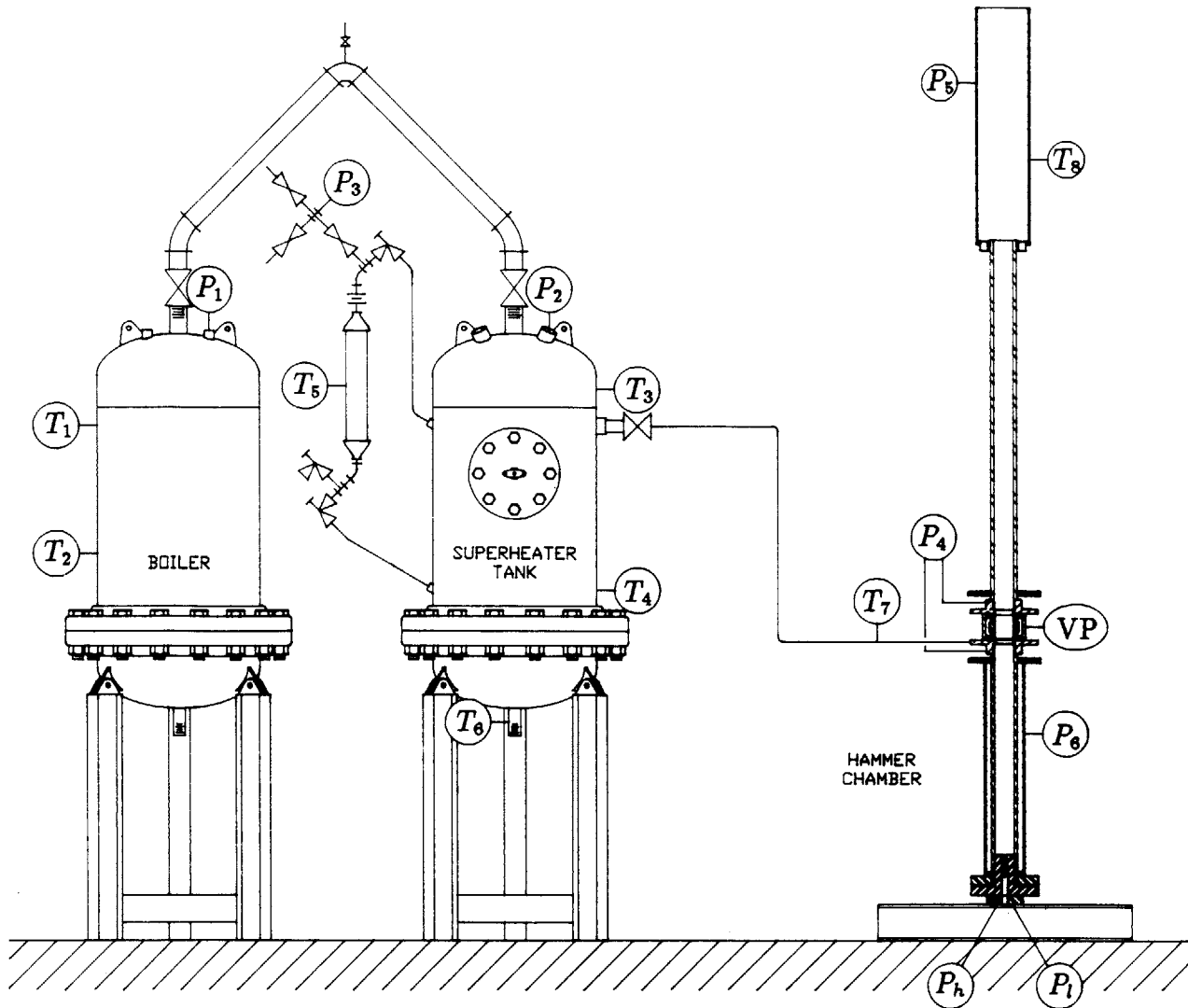
The instruments are shown in Figure 2-6 on page 36. The instrumentation consisted of those instruments necessary for operating the apparatus as well as those required for collecting the data needed for analysis. Specifications for all instruments are given in Appendix I on page 119.

Pressure Gauges

Except for the 0 - 400 psi boiler pressure gauge and the 0 - 400 psi superheater tank pressure gauge, all pressure gauges were calibrated using a dead weight tester. Except for the dump valve differential pressure transducer the gauges were not adjusted. Instead, a calibration curve was developed during calibration and the corrections applied to the reading during data analysis.

The two piezoelectric transducers were paired with a charge amplifier. The transducers were calibrated in both the high pressure and low pressure ranges of their charge amplifiers. Calibrating both transducers in both pressure ranges allowed them to be used to cross-check the high pressure and low pressure measurements. The charge amplifier used for the high pressure measurements had a 10 kHz low pass filter to filter out the transient response of the transducer. The charge amplifier used for the low pressure measurements did not need a filter as the data of interest had a very low frequency content.

The dump valve differential pressure transducer was a variable reluctance type.



- | | |
|--|---|
| P_1 boiler pressure | T_1 boiler steam temperature |
| P_2 superheater tank pressure | T_2 boiler water temperature |
| P_3 gas bottle pressure | T_3 superheater tank gas temperature (top) |
| P_4 dump valve differential pressure | T_4 superheater tank gas temperature (bottom) |
| P_5 ambient pressure | T_5 gas bottle wall temperature |
| P_6 steam jacket pressure | T_6 superheater tank bottom drain temperature |
| P_h high pressure transducer | T_7 steam/gas outlet line temperature |
| P_l low pressure transducer | T_8 subcooled water tank temperature |
| VP Dump Valve Position | |

Figure 2-6: Instrumentation

The transducer was fitted with a 5 psi pressure diaphragm allowing reading to ± 5 psi with an accuracy of ± 0.05 psi. The transducer output was fed to the demodulator and the demodulator produced a ± 10 volt dc signal.

The boiler pressure gauges were fitted with capillary bleeds to remove trapped air in the gauge Bourdon tubes. The capillary bleeds allowed removal of all air in the boiler during startup, even the air trapped inside the Bourdon tubes.

The superheater tank pressure gauges were fitted with diaphragm seals to prevent the steam/gas mixture from entering the pressure gauge Bourdon tubes. Since condensation in the Bourdon tubes would increase the gas fraction in the superheater tank, it was necessary to keep the mixture out of the pressure gauges. With the diaphragm seals the superheater tank pressure was transmitted across a thin stainless steel diaphragm to a reservoir of silicone oil. The oil operated the pressure gauge through a capillary tube so the gauge could be mounted in an area cooler than the diaphragm seals. A bleed screw was fitted in the housing just beneath the diaphragms to remove any trapped air during startup. The housing was designed to allow any condensation that occurred during warm-up to fall back into the tank and be re-vaporized. The diaphragm seals are shown schematically in Figure 2-4 on page 32 and are shown in detail in Figure I-1 on page 123.

Thermocouples

All Thermocouples were the type K. The thermocouples were calibrated using an ice bath and boiling water bath. Since the largest error was only one degree Fahrenheit the thermocouple readings were not corrected for instrument errors. All thermocouple voltages were converted to temperature in degrees Fahrenheit and displayed by a multipoint digital thermometer.

Valve Position Indicator

The dump valve position indicator was a 10 k Ω potentiometer attached to the valve shaft. The potentiometer was supplied by a 10 volt dc power supply. The valve position indicator was calibrated by placing a protractor at the valve shaft and recording

valve angle versus potentiometer output voltage.

Tape Recorder and Structural Dynamics Analyzer

The data from the dump valve differential pressure transducer, the two hammer chamber pressure transducers and the valve position indicator were recorded during a data run on a FM tape recorder. The data was analyzed from the tape recorder using a structural dynamics analyzer. The step response analysis of the transducers, tape recorder and structural dynamics analyzer are given in Appendix H on page 113.

Chapter 3

Noncondensable Gas Tests

The noncondensable gas tests were the central tests of the investigation. The tests were conducted to determine if noncondensable gas could reduce water hammer amplitudes and to determine how much noncondensable gas would be required. The experiments involved placing an air/steam mixture with a known noncondensable gas fraction in the hammer chamber. The water hammer was initiated by opening the dump valve and allowing the subcooled water to condense the steam in the mixture. The details of preparing the air/steam mixture are given in Appendix A.1 on page 71. The water hammer pressure was measured by the piezoelectric transducers located at the bottom of the hammer chamber. Details of the data reduction procedure are given in Appendix B.1 on page 78.

3.1 Experimental Results

3.1.1 Water Hammer Peak Pressure

The water hammer peak pressure versus noncondensable gas fraction data are shown in Figure 3-1 on page 41. The data on the left, noncondensable gas fraction of 0, are peak pressures for 100 percent steam. On the right, noncondensable gas fraction of 100 percent, are the peak pressures for 100 percent air. The noncondensable gas fraction is the ratio of the mass of noncondensable gas to the mass of the steam/gas

mixture as defined by Equation 3.1.

$$Q = \frac{M_{air}}{M_{steam} + M_{air}} \quad (3.1)$$

The experimental data show that adding noncondensable gas to steam can indeed reduce the amplitude of steam bubble collapse induced water hammer. The data show that the amplitude decreases rapidly with increasing gas fraction out to about 12 percent. By a gas fraction of 50 percent the amplitude is down to 5 psi, two orders of magnitude below the zero gas fraction amplitude. The data show that a noncondensable gas fraction of 12 percent produces the maximum amplitude reduction for the minimum amount of noncondensable gas. The optimum amount of gas occurs at the “knee” in the amplitude versus gas fraction data. In Figure 3-2 on page 42 the region from 0 to 15 percent gas fraction has been expanded to show the “knee” region of the data. To reduce water hammer amplitudes in this experimental apparatus, adding gas to establish a gas fraction of 10 to 12 percent appears optimal. The actual pressure versus time data for the points labeled “a” through “g” are presented and discussed in Appendix C.

3.1.2 Water Hammer Momentum

The water hammer momentum is the momentum of the liquid slug that was accelerated by the collapsing steam bubble. For incompressible, irrotational flow the water hammer momentum is proportional to the rate of change of bubble volume and therefore, proportional to the bubble collapse rate $\frac{dr}{dt}$. The noncondensable gas diffusion effect slows the rate of bubble collapse as shown in Section 1.3 on page 22. It does so by providing a mass diffusion resistance that reduces the rate at which steam vapor reaches the subcooled water at the bubble liquid/vapor interface. Impeding the flow of steam vapor to the bubble wall reduces the rate of condensation and therefore reduces the rate of steam bubble collapse. The water hammer momentum is directly related to the rate of steam bubble collapse and therefore indicates the noncondensable gas diffusion effect. The diffusion effect can be observed by plotting water hammer

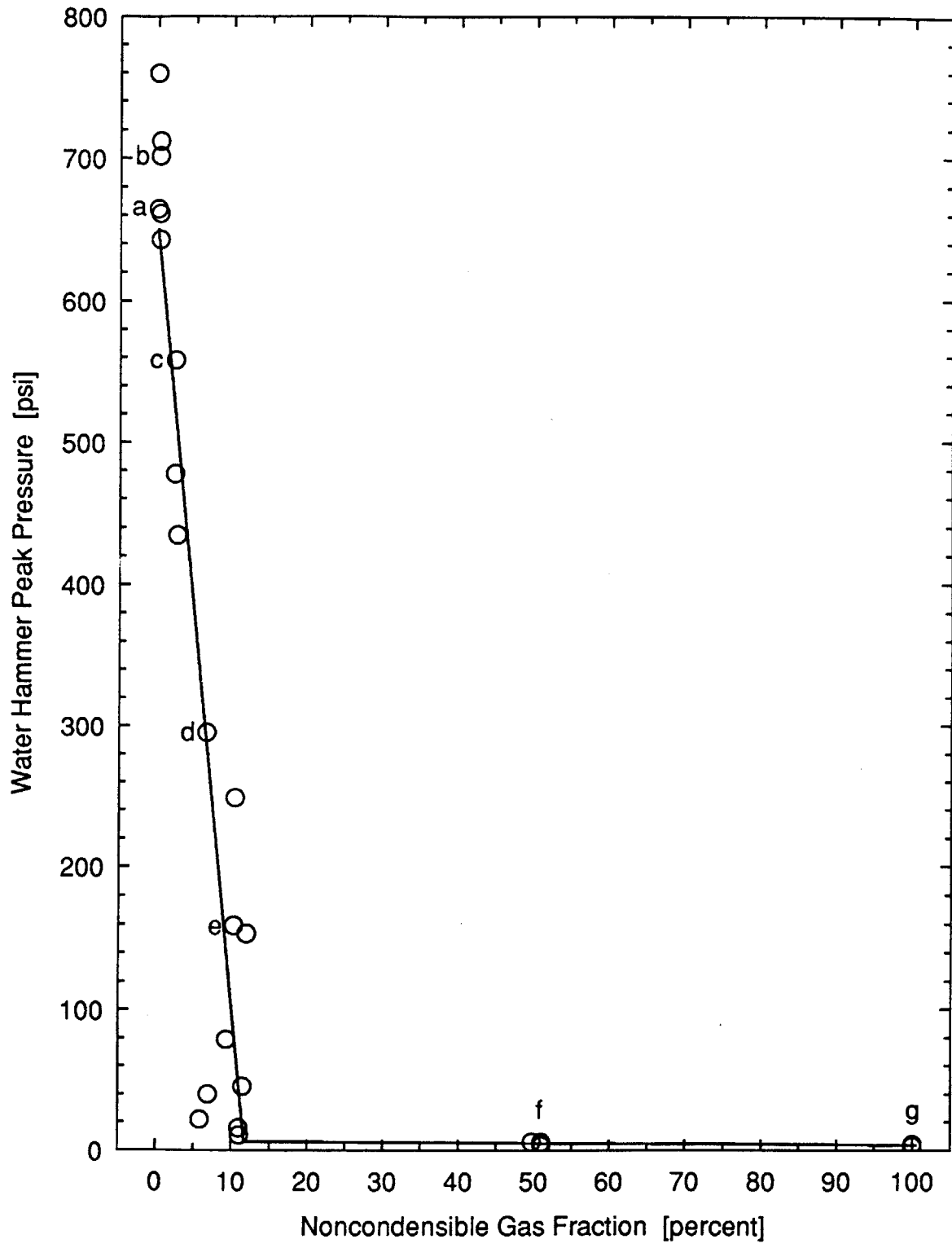


Figure 3-1: Water Hammer Peak Pressure Versus Gas Fraction

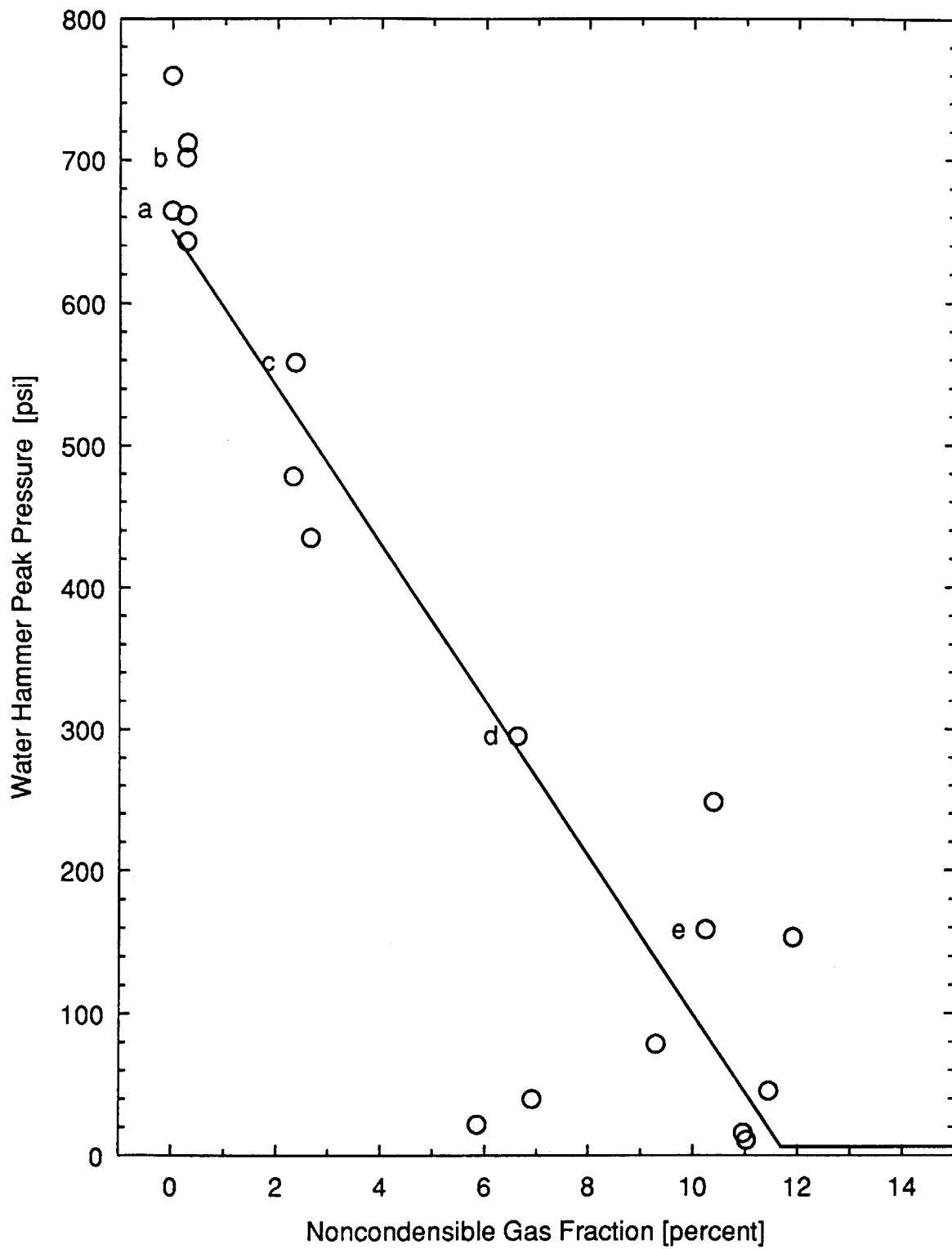


Figure 3-2: Water Hammer Peak Pressure Versus Gas Fraction (Expanded)

momentum versus noncondensable gas fraction.

The water hammer pressure versus time data are a series of pressure spikes of decreasing amplitude as described in Appendix C. The water hammer momentum can be determined by integrating the pressure-time trace of the first pressure spike.

$$\Delta \mathcal{M} = \mathcal{A} g_o \int_{t_0}^{t_1} P_h dt \quad (3.2)$$

where t_0 and t_1 are the beginning and end time of the first pressure spike as shown in Figure 1-3 on page 23.

If the losses are small when the decompression wave reflects as a compression wave from the bottom the hammer chamber then the momentum of the water hammer in the stationary reference frame of the pipe is given by

$$\mathcal{M} = \frac{1}{2} \mathcal{A} g_o \int_{t_0}^{t_1} P_h dt \quad (3.3)$$

The momentum versus gas fraction data are shown in Figure 3-3 on page 44. There is considerable scatter in the momentum data. The data between 0 and 15 percent gas fraction are expanded in Figure 3-4 on page 45 and a least squares straight line fit of the displayed data is shown. The line shows that, at least to first order, that there is no decreasing trend of liquid slug momentum with gas fraction up to a gas fraction of 12 percent. The constant momentum shows that the increase in vapor partial pressure due to the diffusion resistance is insignificant at noncondensable gas fractions below 12 percent. Figure 3-3 shows a decrease in momentum of about 65 percent by a gas fraction of 50 percent and a reduction of 85 percent by a 100 percent gas fraction. The low pressure hammer chamber data described in Appendix C.0.2 on page 90 confirm that the bubble collapse rate is essentially independent of noncondensable gas fraction.

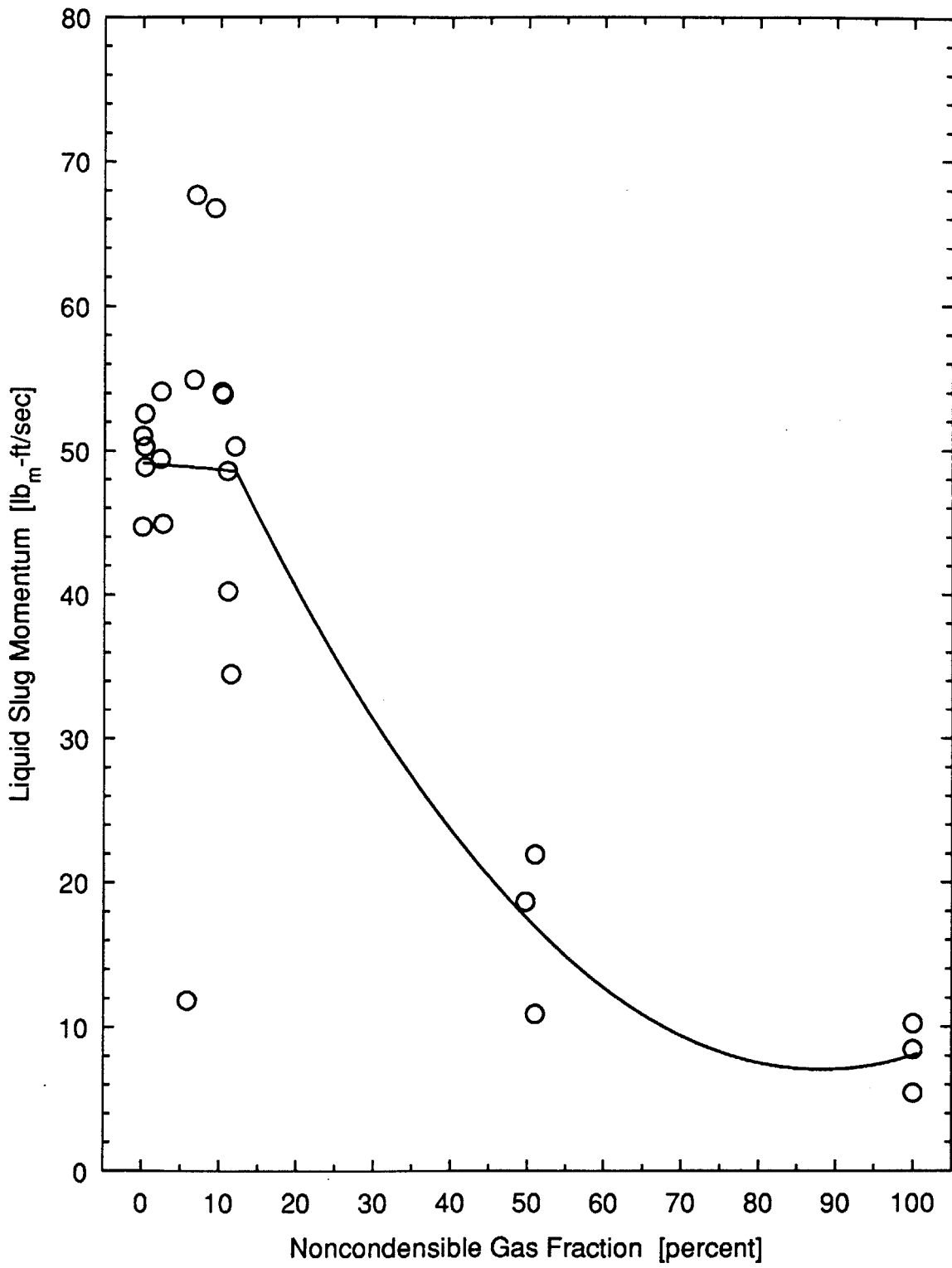


Figure 3-3: Liquid Slug Momentum Versus Gas Fraction

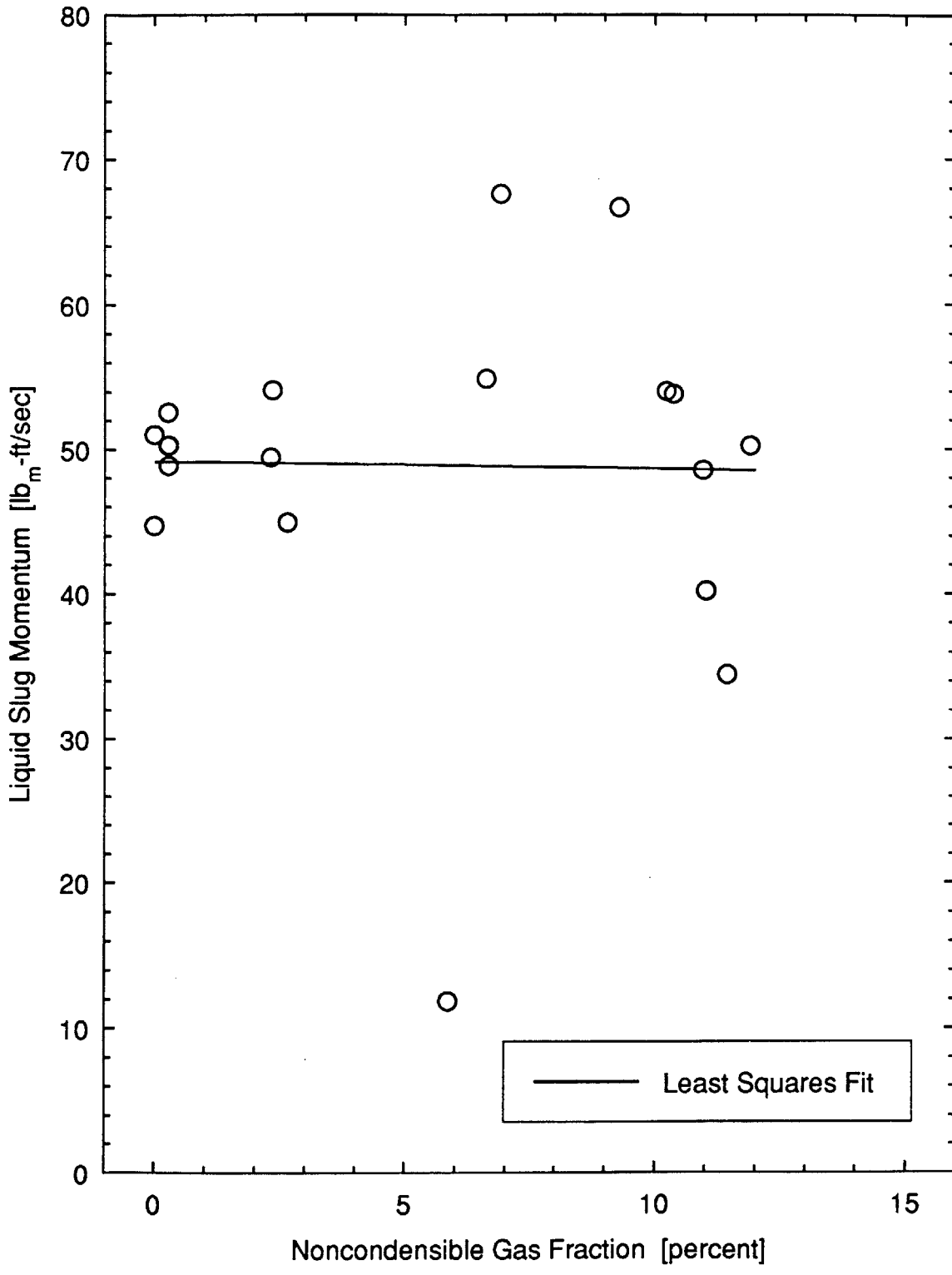


Figure 3-4: Liquid Slug Momentum Versus Gas Fraction (Expanded)

3.2 Discussion

The liquid momentum versus gas fraction data in Figure 3-3 on page 44 show that the momentum of the liquid slug is essentially constant for a gas fraction lying between 0 and 12 percent. The constant momentum indicates that any diffusion resistance being provided by the noncondensable gas has little effect on the rate of steam bubble collapse. The steam bubble is collapsing just as rapidly with 0 percent gas as with 12 percent gas. The constant rate is most likely due to breakup of the liquid/vapor interface preventing a significant boundary layer of noncondensable gas from forming. The breaking up of the interface produces a very large interfacial area allowing more steam to come in contact with the subcooled water. The low pressure data in Figure C-3 on page 91 show that the pressure in the hammer chamber during the interval between valve opening and the water hammer drops only about 1 psi. The pre-water hammer vapor space pressure reduction is remarkably similar from 0 to 12 percent gas fractions which suggests that the liquid slug momentum should be similar as well. Turbulence at the liquid/vapor interface would tend to cause a uniformly low pre-water hammer pressure with increasing gas fraction. The low chamber pressure data, however, show a uniformly high pressure. The high pressure reflects the vaporization of liquid from the heated hammer chamber walls.

Modeling the liquid in contact with the wall as a semi-infinite solid and the wall as a semi-infinite solid, the liquid at the wall attains a temperature of

$$T_{wall} = \frac{k_{steel} T_{steel_o} + k_{water} T_{water_o}}{k_{steel} + k_{water}} \quad (3.4)$$

Since $k_{steel} \simeq 25 \frac{btu}{hr-ft-F}$ and $k_{water} \simeq 0.4 \frac{btu}{hr-ft-F}$ the water at the wall attains a temperature of approximately T_{steel_o} . The liquid in contact with the wall is at the temperature of the steel pipe. If the pre-water hammer chamber pressure were to drop due to condensation of the steam then the liquid on the pipe wall would readily flash generation vapor to maintain the high hammer chamber pressure. It may be that for the gas fractions below 12 percent the wall temperature controls the pre-water hammer pressure, and therefore the momentum, rather than the diffusion resistance

provided by the noncondensable gas. In any case, the experimental data show that the water hammer momentum is essentially independent of gas fraction up to 12 percent. By a 50 percent gas fraction the noncondensable gas reduces the liquid slug momentum by 65 percent. This is a surprising result. Normally 12 percent noncondensable gas in steam would greatly reduce the condensation rate but in this case the diffusion effect of the noncondensable gas is imperceptible. It appears as if the effective resistance of the condensing film is negligible up to a gas fraction of 12 percent. Of course, as the noncondensable gas fraction continues to increase, the air will dominate the chamber pressure being noncondensable but compressible.

Chapter 4

Analytical Model

An analytical model was developed based on the observations of the experimental studies. The proposed model neglects the effects of both the diffusion resistance provided by the noncondensable gas and the compressibility of the liquid. The result of neglecting the interfacial diffusion resistance is to overestimate the water hammer pressure at high gas fractions. The effect of neglecting the liquid compressibility is to overestimate the peak water hammer pressure at low gas fractions. Both of these phenomena tend to make the model a conservative one as the neglected effects tend to reduce the water hammer pressures.

The model considers only the compressibility of the gas and assumes that gas remains below the liquid during the water hammer. The smoothness of the experimental pressure versus time data suggests this to be true as discussed in Appendix C.0.1 on page 89. The model assumes that the liquid can be modeled as a rigid body and that the gas compresses in a polytropic process. Applying $F = MA$ to the liquid

$$\frac{d^2x}{dt^2} = \frac{PAg_o}{M_l} - \frac{P_aAg_o}{M_l} - g \quad (4.1)$$

For the noncondensable gas

$$PV^\gamma = K \quad (4.2)$$

where K is a constant and γ is the polytropic exponent. The equations are coupled

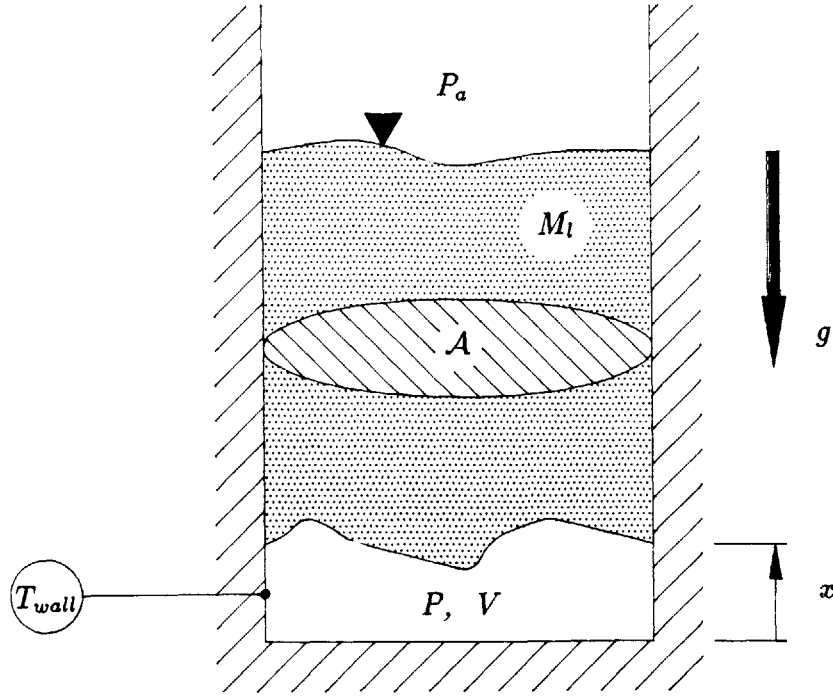


Figure 4-1: Analytical Model Schematic

with the geometric constraint that

$$V = \mathcal{A} x \quad (4.3)$$

Normally this problem would be solved in terms of x and the answer expressed in terms of P but since only P is of interest the equation will be solved directly in terms of P .

From Equation 4.2 and the geometric constraint (Equation 4.3), x may be expressed in terms of P by

$$x = \frac{K^{\frac{1}{\gamma}}}{\mathcal{A} P^{\frac{1}{\gamma}}} \quad (4.4)$$

Differentiating 4.4 twice with respect to time yields

$$\frac{d^2 x}{dt^2} = -\frac{K^{\frac{1}{\gamma}}}{\mathcal{A}} \left(\frac{1}{\gamma}\right) \left[P^{(-\frac{1}{\gamma}-1)} \frac{d^2 P}{dt^2} - \left(\frac{1}{\gamma} + 1\right) P^{(-\frac{1}{\gamma}-2)} \frac{dP}{dt} \frac{dP}{dt} \right] \quad (4.5)$$

Substituting Equation 4.5 into 4.1 yields the following second order nonlinear differ-

ential equation in terms of P and t .

$$\frac{d^2 P}{dt^2} = \left(\frac{1}{\gamma} + 1\right) \frac{1}{P} \left(\frac{dP}{dt}\right)^2 - \mathcal{A} \gamma K^{-\frac{1}{\gamma}} P^{\frac{1}{\gamma}+1} \left[\frac{P \mathcal{A} g_o}{M_l} - \frac{P_a \mathcal{A} g_o}{M_l} - g\right] \quad (4.6)$$

4.0.1 Boundary Conditions

The experimental low pressure data showed that the steam pressure remained at about P_a (the ambient pressure) for most of the time interval between dump valve opening and the water hammer. See Appendix C.0.2 on page 90. It was argued in Section 3.2 on page 46 that the pressure was controlled by the generation or condensation of vapor at the wall. For the purpose of modeling it will be assumed that the condensation process occurs at P_a until all the noncondensable gas is at P_a and after that the pressure begins to rise as the noncondensable gas begins to be compressed in a polytropic process. The boundary condition then is stated as

$$\text{at } t = 0, \quad P = P_a \text{ and } T = T_{wall} \quad (4.7)$$

From the boundary condition in 4.7 and the equation of state for an ideal gas, K can be evaluated as

$$K = P_a \left[\frac{M_g R T_{wall}}{P_a}\right]^\gamma \quad (4.8)$$

The second boundary condition is determined from the momentum of the moving water for the case of no noncondensable gas. The momentum may be experimentally determined or calculated knowing the details of the water hammer initiating event. More will be said about determining \mathcal{M} and what its implications are in Section 4.1.3 on page 60. For now though, it will be assumed to be known. It is also assumed that the momentum for the case of zero noncondensable gas is the same as for the case where it is present. The experimental data show this to be true up to a gas fraction of 12 percent. Since the compression of the gas has no energy dissipative mechanism it seems reasonable to assume the momentum would be unaffected. Pipe friction may cause the momentum in the zero gas fraction case to be different from the case where gas is present but that difference is assumed to be small. The second boundary

condition is then

$$\text{at } t = 0, \quad \frac{dx}{dt} = -\frac{\mathcal{M}}{M_l} \quad (4.9)$$

The boundary condition can be expressed in terms of P by differentiating Equation 4.4 and substituting for K using 4.8.

$$\text{at } t = 0, \quad \frac{dp}{dt} = \frac{\mathcal{M}P_a^2 \mathcal{A} \gamma}{M_l M_g R T_{wall}} \quad (4.10)$$

Then, Equations 4.6, 4.7 and 4.10 fully describe the problem in terms of P .

4.0.2 Nondimensionalization

Using the following nondimensionalizations

$$P^* = \frac{P}{P_a} \quad (4.11)$$

and

$$t^* = t \frac{\mathcal{M} \mathcal{A} P_a}{M_l M_g R T_{wall}} \quad (4.12)$$

Equation 4.6 becomes

$$\frac{d^2 P^*}{(dt^*)^2} = \frac{1}{P^*} \left(\frac{1}{\gamma} + 1 \right) \left[\frac{dP^*}{dt^*} \right]^2 - A P^{*\frac{1}{\gamma}+1} [P^* - (1 + B)] \quad (4.13)$$

where

$$A = \frac{\gamma M_l M_g R T_{wall} g_o}{\mathcal{M}^2} \quad (4.14)$$

and

$$B = \frac{M_l g}{P_a \mathcal{A} g_o} \quad (4.15)$$

The boundary conditions become

$$\text{at } t^* = 0, \quad P^* = 1 \quad (4.16)$$

and

$$\text{at } t^* = 0, \quad \frac{dP^*}{dt^*} = \gamma \quad (4.17)$$

4.0.3 Implementation

Equation 4.13 was integrated numerically using a finite difference technique. The FORTRAN code is listed in Appendix G on page 111. The results from the analytical model are compared to the experimental data in the next section.

4.1 Experimental Versus Analytical Results

The experimental results of the noncondensable gas tests are plotted with the results of the analytical model in Figure 4-2 on page 53. The experimental data had B values of between 0.1071 and 0.1064. The analytical model is plotted for a γ of 1.4 and for B of 1.071 and 1.064. Figure 4-2 shows the curves for $B = 0.1064$ and $B = 0.1071$ to be nearly identical. In fact they differ by less than 0.09 percent.

Figure 4-3 on page 54 shows the region of $A < 2$ expanded. Figure 4-3 shows the analytical model agrees well with the experimental data for values of A greater than 0.02. As A approaches zero the analytical pressure approaches infinity. The pressure from the experimental data remain finite due to the compressibility of the liquid, a factor not considered in the analytical model. In the region where A is very small the pressure is well predicted by the Joukowski limit given by Equation 1.8 on page 22. The analytical model does predict the pressure well in the “knee” of the curve where the pressure begins to level off. Presumably, it is the “knee” region that one would like to operate in when adding noncondensable gas to a system troubled with water hammers. In the “knee” region one obtains the maximum benefit with the minimum amount of noncondensable gas.

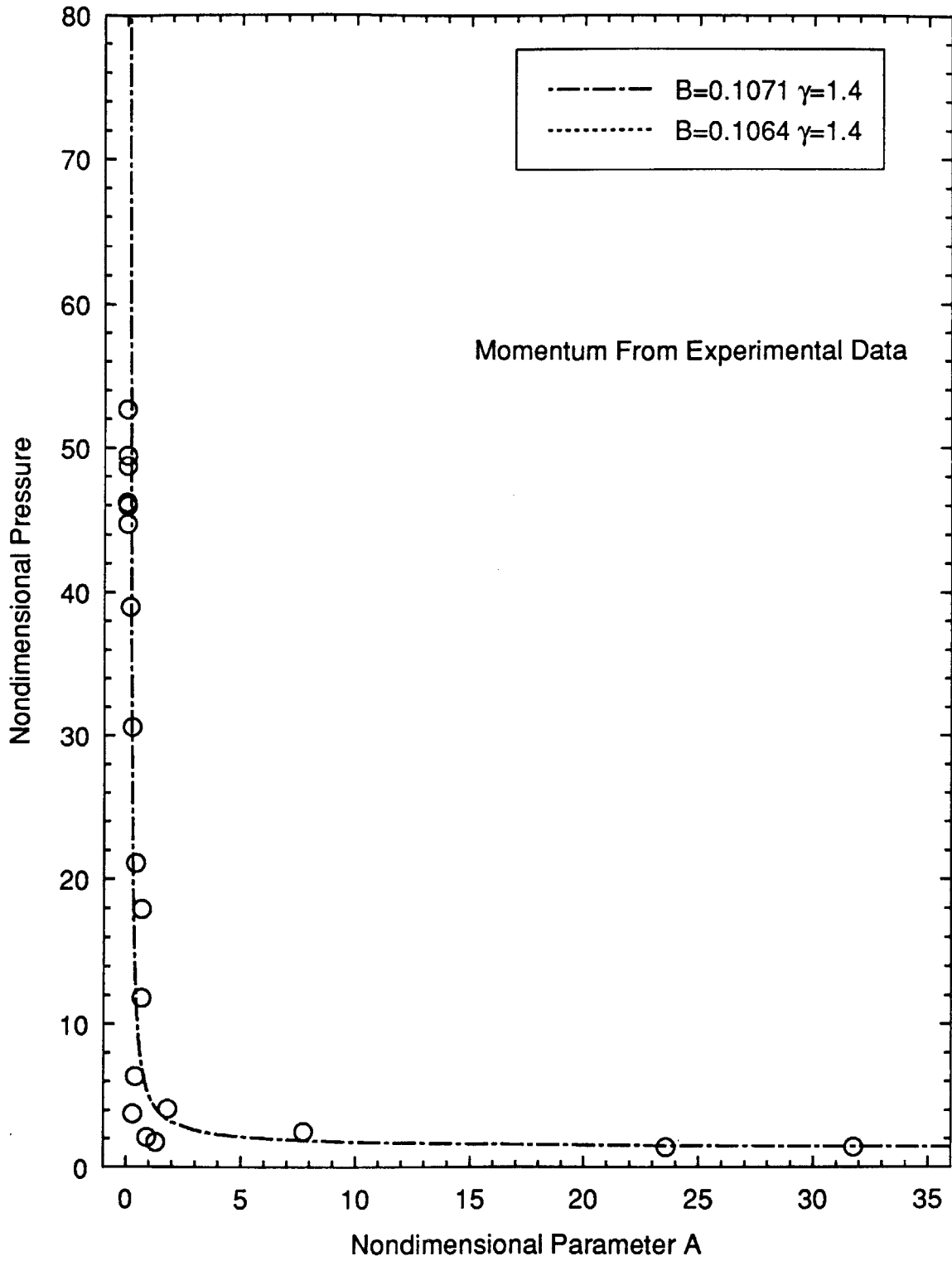


Figure 4-2: Noncondensable Gas Tests - Experimental Versus Analytical Results

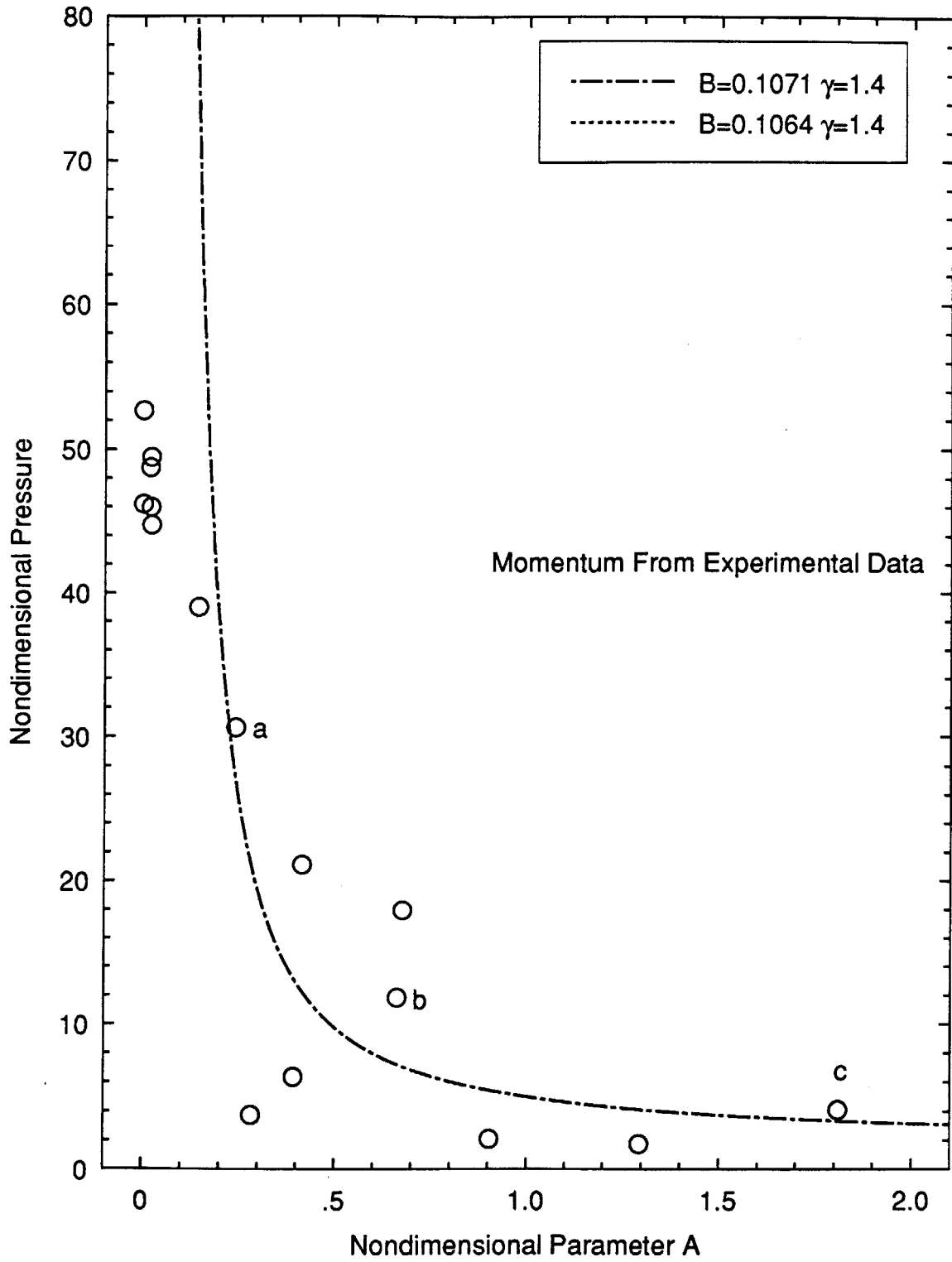


Figure 4-3: Experimental Versus Analytical Results - Expanded

4.1.1 Gamma Sensitivity

Gamma is the only model parameter that was not known or measured from the experimental data. It is, therefore, the only model parameter that can be “tweaked”. Gamma is the exponent of the polytropic compression process and is expected to lie between 1.0, the isothermal compression case, and 1.4 the adiabatic compression case. The isothermal compression case might be expected to represent the actual process if the noncondensable gas were to break up into very small bubbles providing a large liquid/vapor interface area for heat transfer to occur. It might also be expected to well represent the process if the compression were slow enough to allow time for the heat of compression to be transferred out of the gas and into the liquid. The adiabatic case might be expected to better represent the process if the noncondensable gas bubbles remain large and the compression occurs quickly. Since no visualization study was carried out it is not possible to know the bubble size. Figure 4-4 on page 56 shows the limit of 1.4 to better predict the “knee” region of the experimental data. Gamma of 1.4 produces higher peak pressures so produces a more conservative estimate of the water hammer peak pressure. In 1983 Kazama[4] investigated water hammers in closed end pipes using water-methanol mixtures. Kazama found that the methanol behaved isothermally (γ equal to 1) when compressed by the slug of water. The difference in polytropic exponent may be explained by the fact that in Kazama’s experiment the methanol condensed when compressed by the water slug but in this investigation the air did not. Figure 4-4 shows that the difference in the predicted pressure is small whether one uses a γ of 1.0 or 1.4.

4.1.2 Pressure-Time Traces

Figure 4-5, Figure 4-6 and Figure 4-7 beginning on page 57 show the predicted and experimental pressure-time traces for those data points marked “a”, “b” and “c” in Figure 4-3. The figures show that the model predicts the general shape of the pressure-time curve as well as the peak amplitude. The offset correction (Appendix B.2.1 on page 80) has been applied to the experimental data but the thermal effect (Ap-

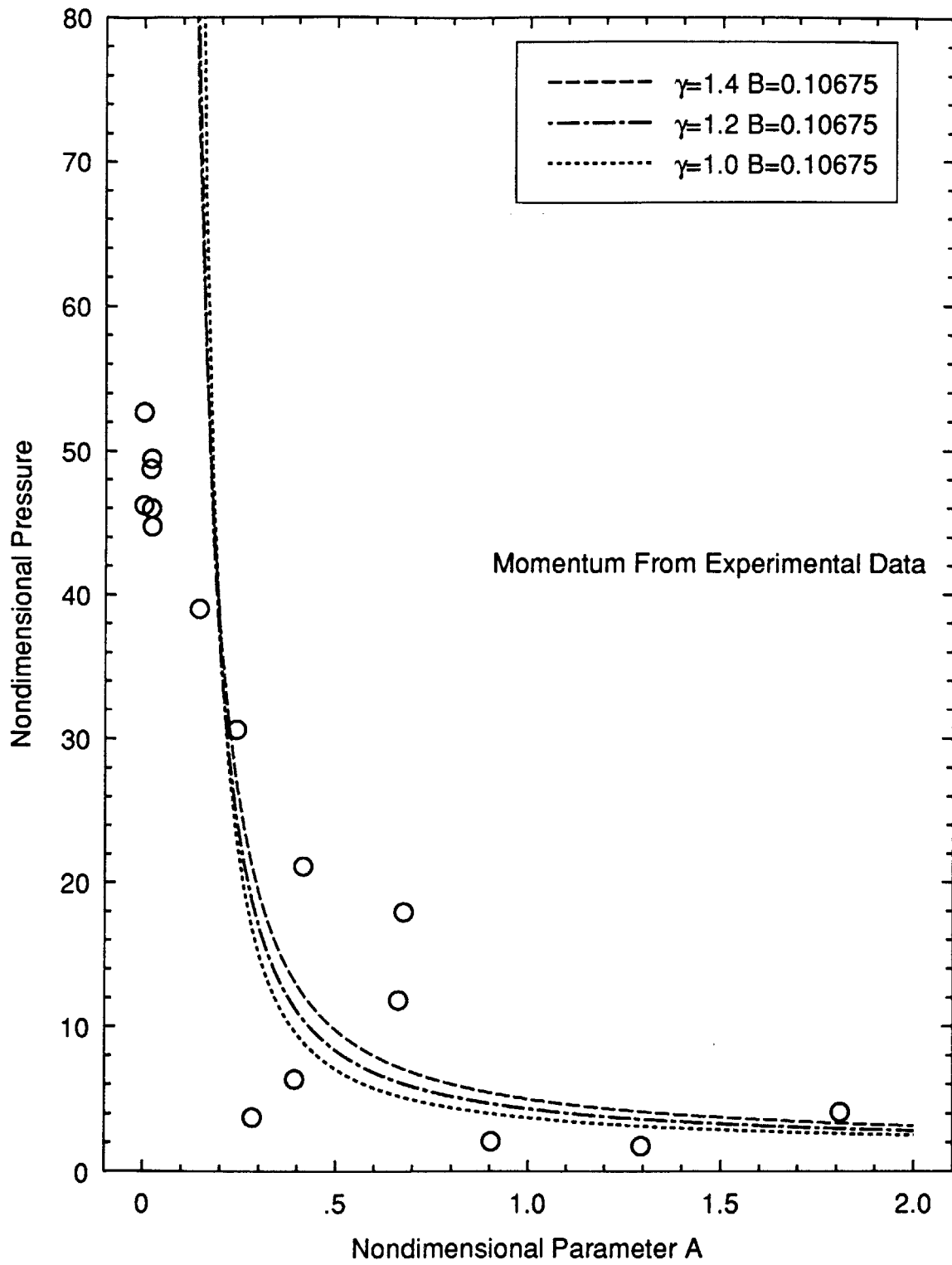


Figure 4-4: Gamma Sensitivity

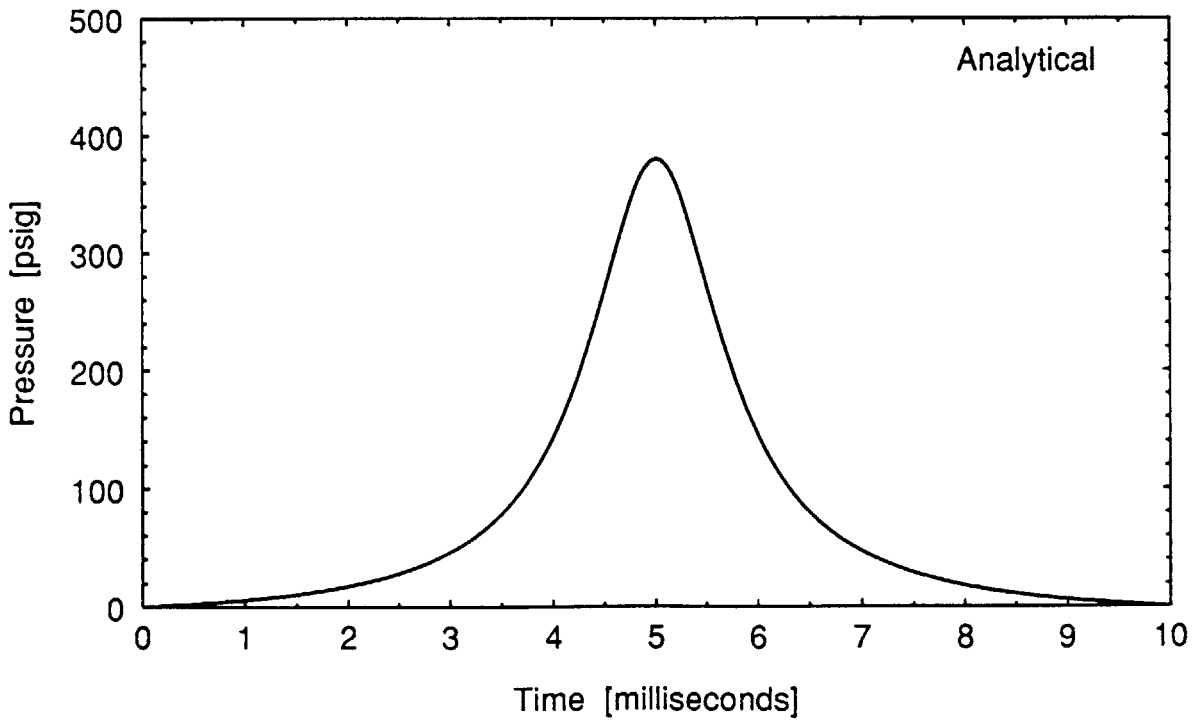
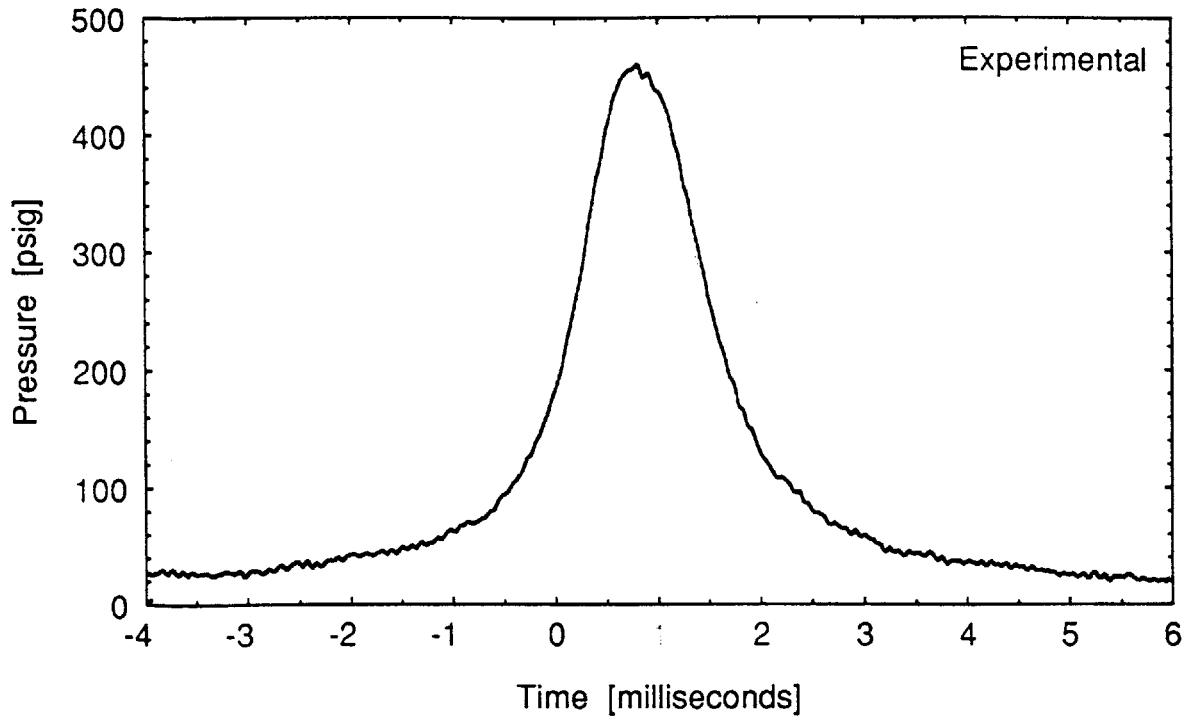


Figure 4-5: Analytical and Experimental Data for Point "a" in Figure 4-3

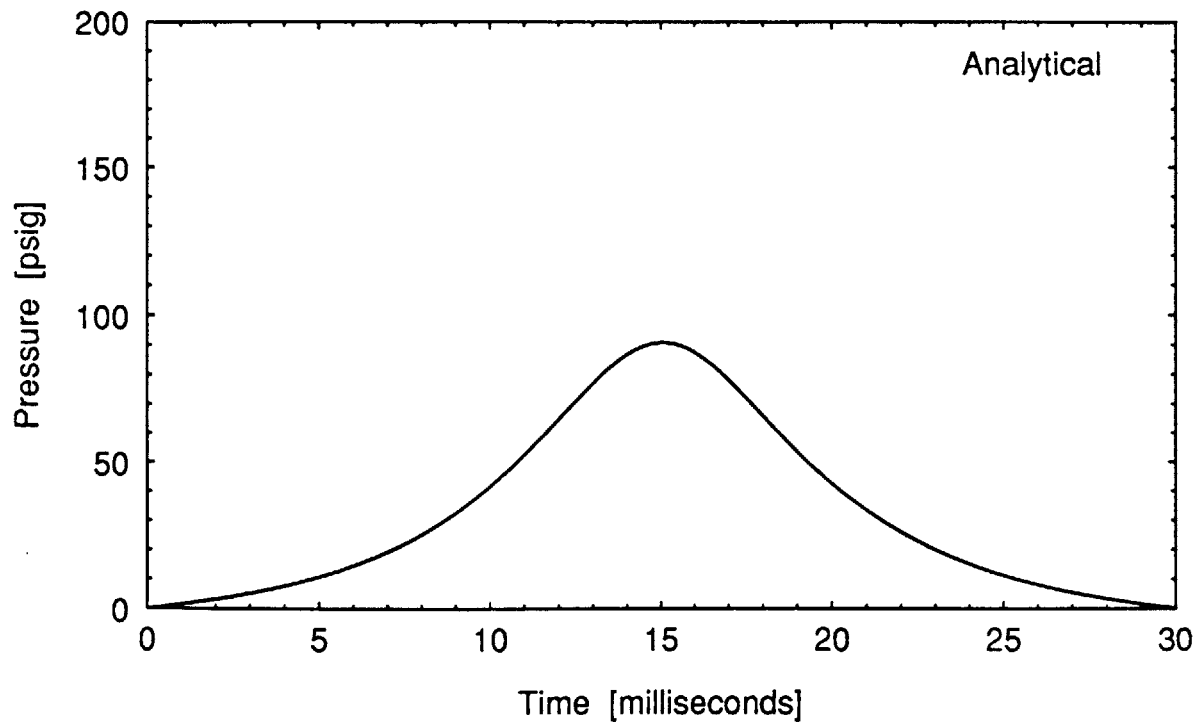
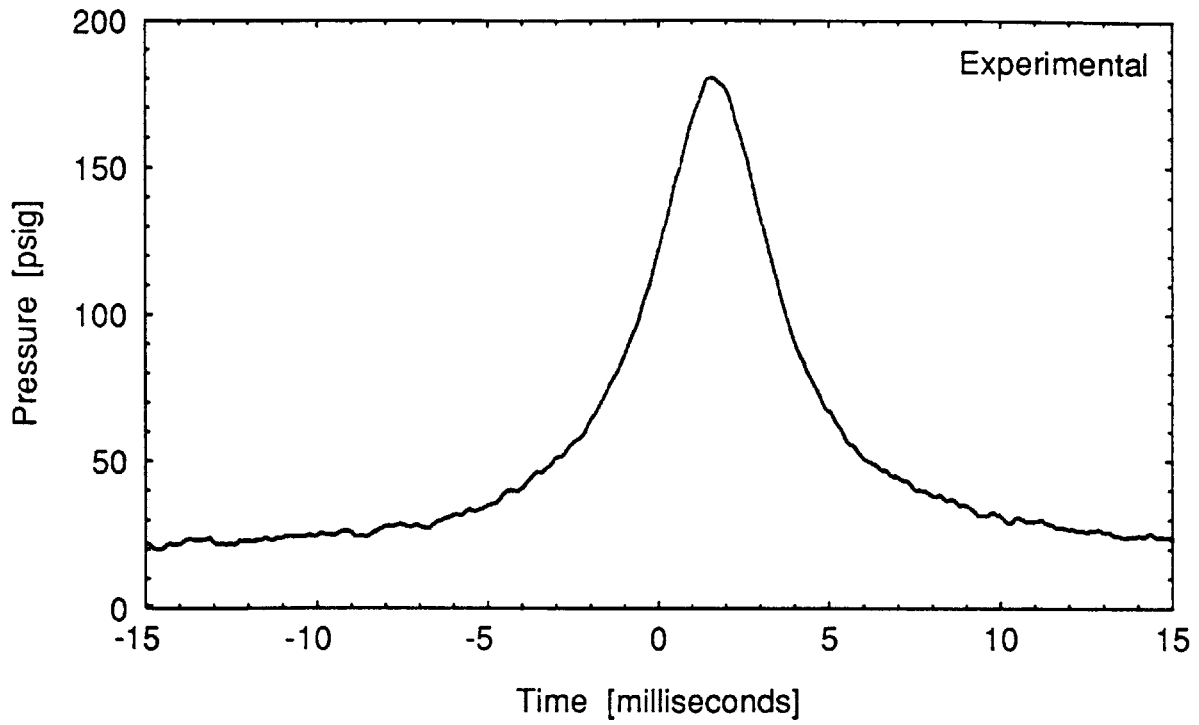


Figure 4-6: Analytical and Experimental Data for Point "b" in Figure 4-3

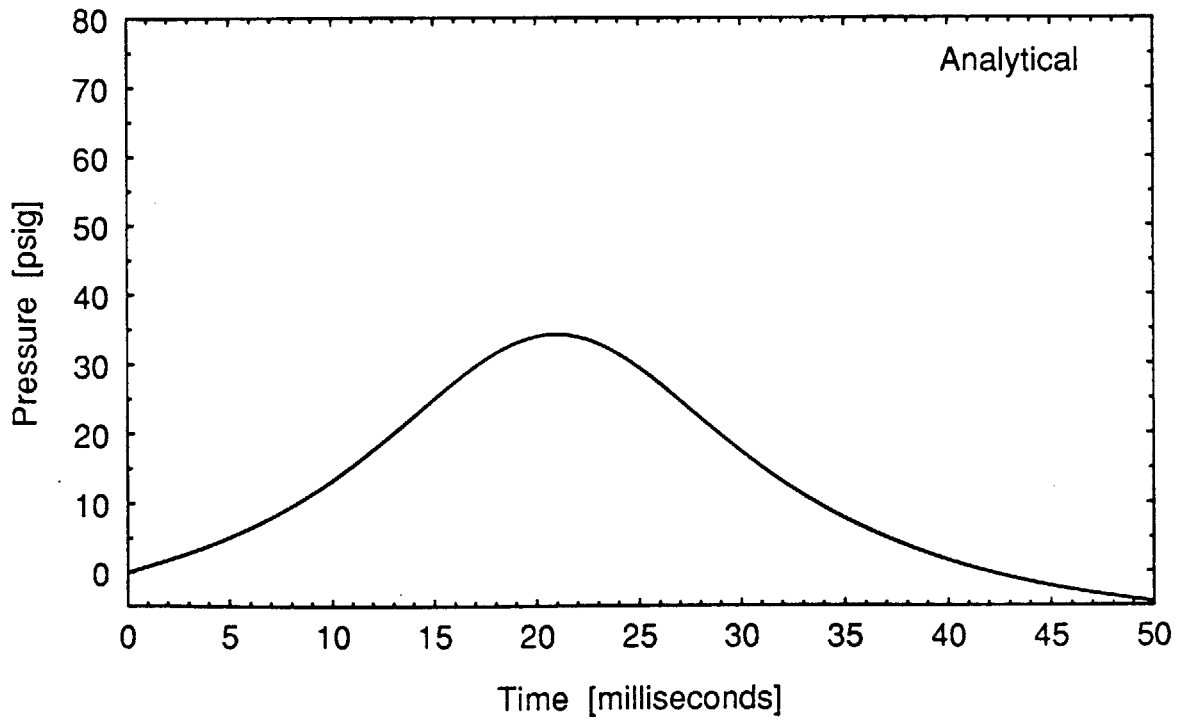
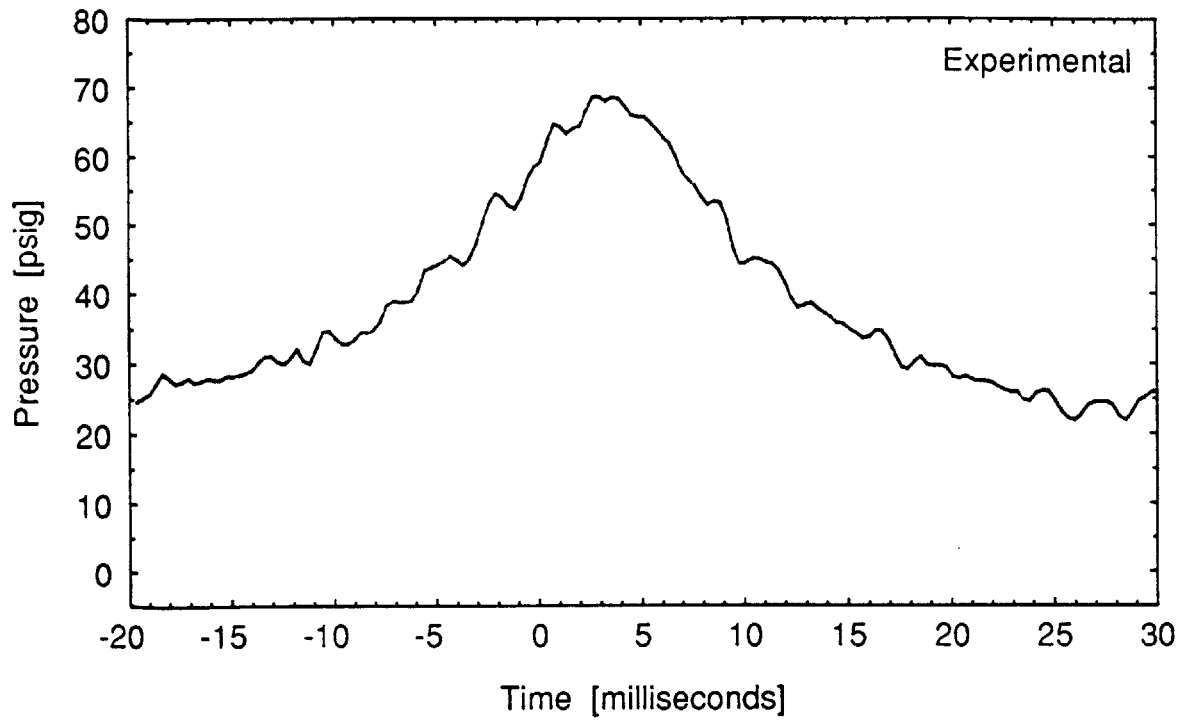


Figure 4-7: Analytical and Experimental Data for Point “c” in Figure 4-3

pendix B.2.2 on page 81) has not. It is the thermal effect that causes the apparent pressure offset between the experimental and analytical data.

4.1.3 Momentum Estimates

The analytical model requires the evaluation of the nondimensional parameter A which is given by Equation 4.14 as

$$A = \frac{\gamma M_l M_g R T_{wall} g_o}{\mathcal{M}^2} \quad (4.18)$$

which requires knowing the momentum of the water slug. The experimental data plotted in Figures 4-2 and 4-3 were plotted against A evaluated with the momentum determined experimentally. If the model is to be useful then it is necessary to know \mathcal{M} beforehand.

One method of estimating \mathcal{M} is simply to use a "freefall" model. The noncondensable gas test low pressure data (Appendix C.0.2) showed the pressure beneath the liquid slug remaining at about P_a . A simple estimate of the momentum is obtained by assuming the liquid simply freefalls from the time the dump valve opens. For freefall:

$$\frac{dx^2}{dt^2} = -g \quad (4.19)$$

and the boundary conditions are:

$$\text{at } t = 0 \quad x = l_{hc} \quad \text{and} \quad \frac{dx}{dt} = 0 \quad (4.20)$$

Integrating and applying the velocity boundary condition yields:

$$\frac{dx}{dt} = -g t \quad (4.21)$$

Integrating again and applying the position boundary condition yields:

$$x = l_{hc} - \frac{1}{2} g t^2 \quad (4.22)$$

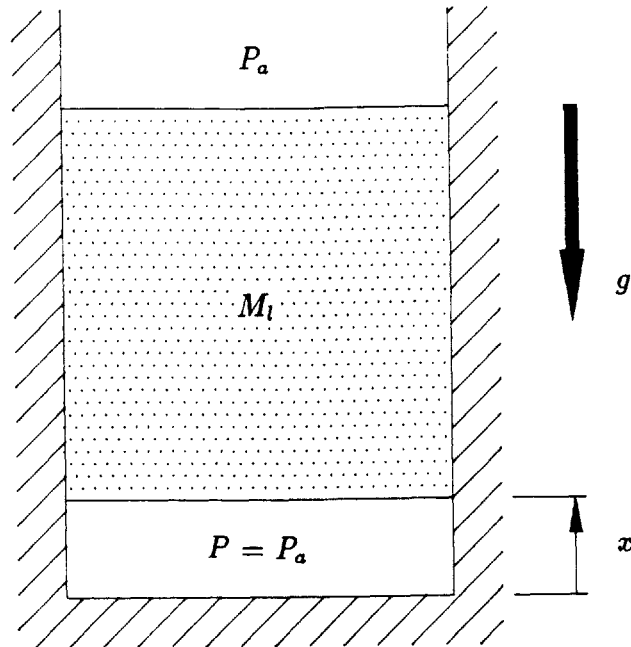


Figure 4-8: Freefall Model

The impact momentum is then

$$\mathcal{M}_{ff} = M_l \frac{dx}{dt} \Big|_{x=0} \quad (4.23)$$

or

$$\mathcal{M}_{ff} = -M_l \sqrt{2g l_{hc}} \quad (4.24)$$

The result is shown plotted against the experimental data in Figure 4-9 on page 62. Figure 4-9 shows the estimate is 29 percent too high for the low gas fraction data and is 402 percent too high for gas fractions above 12 percent.

Figure 4-10 and Figure 4-11 beginning on page 63 show the experimental data plotted against A with \mathcal{M} estimated from the freefall model. The data points are shifted leftward yet the “knee” of the pressure versus A curve is still well predicted by the analytical model. The prediction is good because the momentum in the “knee” region is still well predicted by the freefall model.

If the model were to be used to estimate the mass of air required to operate in the

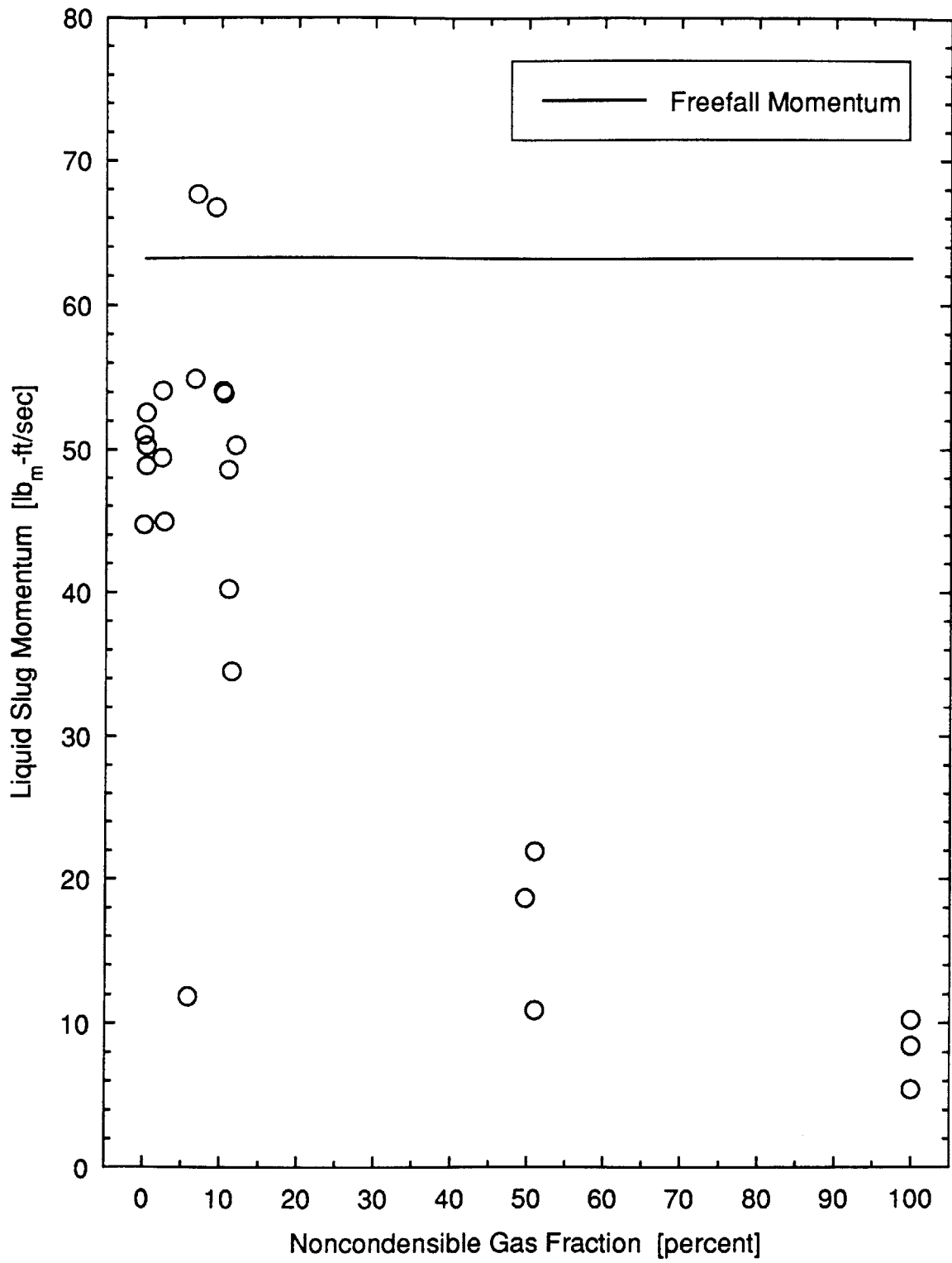


Figure 4-9: Freefall Momentum

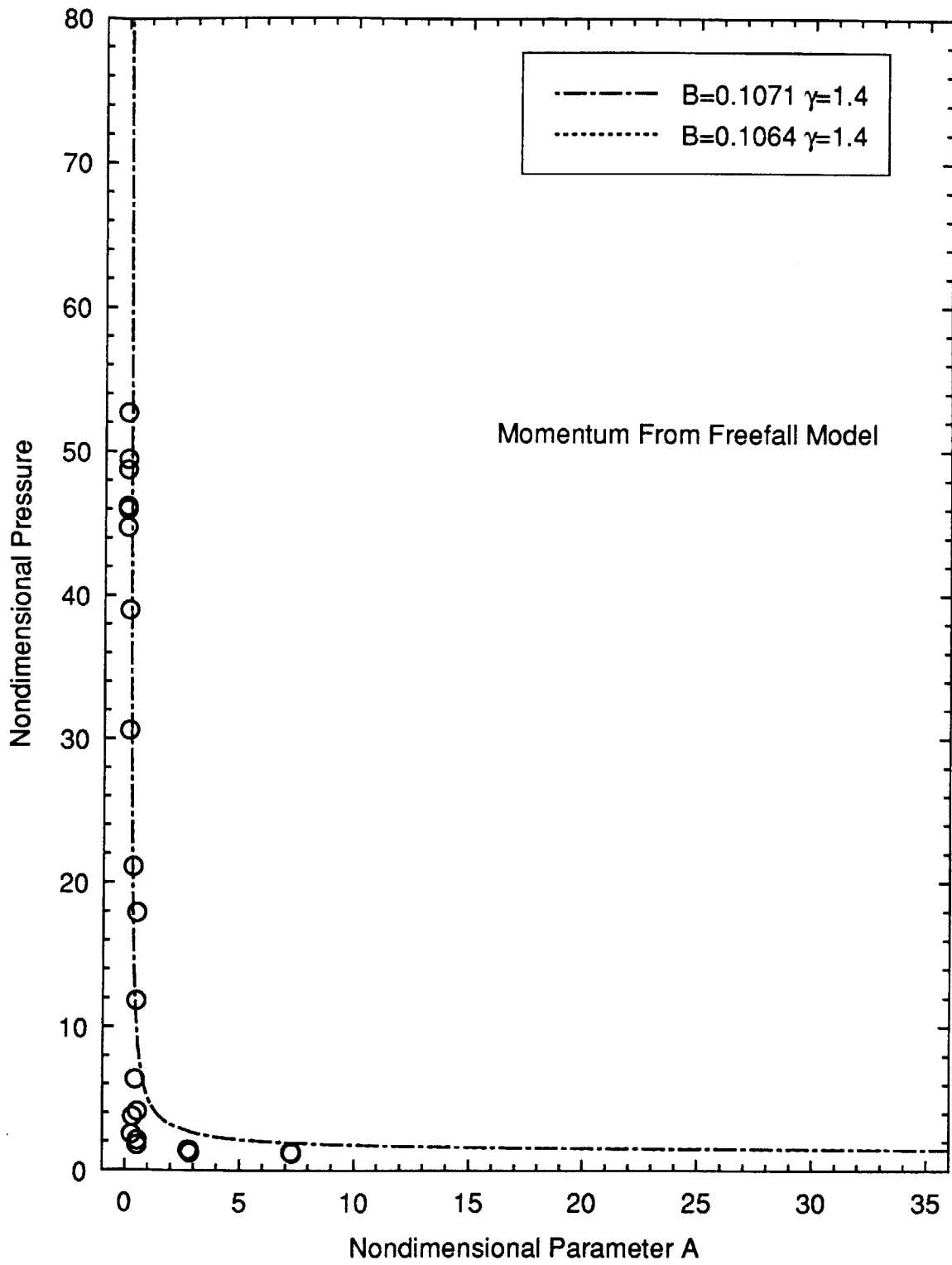


Figure 4-10: "A" Estimated From Freefall

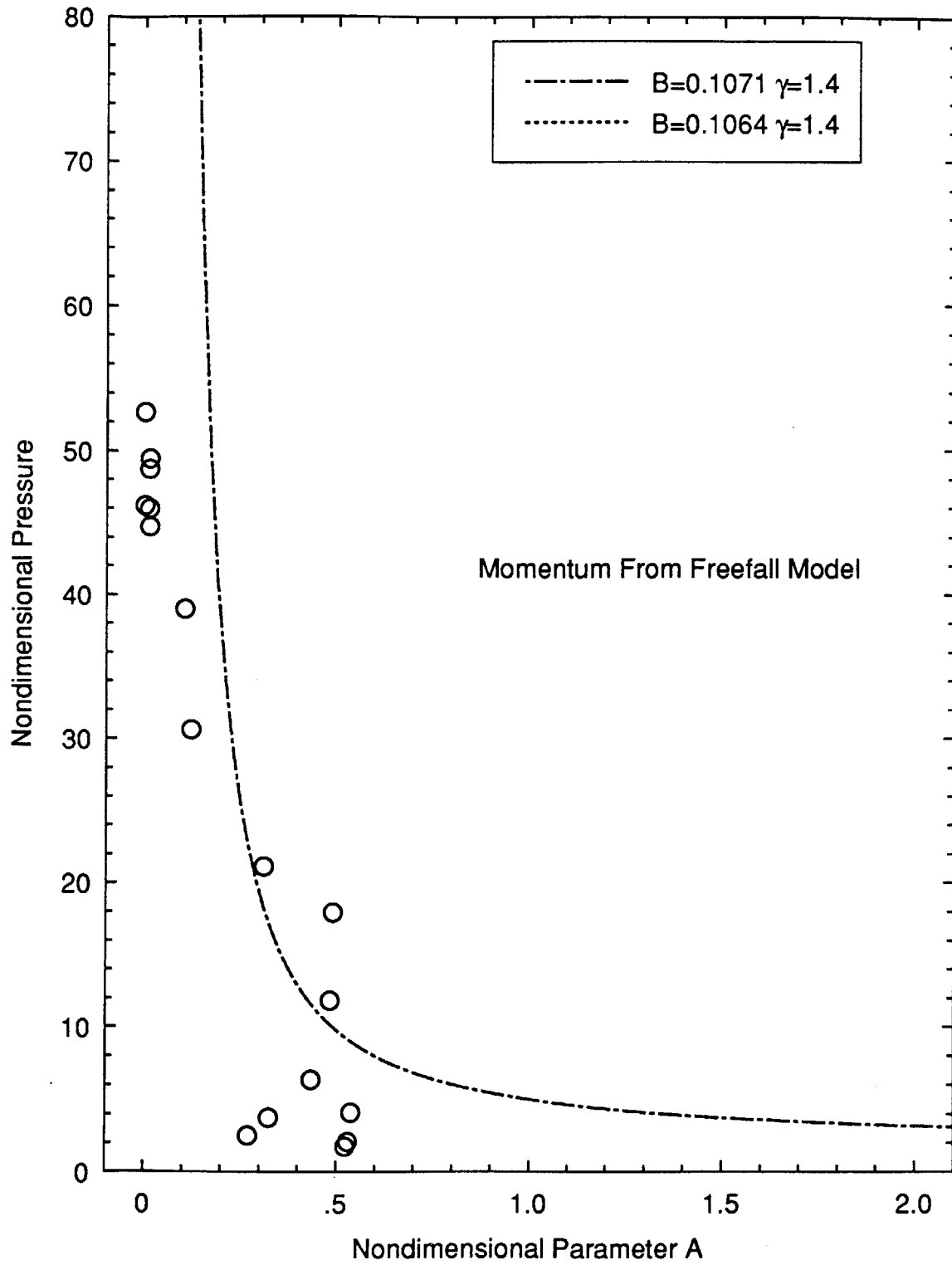


Figure 4-11: "A" Estimated From Freefall (Expanded)

“knee” region then the freefall estimate of the momentum would be adequate. Beyond the “knee” region the predicted pressure is insensitive to the estimate of momentum.

In general, if the pressure difference across the water slug can be evaluated then the momentum of the water slug can be determined. For the case where the pressure “upstream” of the water slug is constant at P_u and the pressure “downstream” is constant at P_d then the momentum can be determined from kinematics and is given by

$$\mathcal{M} = \sqrt{2(P_u - P_d) A l_{hc} M_l g_o} \quad (4.25)$$

Comments concerning estimating the water slug momentum for other systems are given in Appendix F.0.5 on page 109.

Figure 4-12 on page 66 shows the results of the analytical model for B between zero and five and γ equal to 1.4. Based on the comparison of the experimental results to the actual results in Figure 4-3, Figure 4-12 is expected to be able to predict maximum water hammer pressure for A greater than 0.2

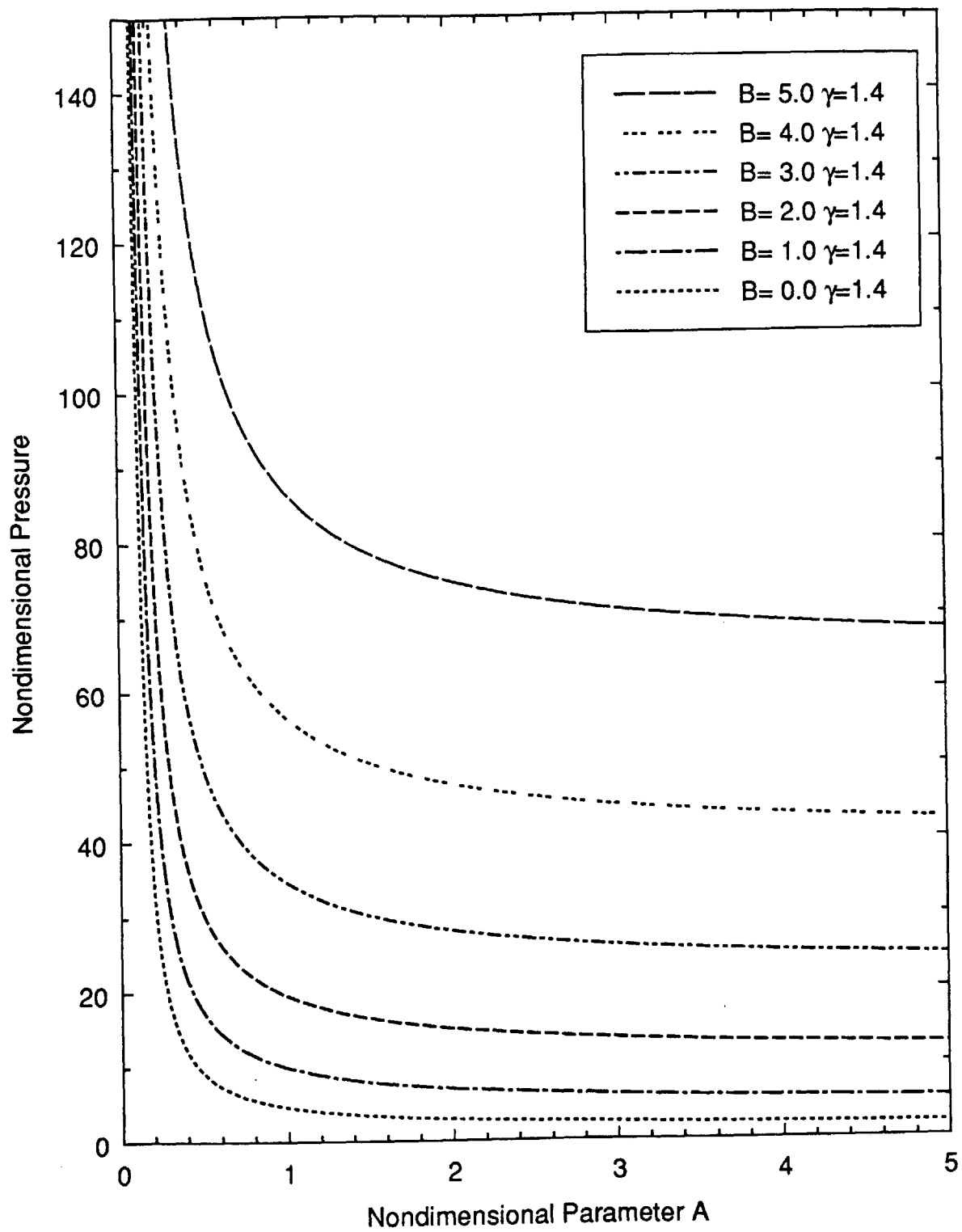


Figure 4-12: Maximum Water Hammer Pressure From Analytical Model

Chapter 5

Conclusion

The experimental results have shown that adding an equal mass of air to steam can reduce the maximum amplitude of steam bubble collapse induced water hammer pressure by two orders of magnitude. A 10 percent mixture of air in steam can reduce the amplitude one order of magnitude. The dominant effect of the noncondensable gas is to provide fluid compressibility. The diffusion resistance provided by the air becomes important only at the very highest gas fractions. The simple analytical model that considers only gas compressibility and neglects diffusion resistance and liquid compressibility predicts the experimental data well except in the region of very low gas fractions where the maximum pressure can be calculated satisfactorily by the Joukowski equation.

The model may be used to predict the mass of air required to reduce water hammer amplitudes by a half order of magnitude or greater. Using the model for amplitude reductions less than a half order of magnitude will over predict the mass of noncondensable gas required because the model does not consider liquid compressibility.

The experimental results showed that the pressure in the steam bubble did not drop to a pressure near the steam saturation pressure for the temperature of the liquid as had been anticipated. The pressure remained near saturation pressure for the wall temperature. The higher pressure may be explained by the generation of vapor by the liquid flowing down the hammer chamber walls.

The analytical model showed the gas fraction to be unimportant so mixing the

noncondensable gas with the steam also seems unimportant. This is consistent with the understanding that the diffusion resistance effect is small. As long as the condensation process can sweep the noncondensable gas toward the region of final impact then the location of gas injection should be unimportant. As long as all the gas makes it to the region of final impact the full effect of the fluid capacitance will be obtained.

While the peak amplitude of the steam bubble collapse induced water hammer decreased two orders of magnitude, the impact momentum decreased by only one half of an order of magnitude. From a piping system response point of view the addition of noncondensable gas reduces the high frequency content of the water hammer more than reducing the destructive energy. The gas reduces the amplitude of the water hammer and spreads it over a longer period of time. In general, the gas "de-tunes" the water hammer. However, it may be possible to excite low frequency vibration modes in piping systems in the process of de-tuning with noncondensable gas. Since the analytical model produces a good estimate of the pressure-time history, the model may be used to investigate potential resonance problems prior to implementing gas addition.

The amount of noncondensable gas needed to reduce water hammer amplitudes was much greater than that suggested by observations made by Bjorge[1]. In his experiments, trace amounts of noncondensable gas were enough to completely eliminate water hammers in his two-phase flow experiments. The reason is probably due to the difference in the way the way the gas alters the water hammer process. If the process is fairly quiescent, that is the interface is flat, the noncondensable gas collects as a layer isolating the water from the steam. It basically stabilizes the stratified flow. Air, having a density greater than that of steam but less than that of water forms a blanket between the steam and water as soon as a little condensation occurs. Without much condensation the flow is stable. Rapid condensation of gas-free steam on cold water however, destabilizes the stratified flow causing still more condensation and a transition to slug flow. Dumping water into steam from above by opening the dump valve is an inherently unstable, turbulent process as predicted from the Taylor stability criterion. In an inherently unstable process, trace amounts of non-

condensable gas hardly alter the interaction between steam and water. There is so much interfacial area already that there is almost no condensation resistance. As the diffusion resistance of the gas is negligible, it is only the compressibility that matters.

At the time this work was undertaken it was thought that a very small amount of gas would eliminate steam bubble collapse induced water hammer. This did not turn out to be the case. The essential difference between stratified steam/water flow in a blind ended pipe (Bjorge's experiment) and the flow of cold water down into steam (this experiment) was not then evident. For certain geometries Bjorge's criterion for stability shows how to categorically eliminate steam bubble collapse induced water hammer. This work shows how, in any geometry, water hammer can be mitigated by the introduction of air. It also suggests how the mitigation effect can be estimated.

The key variable which one needs when trying to estimate the magnitude of the peak pressure arising from a steam bubble collapse induced water hammer is the pressure in the collapsing bubble. In general, this pressure can be expected to lie somewhere between the saturation pressure for the water and the saturation pressure for the walls. These experiments indicate that the best choice is the saturation pressure corresponding to the wall temperature.

It is the compression of the noncondensable gas that mitigates the water hammer. The actual gas compression path followed can be expected to lie between an isentropic and an isothermal process. The choice is not very important but the better one seems to be the isentropic process.

Additional Work

The experimental data were taken at only one pipe diameter, with only one gas and over very limited ranges of ambient pressure and liquid slug mass. Additional studies at higher ambient pressures, larger pipe diameters and with nitrogen as the noncondensable gas may want to be undertaken to determine their effects before introducing noncondensable gas into large systems as a water hammer mitigation procedure. The model developed here, however should work at higher pressures in larger pipes. The model can be used to predict how much gas is needed to prevent a

dangerous fluid transient and determine exactly how much gas is needed.

Appendix A

Experimental Procedures

A.1 Noncondensable Gas Tests

A.1.1 System Startup

The startup of the apparatus took two to three hours. Each startup of the system was performed from a 56 step checklist. The main concern of the startup procedure was to eliminate all noncondensable gas from the system. The following is a summary of the original startup checklist.

The system was purged of air by slowly filling the boiler and superheater tank with water through their bottom drain connections and venting the air through the crossover vent. When full of water the fill rate was adjusted to maintain 5 psig on the system. Pockets of air trapped at the top of the boiler were eliminated by manually lifting the relief valve, opening the vents on the gauge glasses and by bleeding the pressure gauge bourdon tubes (see Appendix I.3 on page 120). The air trapped in the superheater tank and gas bottle were purged by starting the circulation fan then manually lifting the relief valve and opening the bleed screw under the pressure gauge diaphragm seals (see Appendix I.4 on page 120).

The steam/gas line and hammer column were purged by opening the steam/gas outlet valve (Figure 2-1 on page 27) until water spilled from the overflow connection on the subcooled water tank. Next, the water circulation pump was started. The dump

valve was opened and then closed to dislodge any bubbles. After that the hammer chamber drains were opened and shut until only clean water came out. After purging, the steam/gas outlet valve was shut. The crossover vent and water filling valves were shut. A pressure of 5 psig was maintained on the system to prevent air from entering.

A.1.2 Heating Up

Steam was opened to the heating coils in the boiler and superheater tank. The cross-over vent was throttled to maintain 5psi as the water in the tanks expanded. It was important to keep the system pressure above atmospheric pressure to insure the exclusion of atmospheric air.

Once steam issued from the cross-over vent the pressure was increased to 10 psig. The water level in the boiler was dropped until it was just visible in the gauge glasses by opening the the boiler bottom drain. Next, the water in the superheater tank was vented from the bottom drain until steam appeared. Finally, the dump valve was shut and the steam/gas outlet valve was opened to allow steam to blow out the hammer chamber drains. In this configuration then, steam was being generated in the boiler, passed to the superheater tank through the cross-over, circulated through the superheater tank, passed to the hammer chamber through the steam/gas line and vented out through the hammer chamber drain. This venting process continued for thirty minutes to insure that any noncondensable gas would be eliminated from the system. Since the water used in the boiler had not been degassed, the venting process also eliminated the noncondensable gas dissolved in the boiler water.

A.1.3 Making the Mixture

When ready to make the first batch of steam the hammer chamber drains and steam/gas outlet valve were shut. The pressure in the boiler and superheater tank was brought up to 15 psig and held for a few minutes to bring the superheater tank walls up to at least 250F, the saturation temperature at 15 psig. Next the superheater tank steam inlet valve was shut to isolate a batch of steam in the superheater tank.

After the steam had acquired about 5 F of superheat the steam/gas outlet valve and hammer chamber drains were opened to drop the pressure to about 10 psig, depending on the mass of steam desired. Dropping the pressure insured the superheater tank walls would be superheated by about 10F. Readings of the superheater pressure and temperature were recorded for determining the mass of steam in the batch. Next the gas bottle isolation valves were shut and the gas bottle flushed with air then charged to the desired pressure (up to 100 psi). The air was supplied from the lab compressed air line. The gas charge was held in the gas bottle for at least 10 seconds to allow it to come to thermal equilibrium with the heated gas bottle. The temperature and pressure were recorded to determine the mass of air in the charge. The block valve was shut and the isolation valves opened. The gas charge was pushed into the superheater tank and mixed with the steam batch by the circulation fan. For gas fractions greater than 3 percent it was necessary to repeat this charge/dump procedure to introduce the required air. Typically four charges were required for a 10 percent gas fraction. The air was not added in batch process for the 50 percent gas fraction tests. Instead, air was added to a batch of steam in superheater tank until the superheater tank pressure increased from 3 psig to 14 psig.

The 0 percent and 100 percent gas test were conducted without using a batch process for the gas. For the 100 air tests the boiler was not used. The compressed air was supplied to the superheater tank continuously and vented through the crossover vent to maintain 10 psig of air in the superheater tank. The circulation fan and finned tube heating coils were used to heat the air however. The 0 percent gas runs were conducted with the apparatus in a "flow-through" mode described in Appendix A.3 on page 76.

A.1.4 Hammer Column Preparation

The hammer column was prepared by closing the dump valve, filling the water column and subcooled water tank with water and circulating it with the circulation pump. The steam/gas mixture was admitted to the hammer chamber and vented out the hammer chamber drains until the superheater tank pressure dropped from 10 psig to

5 psig. This process pushed 25 chamber volumes of steam/gas through the hammer chamber and insured the sample would be representative of the batch. The hammer chamber drain valves the steam/gas inlet valves were shut isolating the steam/gas charge in the hammer chamber. The subcooled water tank drain was opened dropping the water column to a height of $43\frac{5}{8}$ inches. Next the hammer chamber drain was cracked and the pressure dropped until the dump valve differential pressure gauge indicated zero pressure across the dump valve.

A.1.5 Water Hammer Initiation

With the steam/gas charge isolated in the hammer chamber and zero pressure across the dump valve, the tape recorder was started. The hammer chamber pressure transducer charge amplifiers were grounded to reset them to zero. The dump valve was opened manually. The liquid column descended in the constant diameter pipe through the dump valve and into the hammer chamber. The subcooled liquid condensed the steam in the hammer chamber and impacted at the bottom of the chamber. The data from the resulting water hammer was recorded the on the FM tape recorder and displayed on an oscilloscope.

A.1.6 Post Run Procedures

The tape recorder was stopped and the dump valve shut. The hammer chamber drains were opened and the subcooled water tank refilled. The boiler steam outlet valve was shut and the crossover vent opened. The steam/gas outlet valve was shut and the superheater tank was refilled with water to purge all noncondensable gas introduced from the previous run. When full the trapped air was purged by lifting the relief valve and bleeding the pressure gauge diaphragms and described in Appendix A.1.1 on page 71. The boiler steam outlet valve was opened and the water drained out the bottom drain of the superheater tank. The 30 minute purge was begun and the next steam/gas mixture was prepared as described in Appendix A.1.3 on page 72.

A.2 Pipe Wall Temperature Sensitivity Tests

The startup and heating procedures used were the same as the ones used for the noncondensable gas tests and are described in Appendix A.1.1 on page 71. Since this series of tests was done with 100 percent steam it was not necessary to make the steam in a batch process.

A.2.1 Hammer Column Preparation

Without the batching process the hammer column preparation differed from the procedure used in the noncondensable gas tests described in Appendix A.1.4 on page 73. The steam was generated in the boiler and passed to the superheater tank then to the hammer chamber and out the hammer chamber drain valves in a continuous process. The superheater finned tube heating coil and circulation fan were kept in operation. Venting the steam through the hammer chamber continued for 15 minutes purging the hammer chamber with 1,000 volumes of steam. During the purging process the subcooled water tank was filled and the water circulated with the circulation pump. When ready for a run the subcooled water tank was drained to the $43\frac{5}{8}$ inch level. The hammer chamber drains were shut, then the steam/gas inlet valves were shut. Finally, the hammer chamber drain valve was cracked open and the pressure bled off to establish zero delta P across the dump valve.

A.2.2 Water Hammer Initiation

With the steam/gas charge isolated in the hammer chamber and zero pressure across the dump valve, the tape recorder was started. The hammer chamber pressure transducer charge amplifiers were grounded to reset them to zero. The dump valve was opened manually. The liquid column descended in the constant diameter pipe through the dump valve and into the hammer chamber. The subcooled liquid condensed the steam in the hammer chamber and impacted at the bottom of the chamber. The data from the resulting water hammer was recorded the FM tape recorder and displayed on an oscilloscope.

A.2.3 Post Run Procedures

The tape recorder was stopped and the dump valve shut. The steam/gas inlet valves were opened then the hammer chamber drains were opened thereby beginning the 30 minute "flow-through" process again. The subcooled water tank was refilled and the circulation pump started.

A.3 Ambient Pressure Sensitivity Tests

The startup and heating procedures used in the ambient pressure sensitivity tests were the same as the ones used for the noncondensable gas tests and are described in Appendix A.1.1 on page 71. As with the wall temperature sensitivity tests this series of test was conducted with 100 percent steam so it was not necessary to make the steam in a batch process.

After the startup and heating procedures were completed the apparatus was placed in the "flow-through" mode where steam was generated in the boiler, passed to the superheater tank through the crossover then to the hammer chamber through the steam/gas line and out the hammer chamber drain valves in a continuous process. In the "flow-through" mode the dump valve was closed and the superheater tank circulation fan was in operation along with the superheater tank finned tube heating coil. Venting the steam through the hammer chamber drains continued for 15 minutes purging the hammer chamber with 1,000 volumes of steam.

A.3.1 Hammer Chamber Preparation

The pressurization of the subcooled water tank required modifying the hammer chamber column preparation used in the noncondensable gas tests. The modified procedure is describe below.

While the hammer chamber was being purged, the subcooled water tank was being filled with water and the water recirculated with the circulation pump. When ready for a run the subcooled water tank drain was opened and the water drained to the

43 $\frac{5}{8}$ inch level. The overflow valve was shut and the air supply to the accumulator tank opened. When the subcooled water tank and accumulator tank were pressurized to 10 psig the hammer chamber drain valves were shut. The steam/gas inlet valves were shut then the hammer chamber drain valve was cracked and the pressure bled off until the dump valve differential pressure gauge indicated zero pressure.

A.3.2 Water Hammer Initiation

With the steam/gas charge isolated in the hammer chamber and zero pressure across the dump valve, the tape recorder was started. The hammer chamber pressure transducer charge amplifiers were grounded to reset them to zero. The dump valve was manually opened and the data from the resulting water hammer was recorded on the FM tape recorder and displayed on an oscilloscope.

A.3.3 Post Run Procedures

The tape recorder was stopped and the dump valve shut. The accumulator tank air supply valve was shut and the pressure bled off through the accumulator tank bottom drain. The subcooled water tank was refilled and the tank overflow valve opened. The steam/gas inlet valves were opened, the hammer chamber drain valves were opened and the 30 minute "flow-through" purge cycle begun again.

Appendix B

Data Reduction

B.1 Noncondensable Gas Tests

B.1.1 Gas Fraction Calculations

The mass of steam is determined using measurements of superheater tank pressures and temperatures, superheater tank volume and the steam specific volume as given in the 1967 ASME Steam Tables[2].

The mass of the initial charge of steam in the superheater tank is given by:

$$M_{steam_0} = \frac{V_T}{v_{steam}} \quad (B.1)$$

where v is determined from the steam tables by entering with a pressure of $P_2 + P_{atm}$ and temperature of $(T_3 + T_4)/2$.

The mass of air in the first gas charge is determined from the ideal gas equation of state.

$$M_{air_{charge1}} = \frac{(P_{3_1} + P_{atm}) \times V_B}{R_{air} \times (T_{5_1} + 459.67)} \quad (B.2)$$

After the isolation valves are opened and the noncondensable gas and steam are mixed, the mixture distributes itself uniformly between the superheater tank and gas bottle.

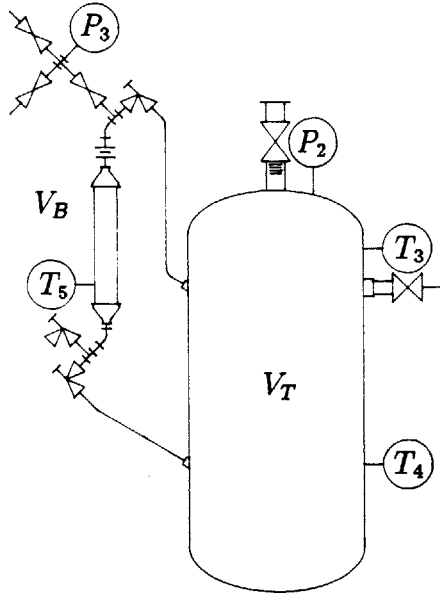


Figure B-1: Instruments Used for Gas Fraction Measurements

The mass of steam in the superheater tank becomes

$$M_{steam_1} = M_{steam_0} \times \frac{V_T}{V_T + V_B} \quad (B.3)$$

and the mass of air in the superheater tank becomes

$$M_{air_{tank1}} = M_{air_{charge1}} \times \frac{V_T}{V_T + V_B} \quad (B.4)$$

For a gas fraction greater than 3 percent it is necessary to add additional charges of noncondensable gas. The isolation valves are then closed and the gas bottle purged with compressed air. The second charge of noncondensable gas has a mass of

$$M_{air_{charge2}} = \frac{(P_{3_2} + P_{atm}) \times V_B}{R_{air} \times (T_{5_2} + 459.67)} \quad (B.5)$$

After opening the isolation valves the uniform mixture will have a mass of steam in the superheater tank given by

$$M_{steam_2} = M_{steam_1} \times \frac{V_T}{V_T + V_B} \quad (B.6)$$

or

$$M_{steam_2} = M_{steam_0} \times \left[\frac{V_T}{V_T + V_B} \right]^2 \quad (B.7)$$

and a mass of air given by

$$M_{air_{tank2}} = M_{air_{charge2}} \times \frac{V_T}{V_T + V_B} + M_{air_{tank1}} \times \frac{V_T}{V_T + V_B} \quad (B.8)$$

or

$$M_{air_{tank2}} = M_{air_{charge2}} \times \frac{V_T}{V_T + V_B} + M_{air_{charge1}} \times \left[\frac{V_T}{V_T + V_B} \right]^2 \quad (B.9)$$

In general then, after the addition of N charges of noncondensable gas

$$M_{steam} = M_{steam_0} \times \left[\frac{V_T}{V_T + V_B} \right]^N \quad (B.10)$$

and

$$M_{air} = \sum_{i=1}^N M_{charge_i} \times \left[\frac{V_T}{V_T + V_B} \right]^i \quad (B.11)$$

Finally, the gas fraction Q is given by

$$Q = \frac{M_{air}}{M_{steam} + M_{air}} \quad (B.12)$$

B.2 Hammer Chamber Pressure Calculations

B.2.1 Offset Corrections

The hammer chamber pressure was measured with piezoelectric pressure transducers. Since the piezoelectric transducers can measure only *changes* of pressure the following procedure was used to relate these pressures to atmospheric pressure.

The pressure in the hammer chamber before the dump valve was opened could be determined by adding the pressure due to the column of subcooled water to the measured pressure differential across the dump valve. Since the dump valve differential pressure was recorded on the tape recorder along with the hammer chamber pressure it was a simple procedure to determine the pressure transducer offset corrections.

The average dump valve differential pressure for the one half second period prior to valve opening was determined from:

$$\overline{\Delta P} = 2 \int_{t_{open}-0.5}^{t_{open}} P_4 dt \quad (B.13)$$

The hammer chamber during that same period is given by

$$\overline{P_{chamber_o}} = \overline{\Delta P} + \frac{\rho g L}{g_o} \quad (B.14)$$

The average hammer chamber pressure as measured by the piezoelectric transducer during the period is

$$\overline{P_h} = 2 \int_{t_{open}-0.5}^{t_{open}} P_h'' dt \quad (B.15)$$

and

$$\overline{P_l} = 2 \int_{t_{open}-0.5}^{t_{open}} P_l'' dt \quad (B.16)$$

The offset correction is a constant equal to the difference between the chamber pressure and the transducer pressure during the one half second period prior to valve opening.

$$P_{h_{correction}} = \overline{P_{chamber_o}} - \overline{P_h} \quad (B.17)$$

and

$$P_{l_{correction}} = \overline{P_{chamber_o}} - \overline{P_l} \quad (B.18)$$

finally

$$P_h'(t) = P_h''(t) + P_{h_{correction}} \quad (B.19)$$

and

$$P_l'(t) = P_l''(t) + P_{l_{correction}} \quad (B.20)$$

B.2.2 Thermal Effect Corrections

At the time a water hammer is initiated the piezoelectric hammer chamber pressure transducers are at a temperature of about 239F (the saturation pressure for 9.8 psig).

When the transducers are hit by the 85F subcooled water during the water hammer they experience strains due to the thermal stresses in their mountings. The strains show up in the transducer outputs as a pressure rise. This thermal effect is shown in Figure B-2 on page 83.

The time scale and magnitude make the effect more significant for the high gas fraction data. For the zero gas fraction data the water hammer amplitude is about 800 psi and the thermal effect about 30 psi. The duration of the zero gas fraction water hammer is about 1.5 ms and the time constant of the thermal effect is about 70 ms. The water hammer is over before the thermal effect becomes important. However, for the 50 percent and 100 percent gas fraction data the water hammer amplitude is much lower and the response time longer so the thermal effect makes up a large part of the measured response. The thermal corrections are critical to the high gas fraction data. The magnitude of the thermal effect corrections as a function of gas fraction are shown in Figure B-3 on page 84.

The thermal effect correction $P_{te}(t)$ is applied to the offset corrected pressure data to determine the hammer chamber pressure

$$P_h(t) = P'_h - P_{te}(t - \tau_{te}) \times f \quad (\text{B.21})$$

where τ_{te} is selected so the initial pressure rise of $P'_h(t)$ and $P_{te}(t + \tau_{te})$ correspond and f is selected so that $P'_h(t) = P_{te}$ as $T \rightarrow \infty$. In other words, f a scale factor selected so the steady state values coincide. It was not necessary to correct the low pressure data for transducer thermal effects. The thermal effect is only important after the transducer and its mounting are contacted by the subcooled water. The low pressure data was used to evaluate the pressure in the hammer chamber prior to the water hammer so the thermal effect was unimportant. This fact is expressed by Equation B.22.

$$P_l(t) = P'_l \quad (\text{B.22})$$

The thermal effect for the high pressure transducer $P_{te}(t)$ is determined experimentally by taking the difference in pressure response of two cases. The first case is

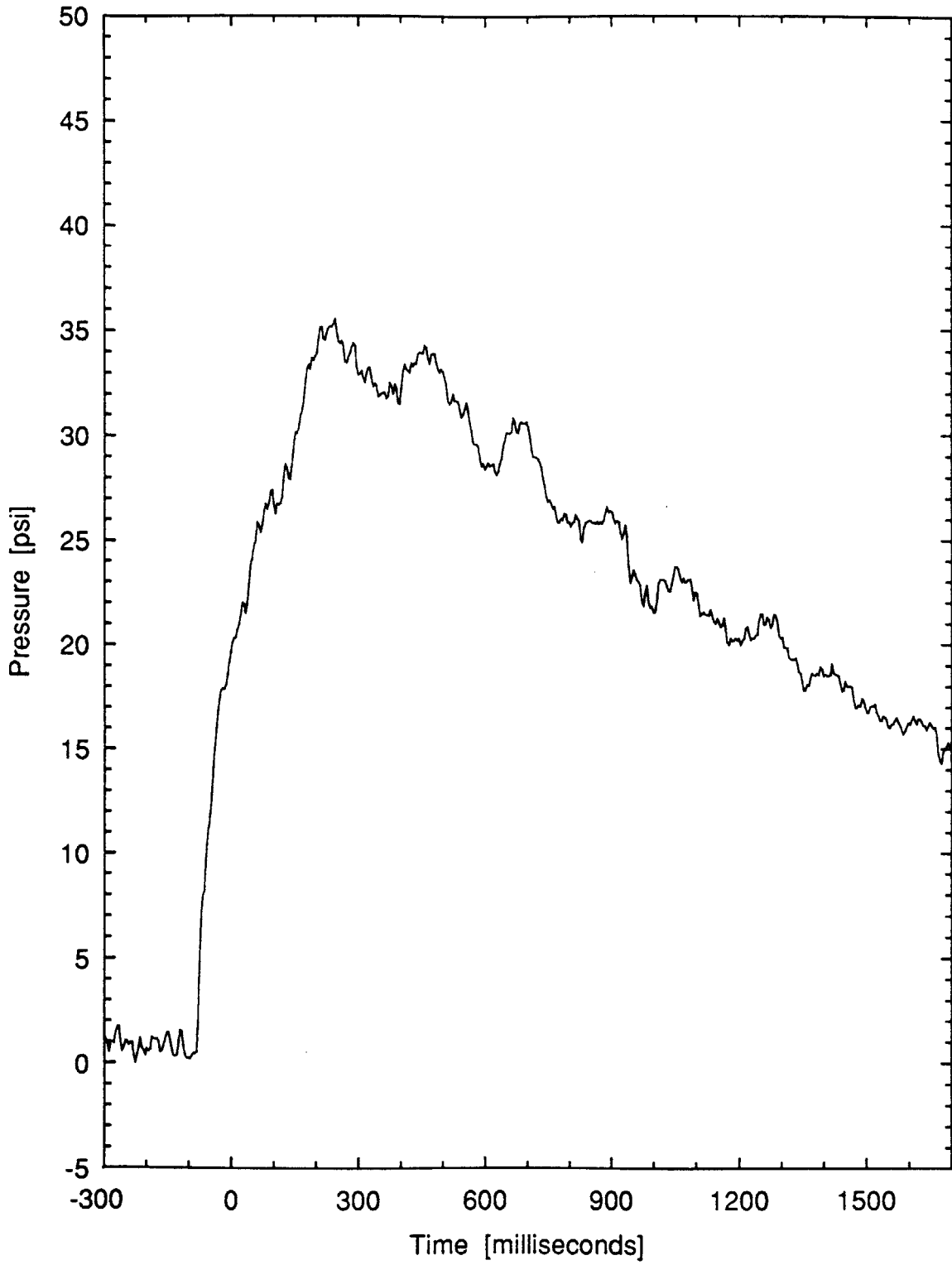


Figure B-2: Hammer Chamber Pressure Transducer Thermal Effect

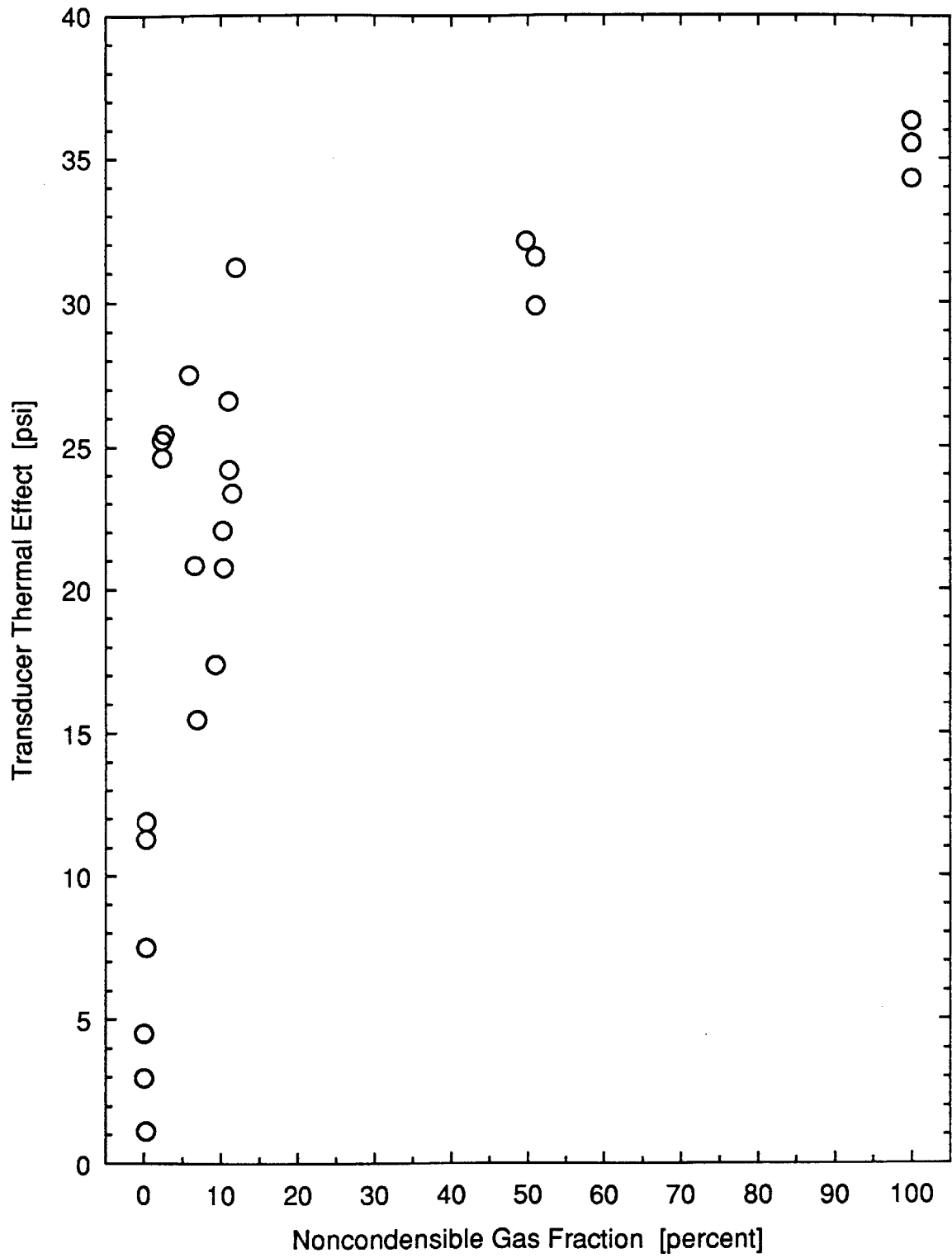


Figure B-3: Thermal Effect Correction Versus Gas Fraction

the 100 percent gas fraction case with jacket temperature of 239F (saturation temperature at 19.8 psig) and subcooled water at 74F. The first case is the average of two runs at those conditions. The second case is also a 100 percent gas fraction case but the jacket steam is shut off and the subcooled water and hammer column are at ambient temperature. The average of five runs at those conditions make up the second case. The difference in the pressures in these two cases is said to be due to the thermal effect of the transducer and called the thermal effect.

B.3 Pipe Wall Temperature Sensitivity Tests

The data reduction procedure for the pipe wall temperature sensitivity test data was simpler than for the noncondensable gas tests. No gas calculations were necessary as the tests were conducted with 100 percent steam. The thermal effect corrections were not applied as the corrections are small for 0 percent gas fraction data. Only the offset corrections (described in Appendix B.2.1 on page 80) were applied to the data.

B.4 Ambient Pressure Sensitivity Tests

The data reduction procedure for the ambient pressure sensitivity tests was the same as used for the hammer chamber wall temperature sensitivity tests and is described in Appendix B.3.

Appendix C

Time Traces of Selected Data

This section contains the pressure/time data for the data points labeled “a” through “g” in Figures 3-1 and 3-2 on page 41. The data is presented to show how the noncondensable gas effects the pressure/time characteristics of the water hammer. The data have noncondensable gas fractions varying from 0 percent at point “a” to 100 percent at point “g”. The hammer chamber high pressure data, low pressure data, dump valve differential pressure data and valve position data are shown for the selected points.

C.0.1 Water Hammer High Pressure Data

The water hammer pressure versus time traces are shown in Figure C-1 on page 87 and Figure C-2 on page 88. The offset correction has been applied to the data but the thermal correction has not. See Appendix B.2.1 on page 80 for details of the offset correction and Appendix B.2.2 on page 81 for the thermal corrections.

The time $t = 0$ is arbitrary and corresponds only to the time at which the hammer chamber pressure reached the triggering threshold of the structural dynamics analyzer. Figure C-1 shows the water hammer to be a series of pressure spikes of decreasing amplitude. In Figure C-2 the first spike has been expanded so that the details of the spike can be seen.

The nature of the 0 percent noncondensable gas fraction traces in Figures C-1 and

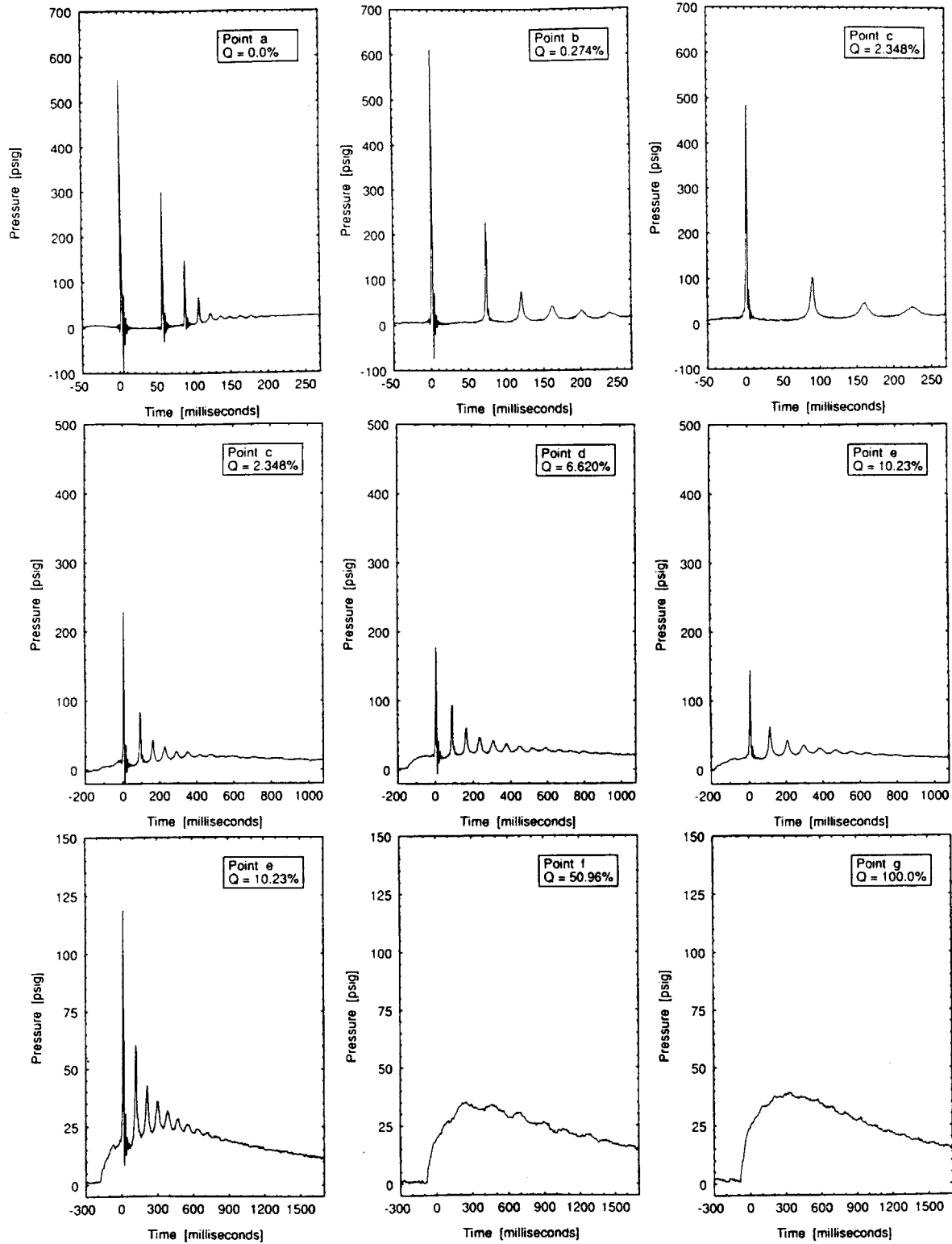


Figure C-1: High Pressure Data for Points in Figure 3-1

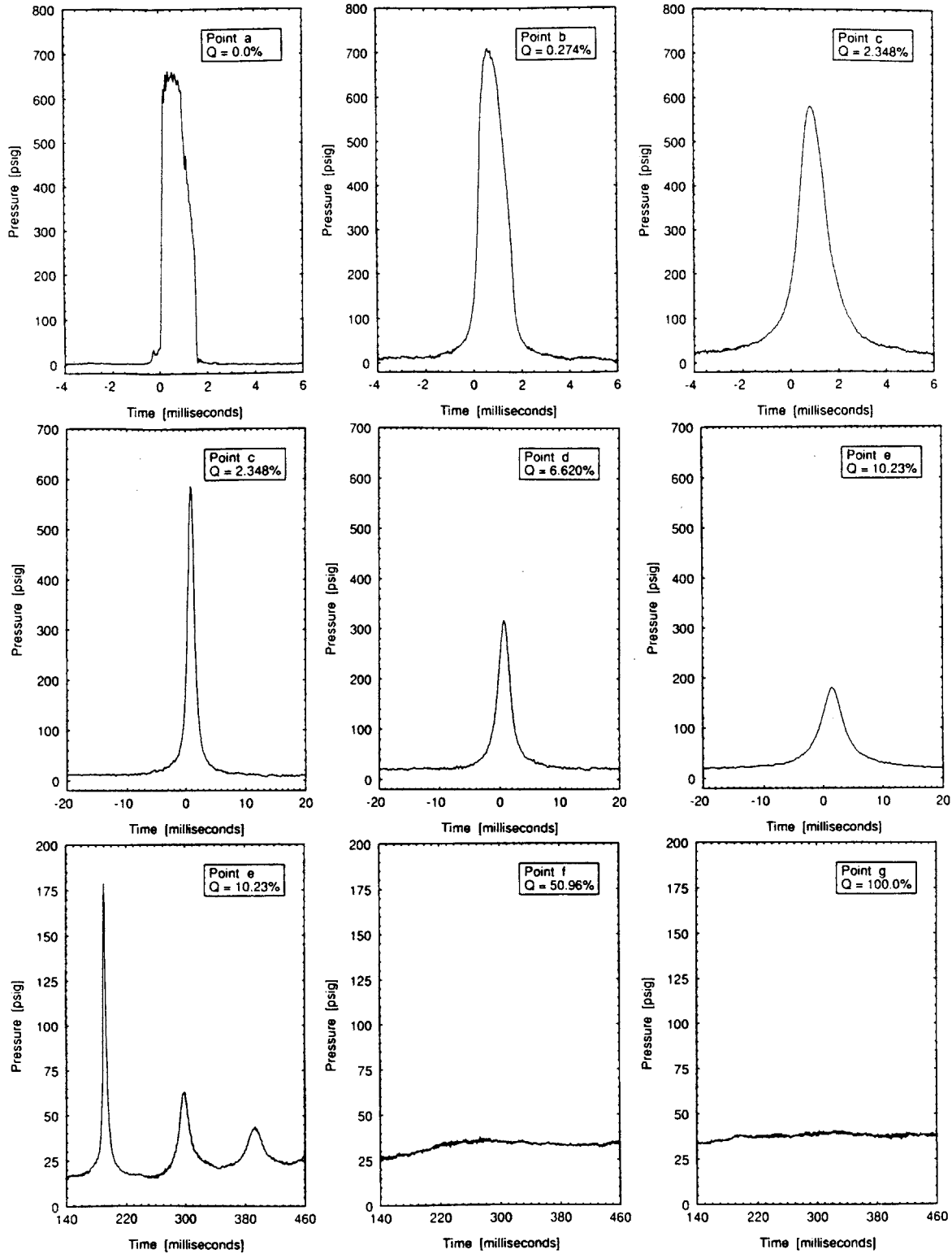


Figure C-2: High Pressure Data for Points in Figure 3-1 (Expanded)

C-2 can be explained from the simple one-dimensional water hammer model presented in Section 1.2 on page 21. The first pressure spike appears as a square wave of duration 1.5 ms which is the travel time of the hydraulic shock wave through the liquid and back at 1,400 meters/second[7] as predicted by the model. The model shows that when the wave reflects at the bottom of the hammer chamber the pressure drops to $-P_j$ and travels back up the liquid to reflect at the top again. In the experimental data however, the pressure below the reflected wave remains at about 0 psig due to the flashing of the liquid. Water near ambient temperature and a pressure of $-P_j$ (-700 psig) is in a non-equilibrium state. The experimental data show the reflected shock wave travels to the liquid surface and down again in 54 ms at an average velocity of 41 meters/second. The low velocity is characteristic of decompression waves having a phase change at the wave front as shown by Moody[7]. Moody shows the decompression wave speed to be as low as 1 meter/second for small decompressions in saturated water.

The model shows the second spike to have the same amplitude as the first because the model has no losses. The experimental data show the amplitude of the second spike is 55 percent of the first spike due to losses in the shock wave propagation and reflections, particularly the reflection at the free surface.

Figure C-2 shows that at 0.274 percent gas fraction the square wave has been transformed into a smooth sine wave due to the compressibility provided by the bubbles of noncondensable gas. If the bubbles were small and uniformly distributed throughout the liquid then the liquid bulk modulus would decrease and, according to the one-dimensional theory, the pressure response would still appear as a square wave but with decreased amplitude. The smooth sine wave shape suggests the bubbles have collected near the bottom of the hammer chamber and are not distributed throughout the liquid.

By a 10.23 percent gas fraction the amplitude is down to less than one quarter of the 0 percent gas fraction amplitude. The propagation and transmission losses have increased so that the amplitude of the second spike is now only 33 percent of the first spike amplitude.

C.0.2 Water Hammer Low Pressure Data

The low pressure data were taken to determine the time history of the hammer chamber pressure in the $\frac{1}{2}$ second interval between the time the dump valve is opened and the water hammer occurs. The pressure drop in the hammer chamber prior to the water hammer is an indication of the rate of condensation of the steam in the steam/gas mixture. Knowing the condensation rate is critical in determining the momentum of the subcooled water and therefore critical in estimating the water hammer amplitude.

The low pressure data are shown in Figure C-3 on page 91. The data have not been corrected for thermal effects as the effect is negligible until the transducer comes in contact with the subcooled water which occurs at approximately $t = 0$. The data show that the pressure drop in the hammer chamber prior to the water hammer is typically less than 1 psi.

C.0.3 Dump Valve Differential Pressure

The dump valve differential pressure data are shown in Figure C-4 on page 92. The data were used only for determining the offset corrections (see Appendix B.2.1 on page 80) but are included here just for completeness.

C.0.4 Dump Valve Position Data

The dump valve position data for the points labeled "a" through "g" in Figure 3-1 on page 41 are shown in Figure C-5 on page 93. The data have been normalized so that a value of 100 corresponds to the position when the valve just begins to open and a value of 0 corresponds to the valve fully open position. The traces begin at values of 135 reflecting the fact that the valve rotates about 15 degrees from the shut position until the valve begins to open. The data show that the valve opening time is about 40 ms and the valve is fully open for 400 ms before the water hammer occurs. The valve opening time should be sufficiently fast to prevent water hammer amplitude reduction by restricting the velocity of the falling liquid. 40 ms represents a freefall

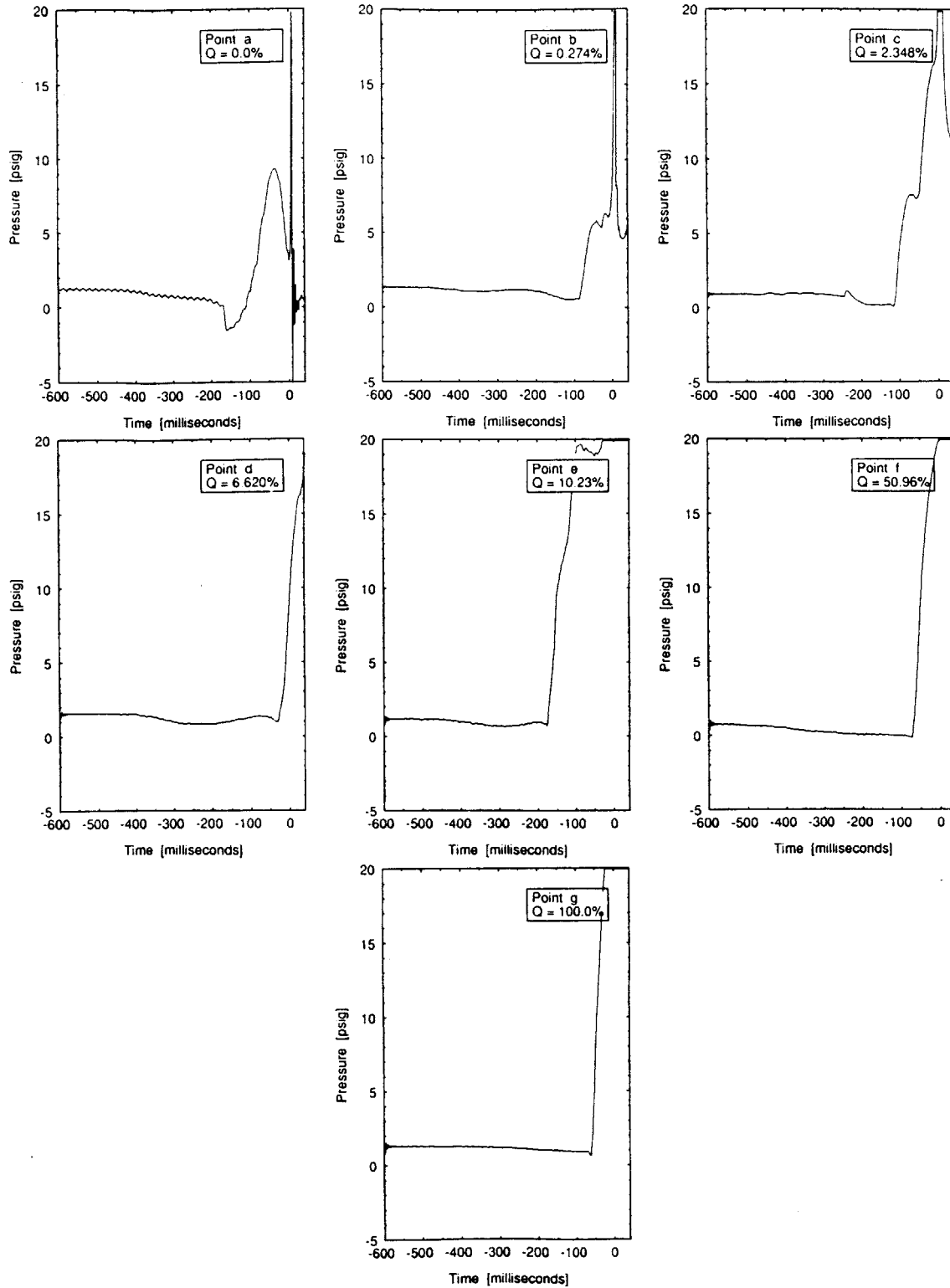


Figure C-3: Hammer Chamber Low Pressure Data for Points in Figure 3-1

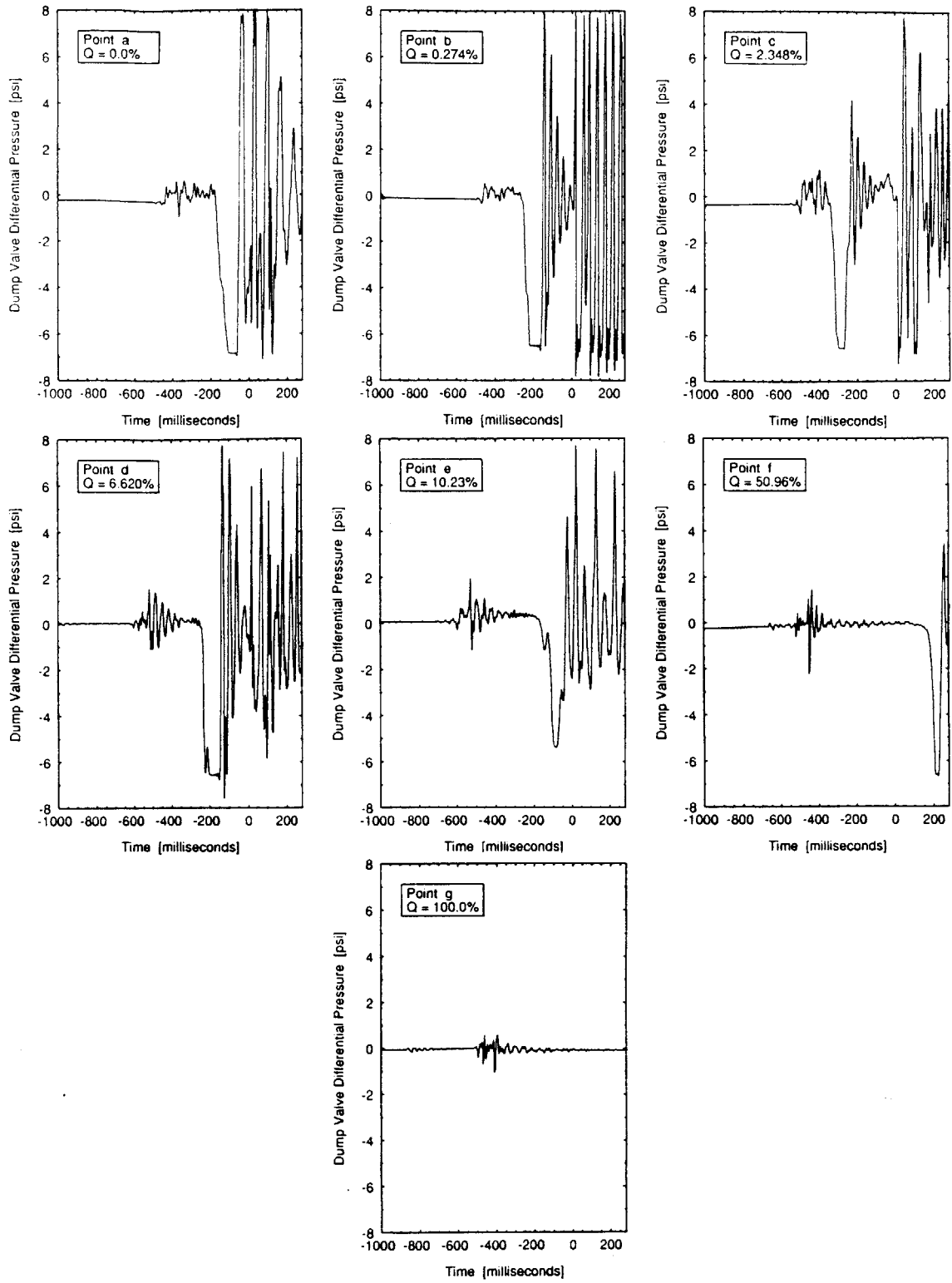


Figure C-4: Dump Valve Differential Pressure Data for Points in Figure 3-1

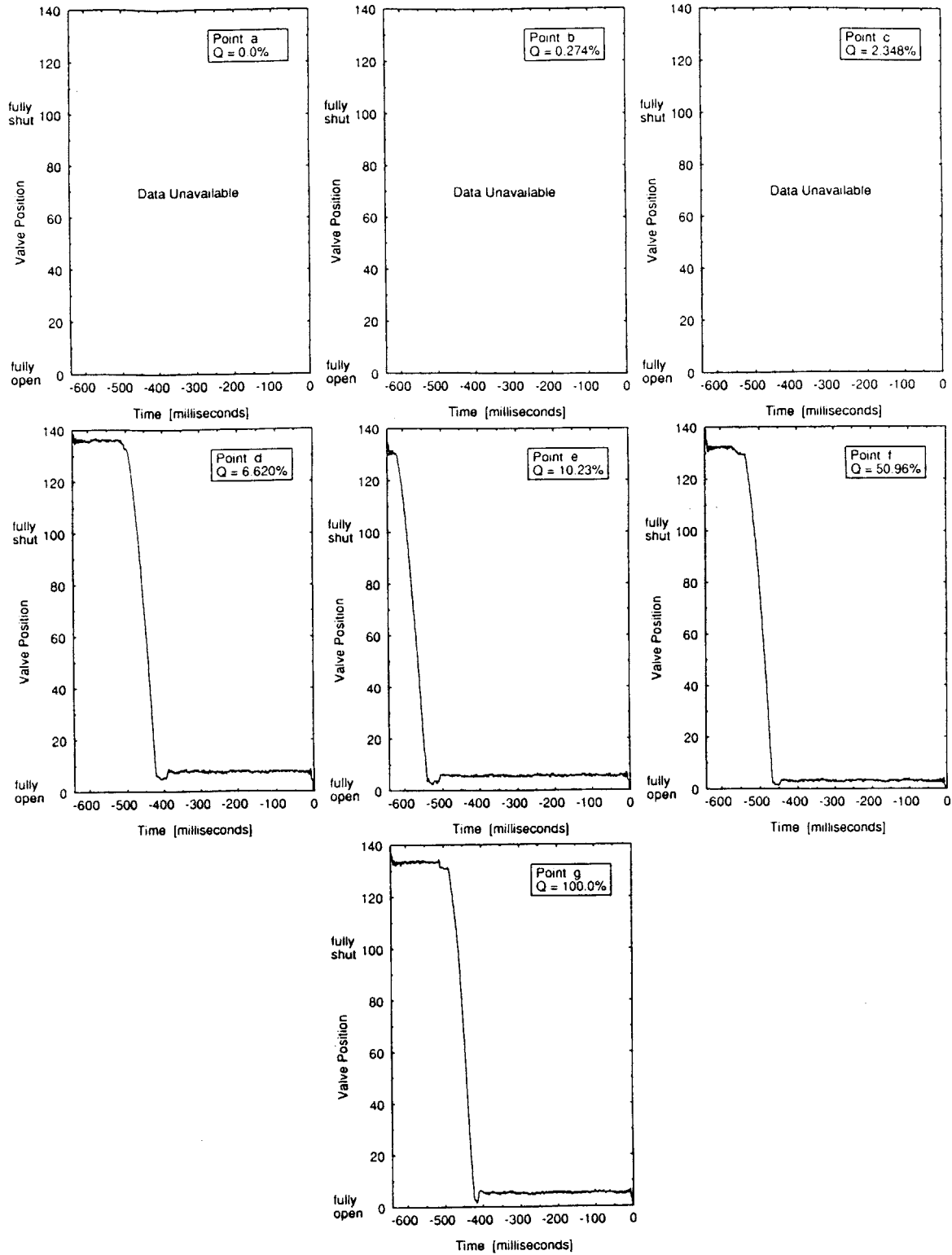


Figure C-5: Dump Valve Position Data for Points in Figure 3-1

distance of $\frac{5}{16}$ inches or 0.15 ball valve diameters.

Appendix D

Ambient Pressure Sensitivity

Tests

The ambient sensitivity tests were conducted to determine the effect of system ambient pressure on steam bubble collapse induced water hammer. The experimental apparatus was modified so that the subcooled water tank could be pressurized to 10 psig. Four runs were conducted at 10 psig with a steam jacket temperature of 268F. All four runs were conducted with 100 percent steam (a noncondensable gas fraction of 0 percent). The experimental procedure used for the ambient pressure sensitivity tests is described in Appendix A.3 on page 76 and the data reduction procedures are described in Appendix B.4 on page 85.

D.1 Apparatus Modifications

For the noncondensable gas tests and wall temperature sensitivity tests the top of the subcooled water tank was open to the atmosphere. For the ambient pressure sensitivity test it was necessary to pressurize the hammer column to 10 psig which required sealing off the top of the subcooled water tank. The overflow connection was connected to a 3.9 cubic foot pneumatic accumulator tank so that when the water column dropped into the hammer chamber the pressure above the water column would remain constant at 10 psig. The accumulator tank was supplied compressed

air through an air pressure regulator that allowed one to set the tank pressure at 10 psig. Measurements in the course of the experiments showed the pressure above the water column dropped less than 0.3 psi. The configuration of the hammer column after the required modifications is shown in Figure D-1 on page 97.

D.2 Experimental Results

The peak pressure versus ambient pressure data are shown in Figure D-2 on page 98. Pressure versus time traces for the two data points labeled “a” and “b” are shown in Figure D-3 on page 99. A comparison of the average pressure at 0 psig ambient pressure and 10 psig ambient pressure, indicates that increasing the ambient pressure 10 psig decreases the water hammer amplitude by 5 percent. Given the variation in the data however, a more reasonable conclusion is that the amplitude change is immeasurable.

The water hammer momentum versus ambient pressure data are shown in Figure D-4 on page 100. As an ambient pressure change of 10 psig has a negligible change on the speed of sound in the liquid, Figure D-4 is essentially the same as Figure D-2 with the vertical axis scaled as $\frac{V_l g_0}{c}$ as predicted by the one-dimensional theory in Section 1.2. From Equation 1.8 on page 22

$$P = \frac{\rho v_i c}{g_0} \quad (\text{D.1})$$

and expressing the velocity as $\frac{M}{M_l}$ and M_l as ρV_l then

$$P = M \frac{c}{V_l g_0} \quad (\text{D.2})$$

D.3 Discussion

The ambient pressure sensitivity tests showed that, when the ambient pressure increased from 0 psig to 10 psig, there was little change in the water hammer peak

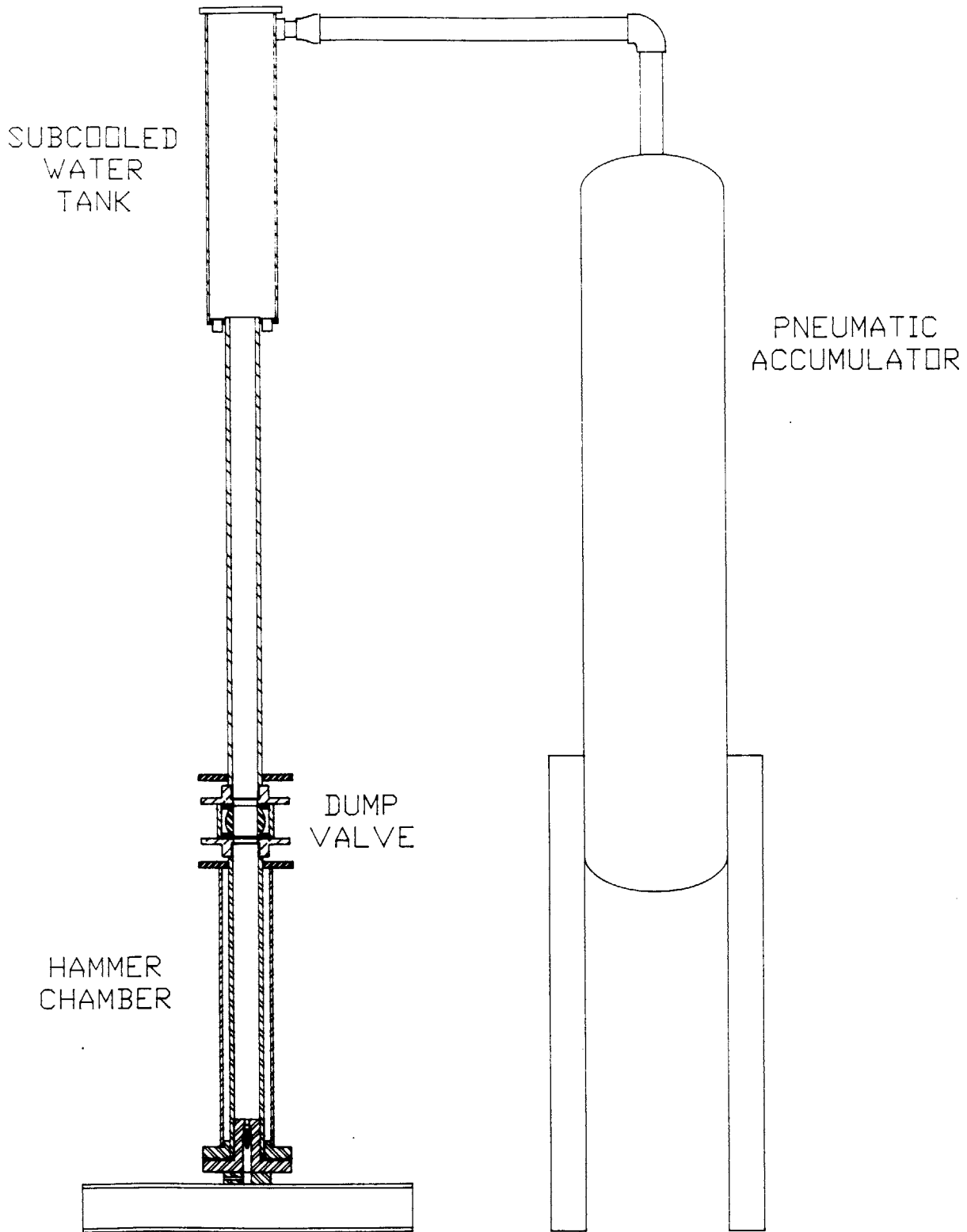


Figure D-1: Apparatus Modified for Ambient Pressure Sensitivity Tests

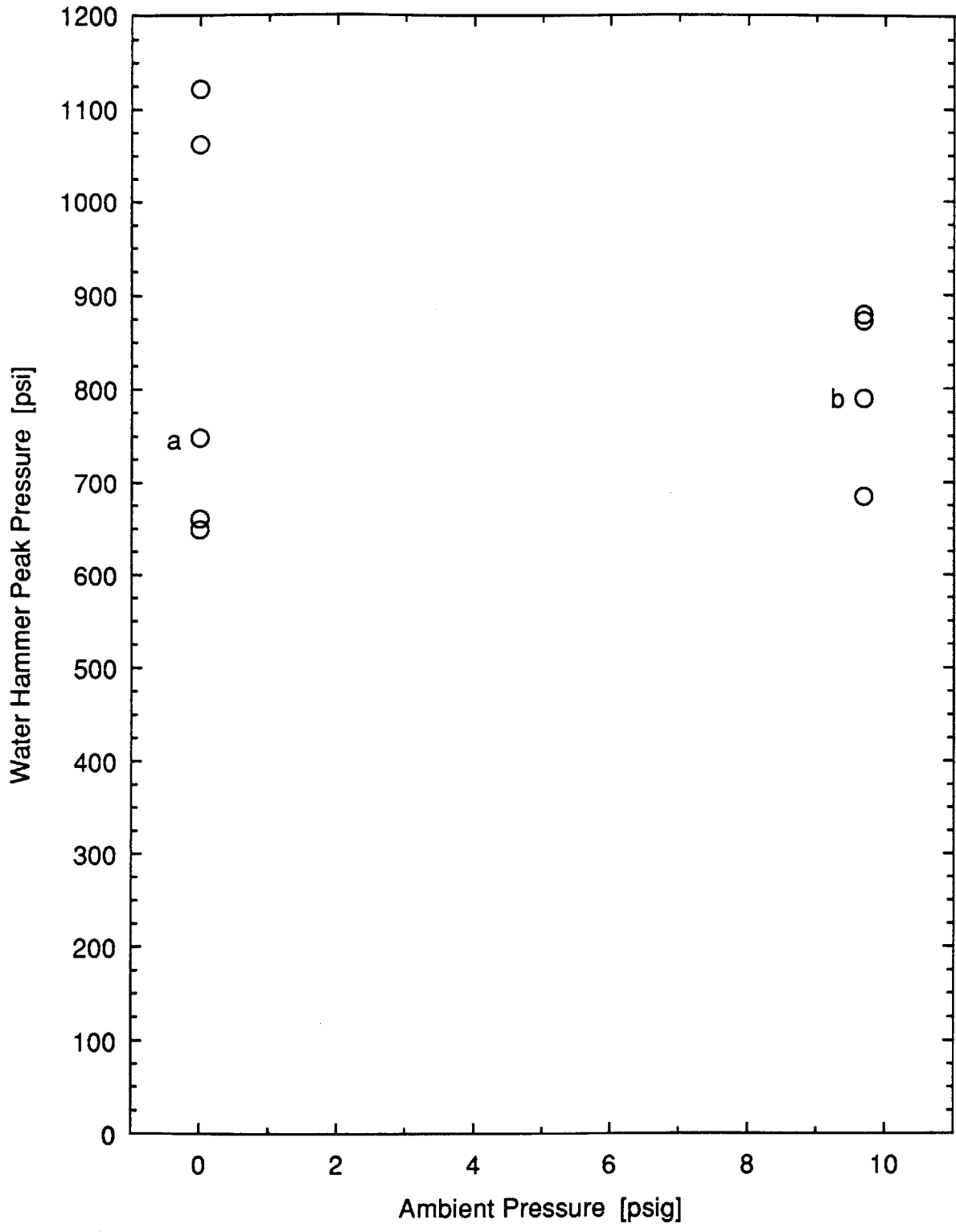


Figure D-2: Water Hammer Peak Pressure Versus Ambient Pressure

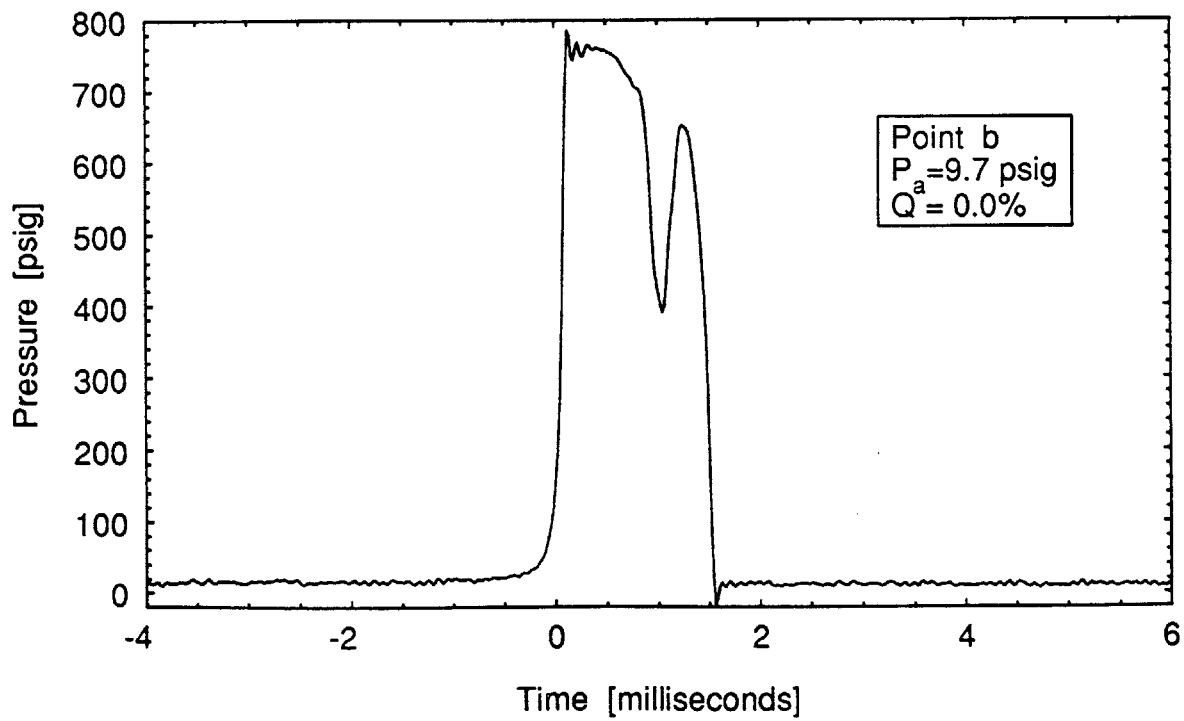
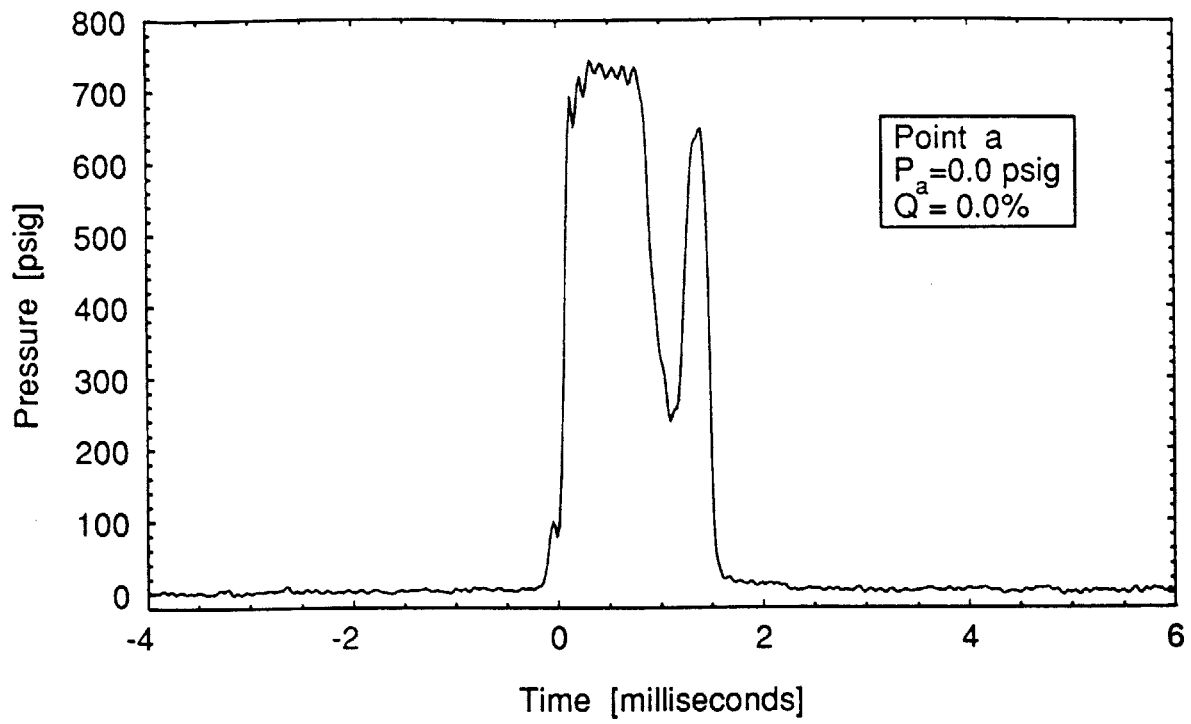


Figure D-3: Pressure Versus Time Data for Points "a" and "b" in Figure D-2

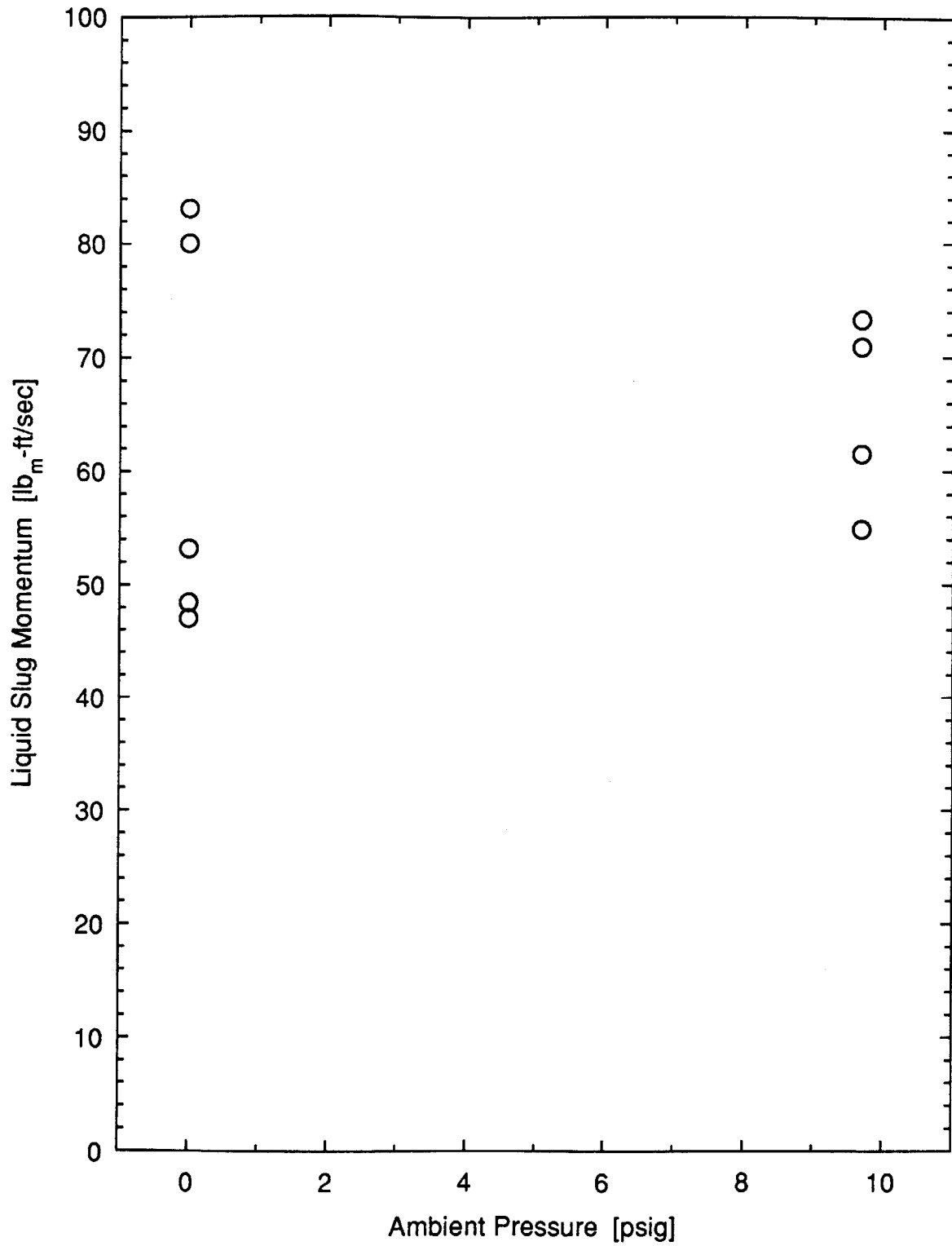


Figure D-4: Liquid Slug Momentum Versus Ambient Pressure

pressure or in the water hammer momentum. The tests were initiated with zero pressure differential across the dump valve so the liquid slug was initially accelerated only by gravity. The constant momentum suggests that the pressure difference across the liquid slug during bubble collapse was essentially the same regardless of ambient pressure. The results show that when estimating the liquid slug momentum for the case of zero noncondensable gas, the ambient pressure will have little effect on the estimate, at least in the range of ambient pressures tested here.

Appendix E

Pipe Wall Temperature Sensitivity Tests

The pipe wall temperature sensitivity tests were conducted to determine the effect of the hammer chamber wall temperature on steam bubble collapse induce water hammer. The hammer chamber wall temperature was varied by adjusting the steam supply pressure to the steam jacket around the hammer chamber. A series of runs was conducted with 0 percent gas fraction (100 percent steam) with nominal jacket steam pressures of 28 and 50 psig which corresponding to a hammer chamber wall temperature of 267F and 298F. The experimental procedure used for the pipe wall temperature sensitivity tests is given in Appendix A.2 on page 75. The data reduction procedures are described in Appendix B.3 on page 85.

E.1 Experimental Results

In Figure E-1 on page 103 shows the water hammer peak pressure versus the temperature difference between the hammer chamber wall and the subcooled liquid. As the liquid temperature varied only $\pm 3F$, the results show the effect of the varying wall temperature. The data show that as the liquid/wall temperature difference increased from 160F to 220F the water hammer peak pressure increased 20 percent. The pressure-time data for the points labeled "a", "b" and "c" are shown in Figure E-3

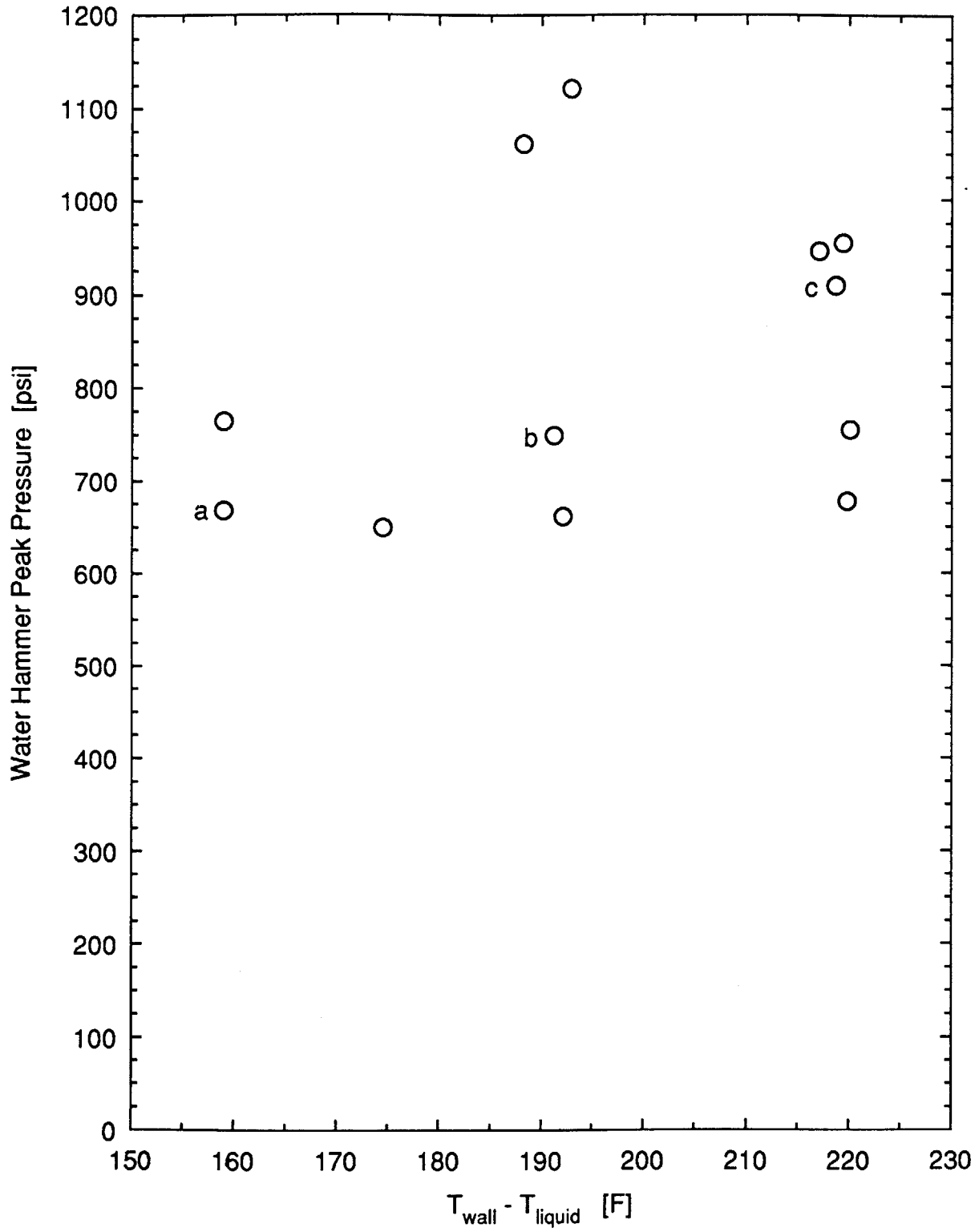


Figure E-1: Water Hammer Peak Pressure Versus Liquid/Wall Temperature Difference

on page 106.

The liquid slug momentum versus liquid/wall temperature difference is shown in Figure E-2 on page 105. Figure E-2 shows that the momentum increases about 20 percent as did the water hammer peak pressure. The momentum increase is almost entirely responsible for the increase in peak pressure.

Figure E-3 on page 106 shows the pressure/time histories for the points labeled "a", "b" and "c" in Figure E-1. The data show not only the peak pressure increase with liquid/wall temperature difference, they also show that the pressure spike begins to split into two separate spikes. The drop in pressure beginning at about 0.7 ms may be due to a decompression wave that has been reflected before reaching the liquid slug free surface. The pressure drop at 1.5 ms is due to the decompression wave that has traveled to the free surface and back. The pressure drop at 0.7 ms may be due to the partial reflection of the upward traveling compression wave reflecting from a bubble located about half way up the liquid column. This reflected wave contains about half the energy of the upward traveling compression wave based on the measured pressure reduction at 0.7 ms.

E.2 Discussion

The pipe wall temperature sensitivity tests show that, for the range of wall temperatures tested, there is little change in water hammer amplitude with wall temperature. The data suggest that what change there is is due to an increase in liquid slug momentum. The pressure/time data show a splitting of the first pressure spike. The splitting does not affect the peak amplitude as the peak has already been reached before the pressure reduction due to the "split". The splitting does have a significant effect on the frequency content of the water hammer however. The sharp decrease in pressure at 0.7 ms followed by a sharp increase suggest that high wall temperature increases the water hammer frequency content. The splitting of the pressure spike it thought to be due to a pressure wave reflection from a bubble surface near the mid-height of the liquid column.

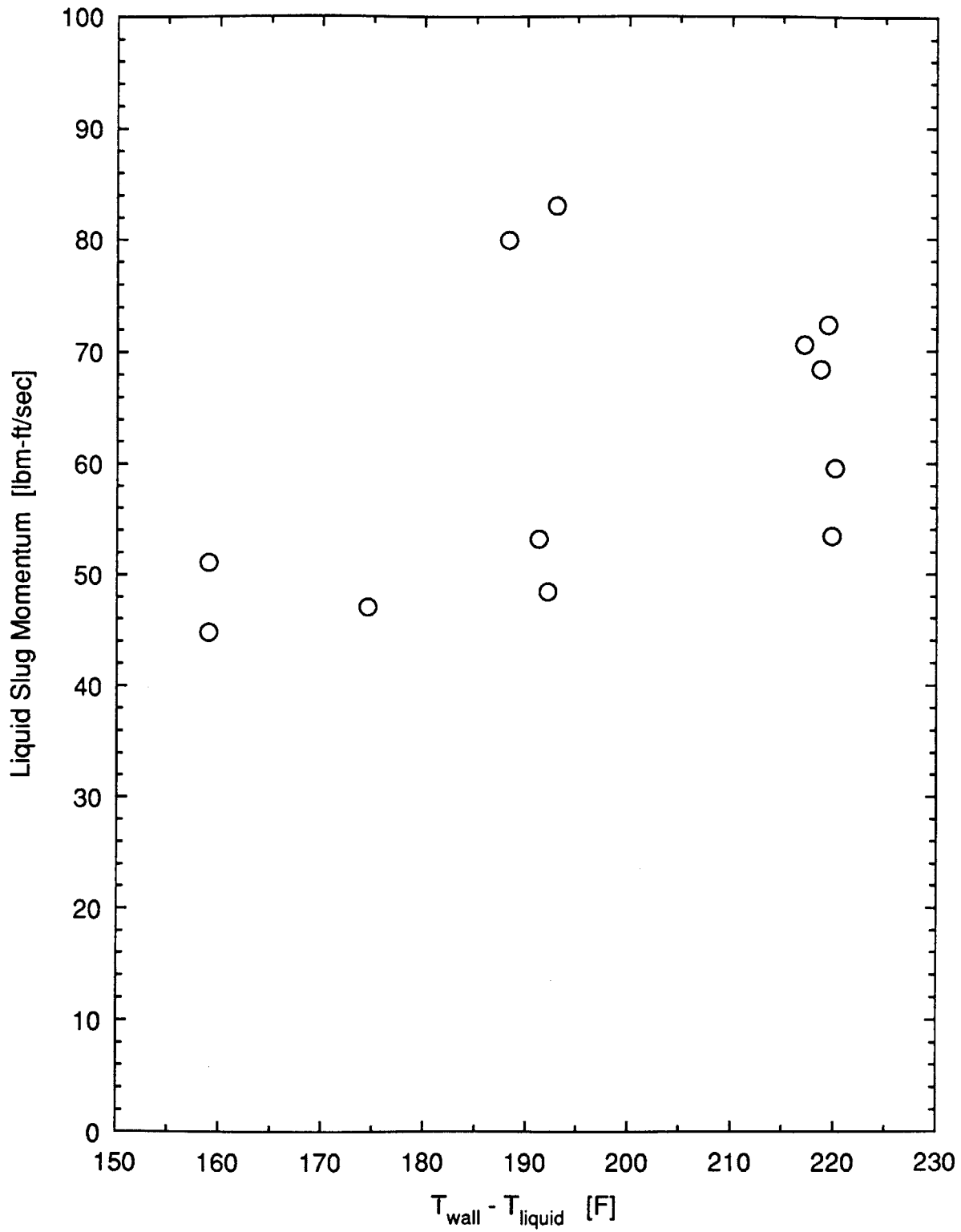


Figure E-2: Liquid Slug Momentum Versus Liquid/Wall Temperature Difference

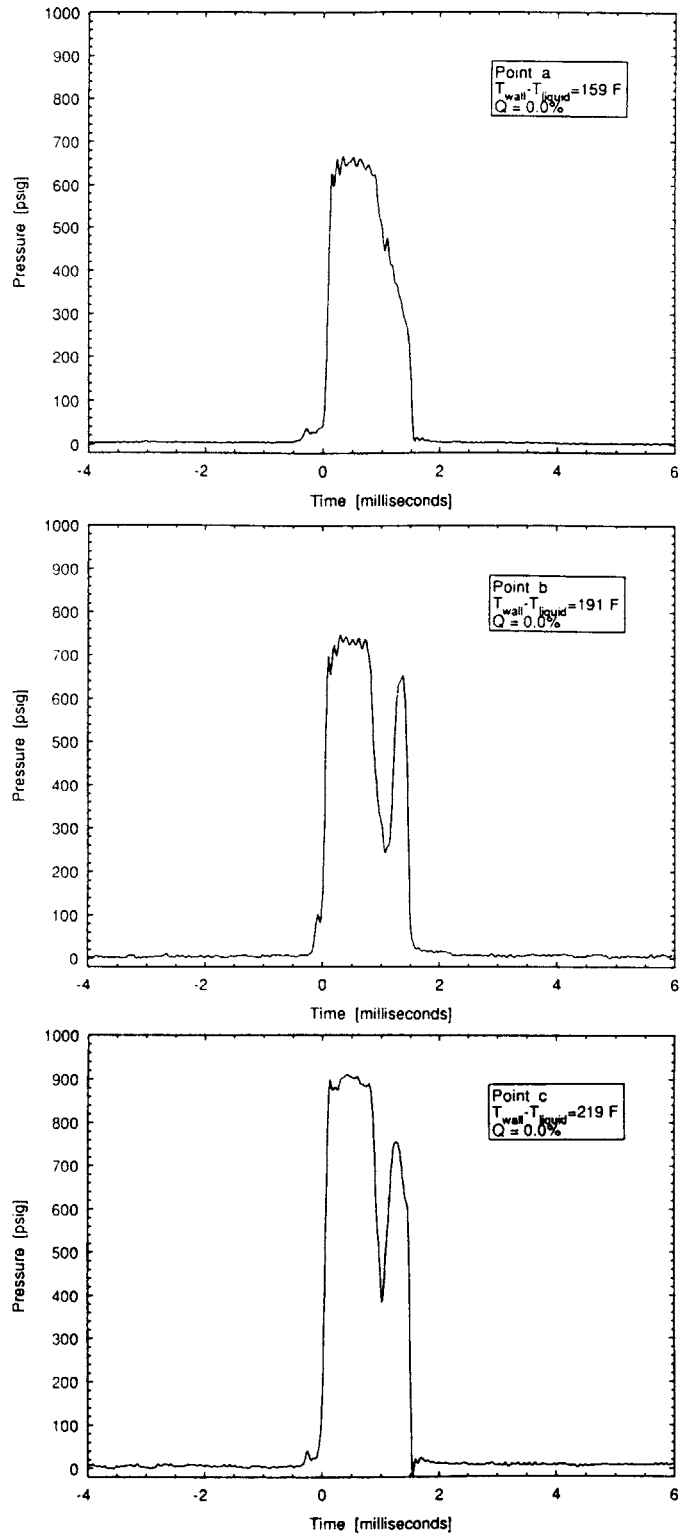


Figure E-3: Pressure Versus Time Data for Points “a”, “b” and “c” of Figure

Appendix F

Application to Other Systems

The experimental water hammer data were collected from the system shown in Figure 2-5 on page 34 and the analytical model was developed to describe that system. However, the data may be useful in predicting the amount of noncondensable gas needed to reduce water hammer amplitudes in other systems as well. The general procedure outlined below should be used to apply the results obtained here to other systems. Each of the items will be discussed in detail in the following sections.

1. Determine the acceptable level of water hammer amplitude in the system
2. Calculate maximum acceptable P^* from Equation 4.11 on page 51
3. Calculate B from Equation 4.15 on page 51
4. Enter Figure 4-12 on page 66 with P^* and B to select the required A
5. Using Equation 4.14 on page 51 solve for M_g
6. Run simulation of *BOING* to confirm maximum pressure and to obtain the pressure-time history for piping system dynamic response tests if desired
7. Evaluate effect of noncondensable gas addition on other system components
8. Determine location of noncondensable gas injection

In some of these steps parameters will need to be estimated. Below are some guidelines one might want to follow in estimating the necessary parameters.

F.0.1 Determine Maximum Pressure (Step 1)

The maximum allowable pressure may be determined from pipe stress analysis. The maximum pressure may be a function of the duration and number of expected water hammer cycles. The duration will be determined later in Appendix F.0.6. For now assume the duration is sufficiently short and readjust the maximum pressure if necessary.

F.0.2 Calculate Maximum P^* (Step 2)

The maximum allowable nondimensional pressure is simply the maximum allowable pressure determined in step 1 divided by the ambient or steady state pressure as defined by Equation 4.11 on page 51. Choosing P_a is not easy for a pipe undergoing a transient. In general choosing a high P_a overestimates the gas required and is therefore a conservative approach.

F.0.3 Calculate B (Step 3)

B is determined from Equation 4.15 on page 51 and is reproduced below.

$$B = \frac{M_l g}{P_a \mathcal{A} g_o} \quad (\text{F.1})$$

In order to evaluate B it is necessary to interpret g , M_l and \mathcal{A} . P_a was interpreted in step 2. For vertical piping systems g is simply 32.2 feet per second per second. For piping systems inclined at an angle θ from the vertical replace g with $g \cos \theta$. The mass of the liquid slug is more difficult to define. Ideally, it should be the mass of the liquid between the steam bubble that is collapsing and the nearest pressure source, such as a tank free surface. If the cross-section of the piping changes in the run to the pressure source then the mass needs to be corrected to reflect the diameter change. The pipe cross-sectional area \mathcal{A} is assumed constant in the model. It should be entered as the cross-section of the pipe in which the final stage of the gas compression will occur.

F.0.4 Determine A (Step 4)

With P^* from step 2 and B from step 3 enter Figure 4-12 on page 66 and select A . If Figure 4-12 does not contain necessary values of B or A the curves can be extended by running *BOING* and plotting the results.

F.0.5 Calculate M_g (Step 5)

From Equation 4.14 on page 51 the mass of noncondensable gas is given by

$$m_g = \frac{A\mathcal{M}^2}{\gamma M_l R T_{wall} g_o} \quad (\text{F.2})$$

In order to determine M_g the terms γ , R , T_{wall} and \mathcal{M} need to be evaluated. γ is the specific heat ratio for the gas to be used. It is 1.4 for air. R is the gas constant for the gas to be used and T_{wall} is the absolute temperature of the pipe wall in the region where the steam bubble exists. The liquid slug impact momentum \mathcal{M} is perhaps the most difficult parameter to estimate and its effect on M_g is squared. To determine \mathcal{M} it may be necessary to run a dynamic simulation of the liquid in the piping system taking into account such things as pipe friction, gravity and pump transient characteristics. If the liquid slug is being propelled by steam then the momentum may be effected by shedding at the steam/water interface. The effect is described and quantified by Fenton[3]. The pressure ahead of the liquid front may be modeled as being at the saturation pressure for the pipe wall temperature if the pipe contains steam.

F.0.6 Run Simulation of *BOING* (Step 6)

Run a simulation of *BOING* with the known values of A and B to confirm that P^* is sufficiently low. Simulation time steps that are too large cause P^* to be overestimated. Decrease Dt until P^* stabilizes. The pressure-time trace produced by *BOING* may be used to evaluate the duration of the maximum pressure selected in step 1 and to evaluate the piping system dynamic response.

F.0.7 Evaluate Effect on Other Components (Step 7)

The added noncondensable gas will remain in the system until removed by air ejectors or vented to the atmosphere. The gas may affect other system components. For example using air as the noncondensable gas may cause oxygen corrosion problems in the boilers. The effect of the amount of gas on the air ejector performance may need to be evaluated. It may be necessary to determine how long it will take to remove the gas from the system and what effect it will have on plant efficiency.

F.0.8 Determine Location of Gas Injection (Step 8)

The gas may be injected at the location where the water hammer occurs or anywhere ahead of the liquid front provided the liquid is able to sweep the gas to the water hammer location. Be aware of "T"s, "Y"s and other piping junctions that may cause the gas to be misdirected. The noncondensable gas may be injected through existing vents, drains or by draining a section of pipe and filling it with air.

F.1 Final Comments

The list above is only a general one. There are other considerations that are too system specific to be mentioned here. The intent is simply to provide a guideline as to some of the items that need to be considered when attempting to use these laboratory results on other systems.

Appendix G

Finite Difference Water Hammer Model

The following page contains a listing of the FORTRAN code BOING (Bubble Only Includes Noncondensable Gas). BOING uses a finite difference integration technique to solve Equation 4.13 on page 51 with the boundary conditions given by Equations 4.16 and 4.17. The program accepts as input A , B , γ and the time step Δt . The output is nondimensional peak pressure and the nondimensional time of that peak pressure.

```

C          PROGRAM:   BOING (Bubble Only Includes Noncondensable Gas)
C          VERSION:   1
C          BY:        BRUCE H. EASOM
C          DATE:      16 SEPTEMBER 1991
C
C          This program simulates the spring action of the noncondensable
C          gas bubble that stops the slug of falling liquid.
C
C*****
C
C          PROGRAM BOING
C
C          DOUBLE PRECISION P(3), T, Dt
C          DOUBLE PRECISION A, B, C
C
C          WRITE(5,1000)' Enter A, B, Gamma and Dt '
C          READ(6,*) A, B, Gamma, Dt
C          WRITE(5,1000)' '
C          WRITE(5,1000)'           Time           Pressure '
C          WRITE(5,1000)'           [nondimensional] [nondimensional]'
C          WRITE(5,1000)' '
C
C          C=1.0/Gamma + 1.0
C
C          initial conditions
C
C          T=0.0-Dt
C          P(1)=1.0 - (Gamma*Dt)
C          WRITE( 5,1010) T, P(1)
C          Pmax=0.0
C          Tmax=0.0
C
C          T=T+Dt
C          P(2)=1.0
C          WRITE( 5,1010) T, P(2)
C
C          10 T=T+Dt
C          P(3) = C/P(2)*((P(2)-P(1))/Dt)**2
C          P(3) = P(3) - A*P(2)**C * (P(2)-(B+1))
C          P(3) = P(3)*Dt**2 + 2.0*P(2) - P(1)
C          IF(Pmax .LT. P(3)) THEN
C             Pmax=P(3)
C             Tmax=T
C          ENDIF
C          IF(P(3) .LT. 0.9*Pmax) THEN
C             WRITE(5,1000)' '
C             WRITE(5,1000)' Time of Maximum Pressure   Maximum Pressure'
C             WRITE(5,1000)'           [nondimensional] [nondimensional]'
C             WRITE(5,1000)' '
C             WRITE(5,1010) Tmax, Pmax
C             WRITE(5,1000)' '
C             STOP
C          ENDIF
C          WRITE( 5,1010) T, P(3)
C          P(1)=P(2)
C          P(2)=P(3)
C          GOTO 10
C
C          1000 FORMAT(1X,A)
C          1010 FORMAT(1X,6X,2(E13.6,11X))
C          END

```


Appendix H

Pressure Transducer System Step Response

This appendix contains the step response analysis of the pressure transducer system. The system consists of the piezoelectric pressure transducers, charge amplifiers, charge amplifier low-pass filter, FM tape recorder and structural dynamics analyzer. This analysis was conducted to show that the response of the transducer system is fast enough to accurately record the water hammer pressure characteristics. The elements of the pressure transducer system are connected as shown in Figure H-1.

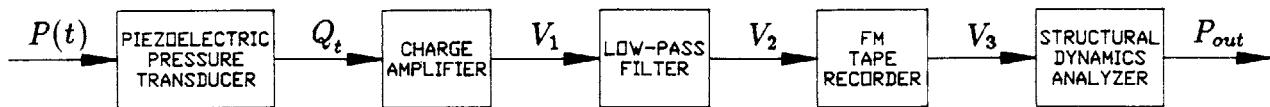


Figure H-1: Piezoelectric Pressure Transducer System Schematic

H.1 Piezoelectric Transducer

The piezoelectric crystal has both mass and compressibility and so responds dynamically to a pressure input. Being a continuous system, the crystal has an infinite number of vibration modes and natural frequencies. Looking only at the fundamental mode, the transducer responds like a second order, underdamped, linear, time-invariant system. The manufacturer's specifications give this natural frequency as 70 kHz and the 10% to 90% rise time as 6 μ s. The transducer damping ratio, ζ_t , determined from the rise time and natural frequency data[8], has a value of 0.84.

The s-plane representation of the transducer transfer function is given by

$$G_t(s) = \frac{Q_t(s)}{P(s)} = \frac{K_t \omega_{n_t}^2}{s^2 + 2 \zeta_t \omega_{n_t} s + \omega_{n_t}^2} \quad (\text{H.1})$$

H.2 Charge Amplifier

The charge amplifier consists of a capacitor and isolating amplifiers. The amplifier behaves as a constant gain device with the gain equal to $\frac{1}{C_a}$. The charge amplifier transfer function is given by

$$G_c(s) = \frac{V_1(s)}{Q_t(s)} = \frac{1}{C_a} \quad (\text{H.2})$$

H.3 Charge Amplifier Low Pass Filter

The charge amplifier is fitted with a 10 kHz low pass filter to filter out the noisy 70 kHz transducer transient response. The manufacturer's filter specifications give the cutoff frequency as 10 kHz, the roll off as 12 dB/octave and the frequency response being down 3dB at 10 kHz. The transfer function of this filter is given by

$$G_f(s) = \frac{V_2(s)}{V_1(s)} = \frac{\frac{1}{T_f}}{s + \frac{1}{T_f}} \quad (\text{H.3})$$

$$\text{where } T_f = \frac{1}{2\pi \times 10,000}$$

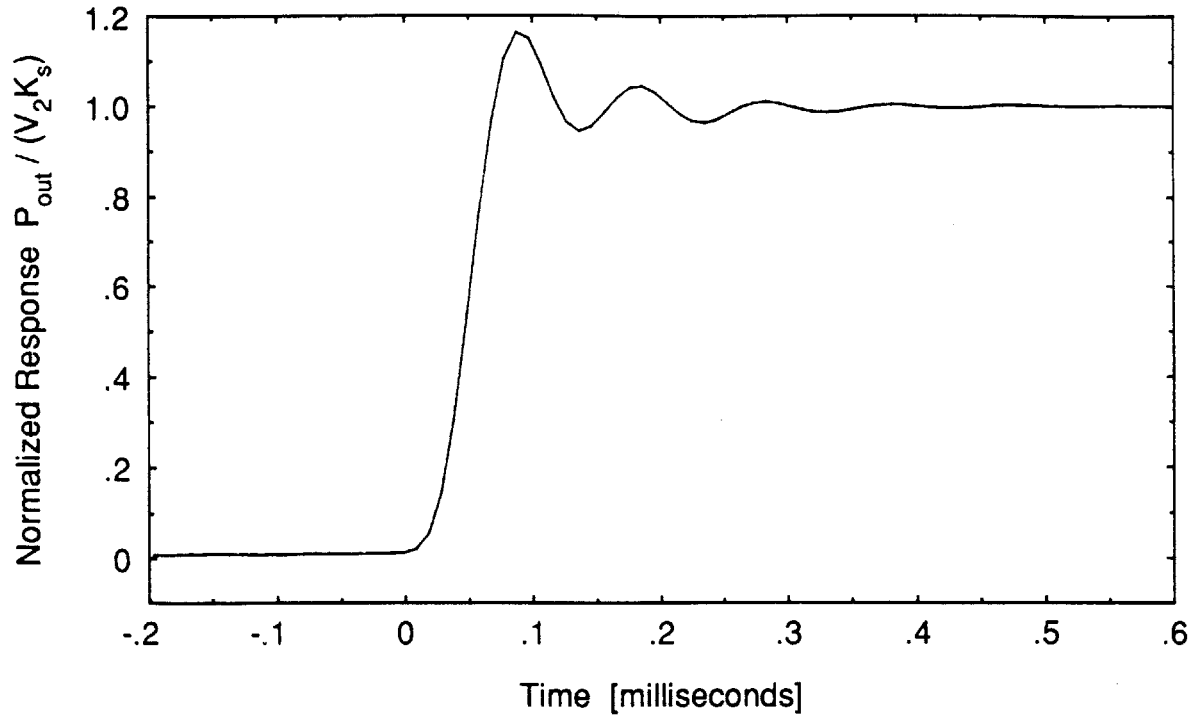


Figure H-2: Step Response of FM Tape Recorder and Structural Dynamics Analyzer

H.4 FM Tape Recorder and Structural Dynamics Analyzer

The step response of the tape recorder and structural dynamics analyzer were determined together experimentally. A 9 volt step input was recorded on the FM tape recorder from a function generator. The recorder was played back into the structural dynamics analyzer. The result is shown in Figure H-2. The step response of the combined system appears as a step response from a second-order, linear, time-invariant system having a natural frequency of 6.73 kHz and a damping ratio of 0.51. The transfer function of the combined FM tape recorder/structural dynamics analyzer system is given by

$$G_s(s) = \frac{P_{out}(s)}{V_2(s)} = \frac{K_s \omega_{n_s}^2}{s^2 + 2\zeta_s \omega_{n_s} s + \omega_{n_s}^2} \quad (\text{H.4})$$

The transfer function of the combined pressure transducer system is given by

$$G(s) = \frac{P_{out}(s)}{P_{in}(s)} = G_t(s) \times G_c(s) \times G_f(s) \times G_s(s) \quad (\text{H.5})$$

or

$$G(s) = \frac{P_{out}(s)}{P_{in}(s)} = \frac{K_t \omega_{n_t}^2 \frac{1}{C_a} \frac{1}{T_f} K_s \omega_{n_s}^2}{(s^2 + 2 \zeta_t \omega_{n_t} s + \omega_{n_t}^2)(s + \frac{1}{T_f})(s^2 + 2 \zeta_s \omega_{n_s} s + \omega_{n_s}^2)} \quad (\text{H.6})$$

The steady state response of this system is given by

$$G(s = 0) = K_t \frac{1}{C_a} K_s \quad (\text{H.7})$$

Equation H.7 is equal to one if all the component calibrations have been done correctly so

$$G(s) = \frac{P_{out}(s)}{P_{in}(s)} = \frac{\omega_{n_t}^2 \frac{1}{T_f} \omega_{n_s}^2}{(s^2 + 2 \zeta_t \omega_{n_t} s + \omega_{n_t}^2)(s + \frac{1}{T_f})(s^2 + 2 \zeta_s \omega_{n_s} s + \omega_{n_s}^2)} \quad (\text{H.8})$$

The step response of this system is given by $\frac{1}{s} G(s)$. Using partial fraction expansion and evaluating the residuals

$$P_{out}(s) = \frac{1}{s} + \frac{2.030E-3 s}{s^2 + 2 \zeta_t \omega_{n_t} s + \omega_{n_t}^2} + \frac{1.169E-9 \omega_{n_t}^2}{s^2 + 2 \zeta_t \omega_{n_t} s + \omega_{n_t}^2} - \frac{0.7534}{s + \frac{1}{T_f}} - \frac{0.2487 s}{s^2 + 2 \zeta_s \omega_{n_s} s + \omega_{n_s}^2} - \frac{2.872E-5 \omega_{n_s}^2}{s^2 + 2 \zeta_s \omega_{n_s} s + \omega_{n_s}^2} \quad (\text{H.9})$$

where	$\omega_{n_t} = 2\pi \times 70,000$	[radians/second]
	$\zeta_t = 0.84$	[nondimensional]
	$T_f = \frac{1}{2\pi \times 10,000}$	[seconds]
	$\omega_{n_s} = 2\pi \times 6,730$	[radians/second]
	$\zeta_s = 0.51$	[nondimensional]

The inverse Laplace transform yields the following time domain step response.

$$\begin{aligned}
P(t) = & 1(t) + 2.030E-3 \frac{-1}{\sqrt{1-\zeta_t^2}} e^{-\zeta_t \omega_{n_t}} \sin(\omega_{n_t} \sqrt{1-\zeta_t^2} t - \phi_t) + \\
& 1.169E-9 \frac{\omega_{n_t}}{\sqrt{1-\zeta_t^2}} e^{-\zeta_t \omega_{n_t}} \sin(\omega_{n_t} \sqrt{1-\zeta_t^2} t) - 0.7534e^{-\frac{t}{\tau}} - \\
& 0.2487 \frac{-1}{\sqrt{1-\zeta_s^2}} e^{-\zeta_s \omega_{n_s}} \sin(\omega_{n_s} \sqrt{1-\zeta_s^2} t - \phi_s) - \\
& 2.872E-5 \frac{\omega_{n_s}}{\sqrt{1-\zeta_s^2}} e^{-\zeta_s \omega_{n_s}} \sin(\omega_{n_s} \sqrt{1-\zeta_s^2} t) \quad (H.10)
\end{aligned}$$

where

$$\phi_t = \tan^{-1} \frac{\sqrt{1-\zeta_t^2}}{\zeta_t} \quad (H.11)$$

and

$$\phi_s = \tan^{-1} \frac{\sqrt{1-\zeta_s^2}}{\zeta_s} \quad (H.12)$$

The transducer response to a step input at $t = 0$ followed by an inverse step at $t = \tau$ is shown in Figure H-3 on page 118. Here τ is equal to $\frac{2L}{c}$. Figure H-3 represents the transducer response to the pressure trace predicted from the one-dimensional model described in Section 1.2 on page 21. Figure H-3 also shows an experimental pressure traces from a zero noncondensable gas run. The comparison of these two curve shows the following.

1. The rate of rise of the experimental pressure trace is limited by the pressure transducer system frequency response
2. The oscillations in the experimental pressure trace at the peak pressure are due to the underdamped nature of the pressure transducer system
3. The experimental peak pressure can be accurately determined after the oscillations die down
4. The pressure transducer system's response is sufficiently fast to preserve the square wave nature of the water hammer pressure

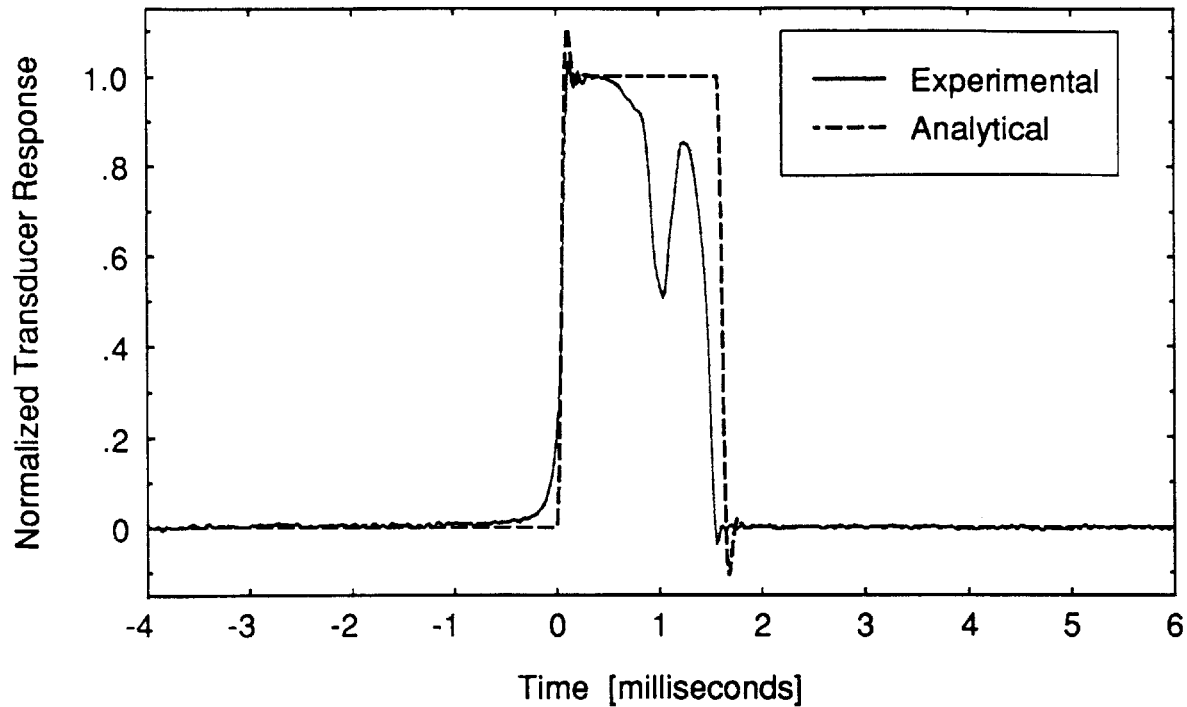


Figure H-3: Transducer System Step Response

5. The smoothness of the pressure traces from the runs with added noncondensable gas are faithfully recorded because the frequency content of those pressure traces is low.

The frequency response of the of the pressure transducer system is limited by the 6.73 kHz natural frequency of the combined FM tape recorder / structural dynamics analyzer. The noncondensable gas tests have a $\frac{1}{2}$ sine wave shape with a frequency of about 300 Hz so this fundamental frequency and up to 10 harmonics can be accurately measured. The sine wave nature of the curve assures that the magnitudes of the higher harmonics are small anyway.

This analysis shows that the pressure transducer system response is fast enough to preserve the square wave nature of the zero noncondensable gas test data. It shows that the peak pressure can be accurately measured and that the system can accurately reproduce the noncondensable gas pressure/time data due to its low frequency content.

Appendix I

Instrumentation

This appendix lists the instruments used in the water hammer experiments. It describes the instruments, calibration procedure and lists the instrument specifications. The instruments are listed by application.

I.1 Hammer Chamber Pressure

The hammer chamber pressure was measured using two piezoelectric pressure transducers and two charge amplifiers. One transducer and charge amplifier were used to measure the pressure of the hammer chamber between the time of dump valve opening and the water hammer event and was referred to as the low pressure transducer. A second transducer and charge amplifier were used to measure the peak water hammer pressure and was referred to as the high pressure transducer. Piezoelectric transducers were chosen because they could measure high pressures of short duration due to their very high frequency response. Both transducers were calibrated with their respective charge amplifier using a deadweight tester. The dead weight tester only went up to 500 psi so the peak pressure measurements required extrapolating the calibration curves. Both transducers were calibrated in the high pressure and low pressure ranges so that each transducer could be used to cross check the other. The transducer was calibrated and all data was taken with the charge amplifier on the “long” time constant setting. The pressure transducer and charge amplifier specifi-

cations are given in Table I.1 on page 121.

I.2 Dump Valve Differential Pressure

The dump valve differential pressure was measured using a variable reluctance pressure transducer and carrier demodulator. The transducer and demodulator were calibrated together using a deadweight tester. The transducer and demodulator specifications are given in Table I.2 on page 122.

I.3 Boiler Pressure

The boiler pressure was measured with a Bourdon tube pressure gauge that was fitted with a capillary bleed to allow removal of noncondensable gas trapped in the Bourdon tube. This bleed feature was used when purging the system as described in Appendix A.1.1 on page 71. The pressure gauge was calibrated using a deadweight tester. The boiler pressure gauge specifications are given in Table I.3 on page 122.

I.4 Superheater Tank Pressure

The superheater tank pressure was measured with a Bourdon tube pressure gauge and a silicone-filled pressure diaphragm. The pressure gauge and diaphragm arrangement are shown in Figure I-1 on page 123. The diaphragm was purchased as a unit but it was necessary to machine a special lower housing to allow condensate to drain from under the diaphragm. A bleed screw was placed in the lower housing to allow venting of trapped noncondensable gas during the tank purging process (see Appendix A.1.1 on page 71). The pressure gauge and diaphragm specifications are given in Table I.4 on page 124. The gauge and diaphragm were calibrated together by pressurizing the superheater tank with air. The gauge reading was compared to a reference gauge that had been calibrated on the deadweight tester. This in situ calibration corrected for the head pressure due to the silicon oil. The generated gauge/diaphragm calibration

	High Pressure	Low Pressure
Transducer		
Manufacturer	Kistler Instrument Corp	Kistler Instrument Corp
Model Number	7001	7001
Serial Number	396182	170324
Sensitivity(nom.)	-5.5 pC/psi	-5.5 pC/psi
Natural Frequency(nom.)	70 kHz	70 kHz
Rise Time (%10 to 90%)	6 μ s	6 μ s
Charge Amplifier		
Manufacturer	Kistler Instrument Corp	Kistler Instrument Corp
Model Number	504A	566
Serial Number	0292	556
Time Constant	Long/Med/Short	Long/Short
Output	± 10 VDC	± 10 VDC
Scale Settings	1 psi/volt	0.05mV/pCb
	2 psi/volt	0.1 mV/pCb
	5 psi/volt	0.2 mV/pCb
	10 psi/volt	0.5 mV/pCb
	20 psi/volt	1 mV/pCb
	50 psi/volt	2 mV/pCb
	100 psi/volt	5 mV/pCb
	200 psi/volt	10 mV/pCb
	500 psi/volt	20 mV/pCb
	1k psi/volt	50 mV/pCb
	2k psi/volt	100 mV/pCb
	5k psi/volt	
Low Pass Filter		
Manufacturer	Kistler Instrument Corp	No Filter Installed
Model Number	545A11	
Frequency	10 kHz	
Rolloff	12 dB/octave	

Table I.1: Hammer Chamber Pressure Instrumentation Specifications

Pressure Transducer

Manufacturer	Validyne Engineering Corporation
Model Number	DP15
Serial Number	27961
Diaphragm Range	± 5 psi
Diaphragm Model Number	P/N3-36

Carrier Demodulator

Manufacturer	Validyne Engineering Corporation
Model Number	CD 15-30
Serial Number	5024
Output	± 10 VDC

Table I.2: Dump Valve Differential Pressure Instrumentation Specifications

Manufacturer	Helicoid Instruments Bristol Babcock, Inc.
Type	410-Bronze
Size	$4\frac{1}{2}$ inch
Accuracy	$\pm\frac{1}{2}$ of 1%
Range	0 to 60 psi

Table I.3: Boiler Pressure Gauge Specifications

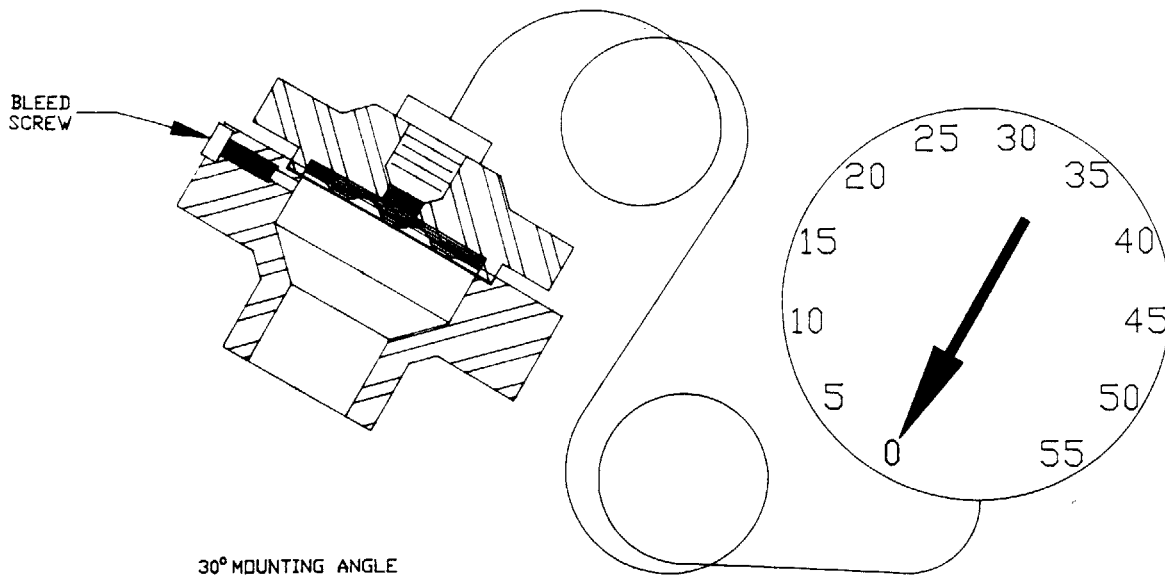


Figure I-1: Superheater Tank Pressure Gauge and Diaphragm Arrangement

curve was used in the gas fraction data reduction procedure.

I.5 Gas Bottle Pressure

The gas bottle pressure was measured with a Bourdon tube pressure gauge. The gas bottle was pressurized with compressed air with the block valve and gauge isolation valves open. The block valve was closed after 10 seconds when the temperature and pressure of the gas in the bottle had stabilized. The block valve was closed so the volume of the pressure gauge Bourdon tube did not effect the volume of noncondensable gas admitted to the superheater tank. The gauge was calibrated with a deadweight tester.

Pressure Gauge	
Manufacturer	Helicoid Instruments Bristol Babcock, Inc.
Type	410-Bronze
Size	4½ inch
Accuracy	±½ of 1%
Range	0 to 60 psi
Diaphragm	
Manufacturer	Helicoid Instruments Bristol Babcock, Inc.
Model Number	1654R
Diaphragm Material	310 Stainless Steel
Filling Liquid	Silicon Oil
Range	0 to 60 psi

Table I.4: Superheater Tank Pressure Gauge and Diaphragm Specifications

Manufacturer	Helicoid Instruments Bristol Babcock, Inc.
Type	410-Bronze
Size	8 inch
Accuracy	±¼ of 1%
Range	0 to 150 psi

Table I.5: Gas Bottle Pressure Gauge Specifications

Manufacturer	John Fluke Mfg. Co.
Model	2166A
Channels	10
Serial Number	3198050
Display	Degrees Fahrenheit to nearest degree

Table I.6: Thermocouple Reader Specifications

I.6 Operating Temperatures

All temperatures were determined using type-K thermocouples and a single multi-channel digital readout. The thermocouples were calibrated by placing them in an ice bath and a boiling water bath. Errors were 1F or less so no calibration curves were used for the temperature data. The specifications for the thermocouple readout are given in Table I.6.

I.7 Dump Valve Position Indicator

The dump valve position indicator consisted of a 1-turn 10 k Ω potentiometer and a DC power supply. The power supply provided 10 volts across the potentiometer. A potentiometer output voltage proportional to the valve angle was displayed on an oscilloscope and recorded on the FM tape recorder. The dump valve position indicator was calibrated by placing a protractor over the valve stem and recording valve angle versus output voltage with the tape recorder and oscilloscope connected into the circuit. The angle at which the valve became full open and fully closed were noted. The potentiometer and DC power supply specifications are given in Table I.7 on page 126.

Potentiometer	
Manufacturer	Clarostat
Model	392C3-10K
Turns	1
Impedance	10 k Ω
DC Power Supply	
Manufacturer	Maxtec International Corp
Model	1630
Serial Number	146-05353

Table I.7: Dump Valve Position Indicator Specifications

I.8 Tape Recorder

The hammer chamber pressures (high and low), dump valve differential pressure and dump valve position signals were recorded on a 16 channel FM tape recorder. The recorder was used because there was no computer available in the laboratory that could sample and digitize fast enough. The data from the tape recorder was played back and analyzed using a Hewlett Packard structural dynamics analyzer located in another laboratory. The tape recorder specifications are given in Table I.8 on page 127. An analysis of the frequency response of the hammer chamber pressure transducers, tape recorder and structural dynamics analyzer is given in Appendix H on page 113. The tape recorder and structural dynamics analyzer were calibrated together each day data was collected. The calibration was done by putting a 0.2 Hz square wave of ± 9.5 volts into the tape recorder from a function generator. The response of the structural dynamics analyzer was then observed and the combined gain and bias were determined. The gain and bias corrections were then applied to all experimental data taken that day.

Manufacturer	Honeywell
Model	101
Part Number	MD101AFNSJAS
Serial Number	0900153VG7SR
S.O. Number	859941
Frequency Response	10 kHz at 30 inches per second tape speed

Table I.8: FM Tape Recorder Specifications

Manufacturer	Hewlett Packard
Model	5423A
Serial Number	2032A00324
Maximum Sampling Frequency	102.4 kHz

Table I.9: Structural Dynamics Analyzer Specifications

I.9 Structural Dynamics Analyzer

The data recorded on the FM tape recorder was analyzed by playing it back into the structural dynamics analyzer. The analyzer digitized, filtered and scaled the data. The analyzer was used to determine the water hammer peak pressure, to integrate the pressure traces to determine the water slug momentum and to correct the pressure traces for the transducer thermal effect. The calibration was done in combination with the FM Tape recorder as described in Appendix I.8. The analyzer specifications are given in Table I.9.

Bibliography

- [1] Robert W. Bjorge. *Initiation of Water Hammer in Horizontal or Nearly-Horizontal Pipes Containing Steam and Subcooled Water*. PhD thesis, Massachusetts Institute of Technology, January 1982.
- [2] Jr. C.A. Meyer; R.B. McClintock; G.J. Silvestri; R.C. Spencer. *1967 ASME Steam Tables*. American Society of Mechanical Engineers, 1970.
- [3] Richard Mark Fenton. The forces at a pipe bend due to the clearing of water trapped upstream. Master's thesis, Massachusetts Institute of Technology, October 1989.
- [4] Tsunenori Kazama. Column separation and waterhammer in binary mixture. Master's thesis, Massachusetts Institute of Technology, June 1983.
- [5] Carlos Alexandre O. C. Lobo. *Filling Strategies for Avoiding Water Hammer In Steam Filled Pipes*. PhD thesis, Massachusetts Institute of Technology, December 1988.
- [6] David Moalem and Samuel Sideman. Bubble condensation with non-homogeneous distribution of non-condensibles. In *International Journal of Heat and Mass Transfer*, August 1971.
- [7] Frederick J. Moody. *Introduction to Unsteady Thermofluid Mechanics*, chapter 2. John Wiley and Sons, 1990.
- [8] Katsuhiko Ogata. *Modern Control Engineering*, chapter 6. Prentice-Hall, Inc., 1970.

- [9] Daniel A. Van Duyne and Wushong Yow. Water hammer prevention, mitigation and accommodation - task 1 - plant water hammer experience. Technical report, Stone and Webster Engineering Corporation, January 1980.

